

## THE GAS-PHASE OXIDATION OF ISOPRENE AND ITS FIRST-GENERATION PRODUCTS

### Abstract

The gas-phase oxidation of isoprene and its major oxidation products are described in detail. The mechanism is developed with the aim of both providing accurate simulations of the impact of isoprene emissions on HO<sub>x</sub> and NO<sub>x</sub> free radical concentrations and to produce realistic representation of the yields of products known to be involved in condensed phase processes. The schemes presented represent a synthesis of recent laboratory studies at the California Institute of Technology and elsewhere that have provided a new wealth of detail on the mechanisms at play. Insights from new theoretical approaches are also incorporated. Finally, we present a reduced mechanism appropriate for implementation in chemical transport models that retains the essential chemistry required to accurately simulate this chemistry under the typical conditions where isoprene is emitted and oxidized in the atmosphere.

### 4.1 Introduction

Volatile organic compounds (VOCs) emitted from vegetation significantly impact atmospheric photochemistry. This biogenic carbon flux is dominated by a single compound, isoprene (C<sub>5</sub>H<sub>8</sub>, 2-methyl-1,3-butadiene). The global budget of isoprene has been estimated by several approaches (Müller *et al.*, 2008; Wang and Shallcross, 2000), typically constrained using surface flux measurements (Guenther and Hills, 1998; Wiedinmyer *et al.*, 2004) and/or satellite observations (Shim *et al.*, 2005). Estimates do not significantly vary between different approaches. The most up-to-date modeling framework suggests that, at roughly 500 Tg y<sup>-1</sup>, the emissions of isoprene alone comprise about half the total biogenic emissions of non-methane VOCs worldwide (Guenther *et al.*, 2012). This emission originates from a broad taxonomic distribution of plants (*e.g.*, mosses, ferns, and trees).

The majority of isoprene's massive flux originates from a light-dependent *de novo* synthesis in plants using carbon from the Calvin cycle; dark production from microorganisms, plants, and animals is only a minor contribution (Sharkey, 1996). The question of why leaves emit isoprene is more complex. A recent unified hypothesis

suggests that isoprene is synthesized in plant tissue to mitigate the compounded effects from several environmental stress factors that produce reactive oxygen species *in vivo* (Vickers *et al.*, 2009), *e.g.*, extreme temperatures, high light, water deficiency, soil salinity, air pollution, and mechanical damage.

Following biosynthesis, isoprene is lost to the atmosphere through stomata and does not significantly accumulate in the leaves (Fall and Monson, 1992). As a result, nearly the entire flux of isoprene occurs during daytime (Loreto and Sharkey, 1990; Monson and Fall, 1989). Further information on the biogenesis of isoprene and historical context of studies is provided by a number of reviews (Kuzuyama and Seto, 2003; Monson *et al.*, 2012; Sanadze, 2004; Sharkey *et al.*, 2008; Sharkey and Yeh, 2001). Here, we focus on isoprene's atmospheric reactions and those of its immediate oxidation products.

As a five carbon conjugated diene, isoprene reacts rapidly with atmospheric oxidants. The high reactivity of isoprene limits its accumulation in the atmosphere, such that despite its large flux, only moderate mixing ratios are observed (0 - 10 ppbv) (Kuhlmann *et al.*, 2004). Under typical atmospheric daytime conditions, the reactive conversion of isoprene into more oxidized VOCs (OVOCs) occurs with a time constant of approximately 1 - 2 h (Atkinson and Arey, 2003b). Reaction with the hydroxyl radical (OH) is the dominant sink ( $\tau_{OH} = 1.25$  h,  $[OH] = 2 \times 10^6$  molec  $\text{cm}^{-3}$ ), followed by ozone ( $\text{O}_3$ ) ( $\tau_{O_3} = 17$  h,  $[O_3] = 50$  ppbv), the nitrate radical ( $\text{NO}_3$ ) ( $\tau_{NO_3} = 16$  h,  $[NO_3] = 1$  pptv), and the chlorine radical (Cl) ( $\tau_{Cl} = 29$  d,  $[Cl] = 1 \times 10^3$  molec  $\text{cm}^{-3}$ ). Because isoprene emissions peak in the daytime, and  $\text{NO}_3$  radical concentrations peak in the nighttime, oxidation by ozone is generally a larger sink for isoprene than by the nitrate radical. Nevertheless, nitrate radical chemistry is an important source of organic nitrates and formation of these nitrates can represent a major pathway for loss of  $\text{NO}_x$  from the atmosphere (Horowitz *et al.*, 2007; Paulot *et al.*, 2012) with significant impacts on [OH] and  $\text{O}_3$  formation (Dunker *et al.*, 2016; Squire *et al.*, 2015; Travis *et al.*, 2016).

The large flux and rapid oxidation of isoprene conspire to make its chemistry, and the chemistry of the associated products, of high global importance. The reactions have broad implications for regional air quality (Chameides *et al.*, 1988; Squire *et al.*, 2015; Trainer *et al.*, 1987) and global climate (Kanakidou *et al.*, 2005). For example, isoprene chemistry significantly affects tropospheric ozone production by perturbing the  $\text{NO}_x$  cycle ( $\text{NO} + \text{NO}_2$ ; Atkinson, 2000), the rate of oxidation of many compounds by impacting  $\text{HO}_x$  ( $\text{OH} + \text{HO}_2$ ; Lelieveld *et al.*, 2008; Peeters *et al.*,

2009), and the Earth's radiative balance and human health through the production of secondary organic aerosols (SOA; Carlton *et al.*, 2009; Claeys *et al.*, 2004). In addition, the precise impact of isoprene chemistry depends on the environment in which it is oxidized. In particular, the levels of anthropogenically emitted pollutants such as  $\text{NO}_x$  and  $\text{SO}_x$  will affect the oxidation pathways of isoprene and its oxidation products.

Quantification of isoprene's global impacts by atmospheric chemical transport models (CTMs) requires, at minimum, an accurate description of oxidation mechanisms and VOC emission fields (Carter, 1996; Dodge, 2000; Mao *et al.*, 2013; Paulot *et al.*, 2012; Zimmermann and Poppe, 1996). Over the past ten years, renewed experimental and theoretical efforts in elucidating the detailed photochemical and dark oxidation mechanisms of isoprene have advanced our understanding of the chemistry substantially (references herein). However, there are still large gaps in our knowledge that preclude the inclusion of an accurate description of isoprene chemistry into CTMs. These lingering kinetic and mechanistic uncertainties translate to uncertainties in the simulations of global air quality and climate feedbacks. In the spirit of past reviews on the isoprene oxidation mechanism (Fan and Zhang, 2004; Jenkin *et al.*, 2015; Paulson and Seinfeld, 1992; Pöschl *et al.*, 2000; Saunders *et al.*, 2003), this work seeks to allay such uncertainties by compiling a state-of-the-science mechanism from recent experimental work, with a particular focus on recent results from the Caltech laboratories.

## 4.2 Mechanism development

This work has three primary goals: (1) to organize the results of recent mechanistic studies undertaken at the California Institute of Technology (hereafter "Caltech") and other laboratories and to place them within the context of current knowledge on the dark and photochemical reactions of isoprene; (2) to provide a recommendation for an explicit and comprehensive mechanism describing the atmospheric reactions of isoprene for use in detailed chemical models; and (3) to synthesize a condensed mechanism that adequately captures the primary features of the isoprene chemistry but with a footprint small enough to be implemented in global CTMs. In order to make our mechanisms widely relevant to CTMs and other broad applications within atmospheric chemistry, we prioritize retaining carbon balance and providing accurate representations of isoprene's impact on  $\text{HO}_x$  and  $\text{NO}_x$  free radical concentrations, as well as the formation of products that may contribute to organic aerosol formation.

The following sections proceed systematically through the steps of isoprene oxidation, detailing recent advances in the measurements of reaction rates and product yields. As oxidation by OH accounts for ~90% of isoprene's atmospheric fate and has been the focus of most recent experimental studies at Caltech and elsewhere, we provide the greatest detail on the first (Section 4.3) and second (Section 4.7) generations of this chemistry. In our mechanism, we attempt to provide reaction recommendations for all products formed in >1% overall yield from isoprene in typical atmospheric conditions, with the exception of ubiquitous fragmentation products (*e.g.* hydroxyacetone, glyoxal, CH<sub>2</sub>O), for which we defer to previous recommendations. We also provide a detailed description and mechanism for the chemistry following isoprene's oxidation by NO<sub>3</sub> (Sections 4.5 and 4.7.5), which has recently been elucidated in multiple studies. While we include descriptions of isoprene's oxidation by ozone (Section 4.4) and chlorine (Section 4.6), we only provide a cursory treatment of the ozone chemistry in our explicit mechanism, and we omit chlorine chemistry altogether.

Our full mechanism recommendations are illustrated in each section's corresponding figures, with yields reported at 298 K and 1 atm, and recommendations for the condensed mechanism are described in the figure captions. More detailed treatments of the reactions can be found in the Supplemental Information, where the full and reduced mechanisms are made available as computer-readable codes for communal use and development. Further description of the codes and the model formulation can be found in Section 4.8. To denote the positions of isoprene's reactions and substituents in the figures and text, we assign numbers to the carbons of isoprene as follows: carbons 1-4 comprise the conjugated butadiene backbone, with the methyl substituent (carbon 5) connected to carbon 2 of the backbone. Throughout the text, we refer to these carbons as "C#" without subscripts (*e.g.* "C2"); subscripted numbers (*e.g.* "C<sub>2</sub>") are used instead to refer to fragmentation products containing a specific number of carbon atoms.

Generally, while the full mechanism treats all isomers of isoprene's oxidation products separately if they are known to have different subsequent reaction rates and products, the condensed mechanism makes use of isomer grouping (*e.g.* "δ-hydroxynitrate" to represent *E*-1-OH,4-ONO<sub>2</sub>-, *Z*-1-OH,4-ONO<sub>2</sub>-, *E*-1-ONO<sub>2</sub>,4-OH-, and *Z*-1-ONO<sub>2</sub>,4-OH-hydroxynitrates) to minimize the number of species and reactions included in the mechanism while retaining an accurate description of the oxidative fate of those grouped species. The condensed mechanism also

uses a steady-state approximation for the initial isoprene-hydroxy-peroxy radical distribution, enabling the removal of many intermediate species and reactions. The mechanism is further reduced by ignoring some particularly minor pathways (<2% branching ratio) of later-generation reactions. The condensed mechanism thus includes 105 compounds and 285 reactions, compared to the 330 compounds and 812 reactions included in the full mechanism.

Our recommended reaction rate coefficients, including their temperature dependences, and product yields are described in the following sections. Those that are not directly addressed are either taken from IUPAC recommendations or MCM v.3.3.1 (Jenkin *et al.*, 2015), or, when no experimental data have previously been reported in the literature, extrapolated from analogous reactions. For some classes of reactions we use a single generic rate parameterization. For example, the overall rates of reactions between NO and RO<sub>2</sub> (excluding acyl peroxy radicals) have been shown not to vary significantly with the structure of the peroxy radical (Miller *et al.*, 2004); we therefore use a single temperature-dependent rate coefficient formula for all non-acyl peroxy radical + NO reactions in our mechanism:

$$k_{RO_2+NO} = 2.7 \times 10^{-12} \times \exp(350/T) \text{cm}^3 \text{molec}^{-1} \text{s}^{-1} \quad (4.1)$$

Accurate simulation of organic nitrate formation in these reactions is essential for properly describing the influence of isoprene chemistry on NO<sub>x</sub>, and therefore ozone formation as well (Dunker *et al.*, 2016; Squire *et al.*, 2015). These nitrates are produced *via* the reaction of RO<sub>2</sub> with NO and *via* nitrate radical addition to alkenes. Because different isomers of the same compound have significantly different subsequent chemistry, it is also necessary to capture the distribution of isomers formed correctly.

The yields of organic nitrates from reaction of NO with individual peroxy radicals are complicated functions of pressure, temperature, molecular size and structure. While it is not possible to encompass this diversity in a simple set of rules, we take as a starting point the parameterization developed by Arey *et al.* (2001) for the temperature, pressure, and molecular size dependent yields of organic nitrates, which is derived from earlier formulations by Carter and Atkinson (1985) and Carter and Atkinson (1989). Arey *et al.* (2001) constrained their parameterization with data only for simple alkanes. As with the HO<sub>2</sub> chemistry, we modify their approach to use the sum of all heavy atoms rather than just carbon, consistent with the recommendation of Teng *et al.* (2015), who measured the hydroxynitrate yields

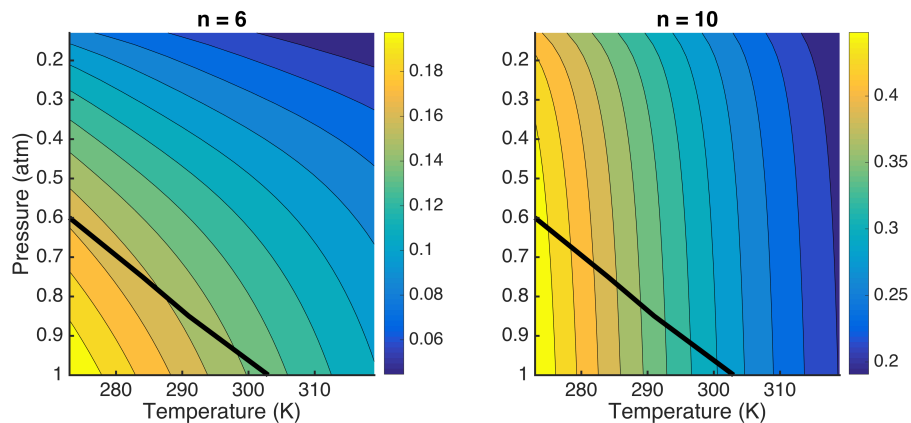


Figure 4.1: Nitrate yield ( $\alpha$ , on color scales) as a function of temperature and pressure for a peroxy radical with  $n$  (= the number of non-hydrogen atoms, not including the peroxy moiety) = 6 (left) and  $n = 10$  (right), using the parameterization in Equations 4.2-4.4. The thick black lines show typical altitude profiles of temperature and pressure over a tropical continent.

( $\alpha$ ) from a variety of alkenes at 293 K and 993 hPa to derive the formula:

$$\alpha_{RONO_2}(n) = \frac{k_{RO_2+NO \rightarrow RONO_2}}{k_{RO_2+NO, total}} = (0.045 \pm 0.016) \times n - (0.11 \pm 0.05) \quad (4.2)$$

where  $n$  again represents the number of heavy atoms excluding the peroxy moiety. Taking this formula as a baseline yield ( $\alpha_0$ ), we add the temperature and pressure dependence from Arey *et al.* (2001) to derive the following parameterization:

$$\alpha_{RONO_2}(T, P, n) = \frac{A(T, P, n)}{A(T, P, n) + A_0(n) \times \frac{1-\alpha_0}{\alpha_0}} \quad (4.3)$$

where  $A_0(n) = A(293 \text{ K}, 993 \text{ hPa}, n)$ , and  $A(T, P, n)$  is given by the Arey *et al.* (2001) formula:

$$A = \frac{\gamma \times e^n \times [M]}{1 + \frac{\gamma \times e^n \times [M]}{0.43 \times (T/298)^{-8}}} \times 0.41^{(1 + [\log(\frac{\gamma \times e^n \times [M]}{0.43 \times (T/298)^{-8}})]^2)^{-1}} \quad (4.4)$$

where  $\gamma = 2 \times 10^{-22} \text{ cm}^3 \text{ molec}^{-1}$ ,  $[M]$  is the number density of air ( $\text{molec cm}^{-3}$ ), and  $n$  is again the number of heavy atoms excluding the peroxy moiety. The pressure and temperature dependences of the nitrate yield resulting from this parameterization are shown in Figure 4.1 for  $n = 6$  and  $n = 10$ .

Laboratory measurements of the nitrate yields for multifunctional compounds often fall below this recommendation, likely reflecting a shorter lifetime for the OONO group. In our mechanism, we use insight gleaned from these studies to modify Equation 4.3 to account for molecular structure. For example, we reduce

nitrate yields from primary peroxy radicals by 50%, following substantial experimental evidence (Arey *et al.*, 2001; Carter and Atkinson, 1985, 1989; Teng *et al.*, 2015), and increase those from tertiary peroxy radicals by 50%, following studies by Teng *et al.* (2015). Additionally, we reduce by 90% the nitrate yields from reactions of  $\beta$ -carbonyl peroxy radicals + NO, following insights from observed nitrate yields of MVK and MACR (Praske *et al.*, 2015); we similarly reduce nitrate yields from  $\beta$ -hydroxy,  $\beta$ -hydroperoxy, and  $\beta$ -nitrooxy peroxy radicals by 30%, 60%, and 90%, although we note that these adjustments are poorly constrained, and further experimental evidence could substantially improve this parameterization.

Where laboratory measurements of nitrate yields have been made, these are explicitly noted, and are used in place of the formula described above. Finally, for many of the larger peroxy radicals considered here, the pressure and temperature dependence of the yields largely compensate so that the yield calculated using the modified Arey approach at conditions throughout the lower atmosphere is not significantly different than the yield at the surface (Figure 4.1).

Reactions of RO<sub>2</sub> with HO<sub>2</sub> have been shown to follow a simple pattern that depends both on temperature and the number of carbon atoms in the peroxy radical (Jenkin *et al.*, 1997; Saunders *et al.*, 2003):

$$k_{RO_2+HO_2} = 2.91 \times 10^{-13} \times \exp(1300/T) \times [1 - \exp(-0.245 \times n)] \text{cm}^3 \text{molec}^{-1} \text{s}^{-1} \quad (4.5)$$

where  $n$  represents the number of carbon atoms in the peroxy radical molecule. We suggest, similarly to the organic nitrate yield parameterization, that  $n$  should be the number of heavy (non-hydrogen) atoms other than the peroxy moiety – not just carbon. Refitting the HO<sub>2</sub> + RO<sub>2</sub> data, using IUPAC recommended rates where available and rates from Boyd *et al.* (2003) for additional species, with  $n=C+O+N-2$  (subtracting off the peroxy moiety) gives an improved fit to the experimental data, with a slightly different formula:

$$k_{RO_2+HO_2} = 2.82 \times 10^{-13} \times \exp(1300/T) \times [1 - \exp(-0.231 \times n)] \text{cm}^3 \text{molec}^{-1} \text{s}^{-1} \quad (4.6)$$

We therefore use this new rate coefficient formula for all peroxy radical + HO<sub>2</sub> reactions in our mechanism.

While reactions of organic peroxy radicals with HO<sub>2</sub> are generally expected to form hydroperoxides, terminating the radical chain, they may also result in radical propagation *via* a channel that forms an alkoxy radical and OH (see Orlando and

Tyndall, 2012). This channel was initially identified for acylperoxy radicals (Dillon and Crowley, 2008; Hasson *et al.*, 2004, 2012; Hurley *et al.*, 2006; Jenkin *et al.*, 2007), but has recently been shown to occur in other peroxy radical species as well, with higher yields for  $\alpha$ -carbonyl and more highly substituted species (Hasson *et al.*, 2012; Jenkin *et al.*, 2008, 2010). Insight from theoretical studies suggests that the radical recycling pathway proceeds through a singlet tetroxide intermediate (ROO-OOH), which, when stabilized by hydrogen bonding between the -OOH hydrogen and other functional groups on the RO<sub>2</sub> radical, may decompose to RO, O<sub>2</sub>, and OH (Hasson *et al.*, 2005; Hou *et al.*, 2005a,b; Hou and Wang, 2005). Here, we use measured hydroperoxide yields wherever possible to constrain the branching between radical terminating and recycling pathways; where such data do not exist, we extrapolate from related compounds using the observations compiled in Orlando and Tyndall (2012) – namely, that increased functionalization of the peroxy radical (particularly  $\alpha$ -carbonyl and  $\beta$ -nitrate substituents, and other functional groups enabling intramolecular hydrogen bonding of the tetroxide intermediate) tends to increase the yield of OH + RO.

Additional details regarding rate coefficient formulas, photolysis parameterizations, and the naming scheme used in the explicit model can be found in Section 4.8.

### 4.3 The reaction of OH with isoprene

Reaction with OH represents the largest loss pathway for isoprene in the atmosphere, owing both to the two species' synchronous diurnal cycles of production and their fast reaction rate. Globally, oxidation by OH is estimated to account for ~85% of the reactive fate of isoprene (Paulot *et al.*, 2012).

The rate coefficient for the reaction of OH with isoprene has been measured numerous times and the JPL Burkholder *et al.* (2015) and IUPAC (Atkinson *et al.*, 2006) reviews provide consistent recommendations:

$$k_{OH+ISOP} = 3.0 \times 10^{-11} \times e^{(360/T)} \text{ cm}^3 \text{ molec}^{-1} \text{ s}^{-1} \text{ [JPL]}$$

$$k_{OH+ISOP} = 2.7 \times 10^{-11} \times e^{(390/T)} \text{ cm}^3 \text{ molec}^{-1} \text{ s}^{-1} \text{ [IUPAC]}$$

As isoprene is oxidized in the atmosphere over a rather small temperature range (*e.g.* 280-315 K), either expression can be used (these parameterizations are within 1%). The estimated uncertainty in this rate coefficient ( $T = 300$  K) is less than 10% (Atkinson *et al.*, 2006; Burkholder *et al.*, 2015). Here, we use the IUPAC expression.

Our recommendation for the complex peroxy radical chemistry that follows addition of OH to isoprene follows the structure described by Peeters *et al.* (2014, 2009). The dynamic nature of the isomer-specific chemistry results in variable product yields that depend on atmospheric conditions. In particular, the pathways followed change depending on the bimolecular lifetime of the hydroxy peroxy radicals and temperature. The recommended reaction rate coefficients, thermochemistry, and product yields needed to capture this chemistry are those determined by Teng *et al.* (2017). One essential aspect of our recommendation is that the chemistry following addition of OH to either C1 or C4 (see numbering in Figure 4.2) is sufficiently distinct that these systems must be treated separately. Finally, in addition to the explicit rates and yields as detailed in Teng *et al.* (2017), we provide a recommendation for parameterizations that capture this highly complex chemistry for most atmospheric conditions.

#### 4.3.1 Location of OH addition to isoprene

The reaction of OH with isoprene at temperatures relevant for atmospheric chemistry goes *via* addition to the unsaturated backbone. Despite the allylic resonance, abstraction of the methyl hydrogen is likely less than 1% of the total reaction (see recent calculations on propene, Zador *et al.*, 2009).

OH can add at any of four positions on the conjugated carbon chain (Figure 4.2). Consistent with both theory and experiments, the majority of the addition occurs at the terminal (primary) carbons. On the basis of theoretical calculations by Greenwald *et al.* (2007), IUPAC recommends a ratio of 0.67:0.02:0.02:0.29 for isomers 1,2,3,4. Work in Simon North's laboratory has suggested that following internal addition, isomerization *via* a cyclopropane-like structure leads to the formation of an unsaturated ketone (*via* C2 addition) or aldehyde (*via* C3 addition), as shown in Figure 4.2 (Greenwald *et al.*, 2010; Park *et al.*, 2003). Recent laboratory studies at Caltech suggest that formation of  $\beta$  hydroxyperoxy radicals *via* OH addition at C2 and C3 is less than 1% of the total (Teng *et al.*, 2017).

Given the lack of experimental evidence and the need to simplify the mechanism, we suggest that the internal channels be ignored in atmospheric modeling for now, though their importance should be revisited with an additional focus on potential for aerosol formation *via* H-shift autoxidation (Crouse *et al.*, 2013).

Here, we recommend yields of: 0.635:0.00:0.00:0.365 for OH addition to C1-C4 Teng *et al.* (2017). It is essential to treat the C1 and C4 addition channels separately

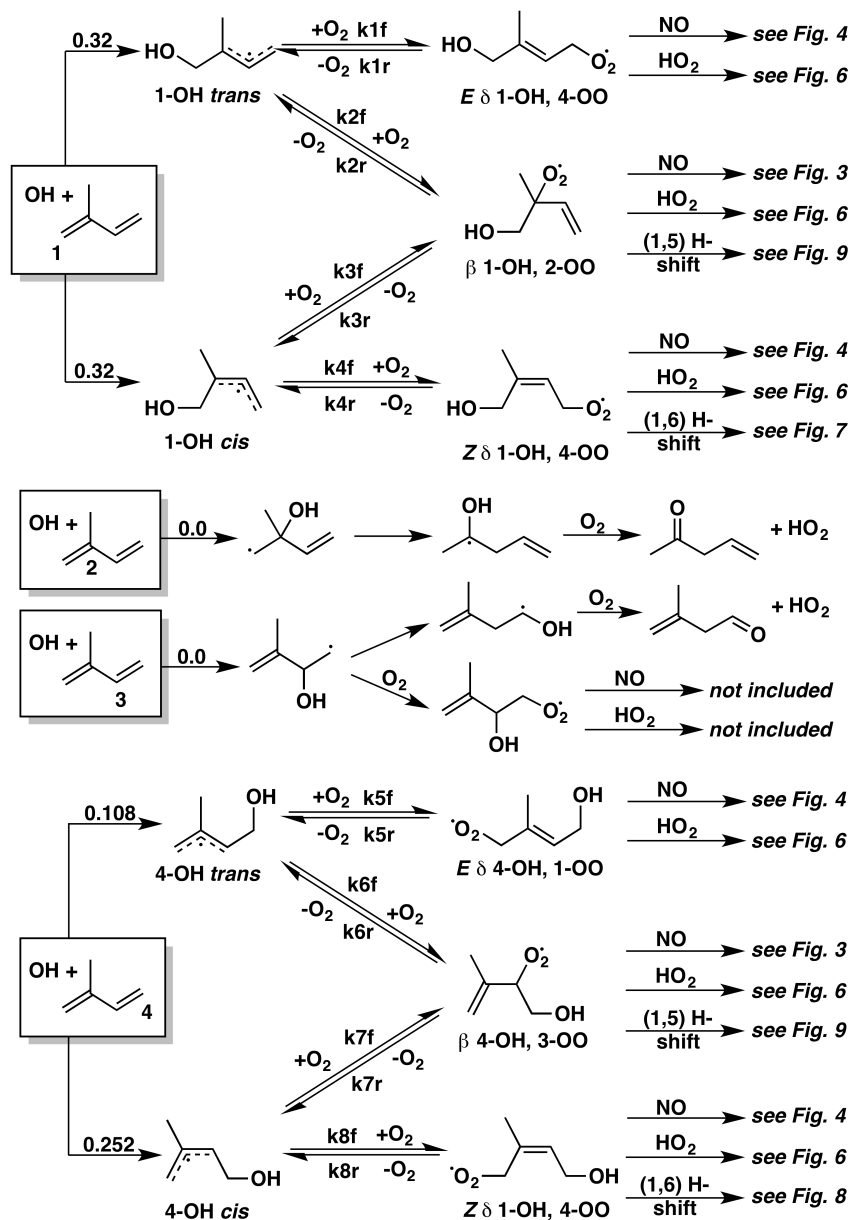


Figure 4.2: Dynamics of the isoprene + OH + O<sub>2</sub> system; 1-OH addition (top) accounts for 64% of isoprene + OH reactivity, while the 4-OH addition system accounts for the remaining 36%. For the full mechanism, we explicitly treat all forward and backward reaction rates. For the reduced mechanism, we treat the peroxy radical pool as a steady-state distribution, using bimolecular chemistry only for the  $\beta$  and  $E$ - $\delta$  isomers, and parameterizing the isomerization loss of the  $Z$ - $\delta$  isomers, as described in Section 4.3.2. These reductions are appropriate for atmospheric conditions where  $k_{bimolecular} < 1 \text{ s}^{-1}$ , at  $>280 \text{ K}$  and  $0.5\text{-}1 \text{ atm}$ .

as the subsequent product yields and mechanisms are not sufficiently similar to allow traditional lumping.

### 4.3.2 Addition of O<sub>2</sub> to the hydroxy allylic radicals

#### 4.3.2.1 *Cis/trans* allylic radical distribution

Following addition of OH to the unsaturated backbone, two separate pools of allylic radicals are established – one each for the 1-OH and 4-OH adducts (Figure 4.2). In each pool, the rotation of the internal carbon bond between *cis* and *trans* OH-isoprene adducts is rapid upon OH addition but slows upon thermalization (Peeters *et al.*, 2009). The initial distribution of *cis* to *trans* adducts is therefore set by the steady-state distribution upon collisional thermalization. Without any experimentally available constraints, we recommend the Peeters *et al.* (2014) computational estimate for the distribution of *cis:trans* allylic radicals of 0.5:0.5 for the 1-OH adducts and 0.7:0.3 for the 4-OH adducts. In the atmosphere, where the peroxy radical pools generally live for longer than 1 s, this choice does not substantially impact the final product distribution.

#### 4.3.2.2 Initial (kinetic) distribution of isoprene hydroxy peroxy radicals (ISOPOO)

Following collisional thermalization, each OH- isoprene allylic radical will add oxygen at either the  $\beta$  or  $\delta$  position to form three distinct hydroxy peroxy radicals (Figure 4.2). The overall distribution of ISOPOO is therefore initially set by both the *trans/cis* allylic distribution and the oxygen forward addition rates for the  $\beta$  and  $\delta$  positions. Isomer-specific O<sub>2</sub> addition rates are not experimentally constrained, and therefore provide little insight into the initial ISOPOO distribution. Previous estimates for the initial distribution of peroxy radicals have been based on computational estimates (Lei *et al.*, 2001) or bulk product analysis (Paulot *et al.*, 2009a). Using speciated distribution of isoprene nitrates measured at very short RO<sub>2</sub> lifetime (<10 ms, ~2 ppmv NO), Teng *et al.* (2017) constrain the product of the thermalized radical isomer distribution (*cis/trans*) and the ratios of the forward O<sub>2</sub> addition rates to form either  $\beta$  or  $\delta$  ISOPOO (Tables 4.1 and 4.2). Table 4.3 provides a summary of the recommendations for the initial (kinetic) RO<sub>2</sub> distribution resulting from OH + isoprene + O<sub>2</sub> system at 296K, as well as the MCM 3.3.1 recommendations for reference. Our recommendation is slightly modified by that presented in Teng *et al.* (2017) as we adopt isomer-dependent yields for the hydroxy nitrates yields as

reaction - see labeling in Figure 4.2	relative rate
$k_1$ : 1-OH <i>trans</i> + O <sub>2</sub> → <i>E</i> - $\delta$ 1-OH,4-OO	0.48
$k_2$ : 1-OH <i>trans</i> + O <sub>2</sub> → $\beta$ 1-OH,2-OO	1
$k_3$ : 1-OH <i>cis</i> + O <sub>2</sub> → $\beta$ 1-OH,2-OO	1
$k_4$ : 1-OH <i>cis</i> + O <sub>2</sub> → <i>Z</i> - $\delta$ 1-OH,4-OO	0.18

Table 4.1: O<sub>2</sub> addition rates for 1-OH isoprene adducts, relative to that of 1-OH-*cis* + O<sub>2</sub> →  $\beta$  1-OH,2-OO.

reaction - see labeling in Figure 4.2	relative rate
$k_5$ : 4-OH <i>trans</i> + O <sub>2</sub> → <i>E</i> - $\delta$ 4-OH,1-OO	0.75
$k_6$ : 4-OH <i>trans</i> + O <sub>2</sub> → $\beta$ 4-OH,3-OO	1
$k_7$ : 4-OH <i>cis</i> + O <sub>2</sub> → $\beta$ 4-OH,3-OO	1
$k_8$ : 4-OH <i>cis</i> + O <sub>2</sub> → <i>Z</i> - $\delta$ 4-OH,1-OO	0.33

Table 4.2: O<sub>2</sub> addition rates for 4-OH isoprene adducts, relative to that of 4-OH-*cis* + O<sub>2</sub> →  $\beta$  4-OH,3-OO.

peroxy radical	distribution	
	our recommendations	MCM 3.3.1
1-OH 2-OO	0.46	0.415
<i>E</i> 1-OH 4-OO	0.10	0.045
<i>Z</i> 1-OH 4-OO	0.05	0.169
4-OH 3-OO	0.26	0.262
<i>E</i> 4-OH 1-OO	0.06	0.014
<i>Z</i> 4-OH 1-OO	0.07	0.095

Table 4.3: Kinetic RO<sub>2</sub> isomer distributions at 297 K from Teng *et al.* (2017), adjusted slightly to account for our recommended nitrate yields from each isomer (Section 4.3.3.1) along with the kinetic distribution inferred from MCM 3.3.1 (Jenkin *et al.*, 2015). The MCM values are reported only as a fraction of the total RO<sub>2</sub> arising from external addition of OH; MCM 3.3.1 apportions 8.4% of total OH reactivity to internal addition.

discussed below.

Assuming the ratio of *cis:trans* allylic radicals calculated by Peeters *et al.* (2014) is accurate, the isomer distribution of the organic nitrates produced from ISOPOO implies a similar oxygen addition ratio at the  $\delta$  position in the *cis* and *trans* OH-isoprene allylic radicals (Teng *et al.*, 2017). There exists, however, significant disagreement between the experimentally-derived O<sub>2</sub> addition rate coefficient recommendations here and recent theoretical calculations. Peeters *et al.* (2014), for example, suggest

that the O<sub>2</sub> addition rate to the *cis*  $\delta$  position is significantly faster than to the *trans*  $\delta$  position in both 1-OH and 4-OH systems. For both the theory and experiments, the absolute recommendations for individual isomer O<sub>2</sub> addition rates are constrained only by the assumed bulk O<sub>2</sub> addition rates. Here, we recommend an overall O<sub>2</sub> addition rate constant of  $2.3 \pm 2.0 \times 10^{-12} \text{ cm}^3 \text{ s}^{-1}$  at 298K (Park *et al.*, 2004) though, within the framework for our recommendation, this choice has little impact on the product yields.

#### 4.3.2.3 The reversibility of O<sub>2</sub> addition

Peroxy radicals formed  $\beta$  to olefinic carbon centers, such that electronic resonance is established upon loss of molecular O<sub>2</sub>, have relatively small R-OO bond dissociation energy (BDE) (<20 kcal mol<sup>-1</sup>; *e.g.*, Benson and Shaw, 1968; Howard, 1972; Pratt *et al.*, 2003, and references therein). For such RO<sub>2</sub>, the addition of O<sub>2</sub> is reversible at 300 K for typical peroxy radical lifetimes in the atmosphere. Using theoretical calculations, Peeters *et al.* (2009) suggested that this reversibility is essential to capture for ISOPOO, as it is fast relative to the timescale of the peroxy radicals' lifetime in the atmosphere. This proposal has subsequently been confirmed experimentally (Crouse *et al.*, 2011; Teng *et al.*, 2017). The importance of this reversibility is that the six major RO<sub>2</sub> radicals formed from OH + isoprene + O<sub>2</sub> interconvert (two subgroups of three defined by a common OH position can interconvert with the subgroup, but not between the subgroups – see Figure 4.2). The interconversion has significance in that the subsequent chemistry of the individual RO<sub>2</sub> isomers is distinct, both in terms rates of reaction and product distribution. In addition, there is now strong evidence (Teng *et al.*, 2017) that the kinetic RO<sub>2</sub> distribution from OH + isoprene + O<sub>2</sub> is substantially different than the equilibrated thermal RO<sub>2</sub> distribution. From estimated daytime RO<sub>2</sub> lifetimes in the atmosphere (20-120 s, equivalent to 200-40 pptv NO at pressure of 1 atm), the average isoprene RO<sub>2</sub> distribution is close to the thermal equilibrium distribution (Teng *et al.*, 2017). In contrast, most laboratory studies of the product distribution from OH + isoprene have been at or near the initial (or kinetically-determined) RO<sub>2</sub> distribution.

In addition to constraining the kinetic RO<sub>2</sub> distribution from isoprene + OH, Teng *et al.* (2017) use the observed change in the isomeric distribution of isoprene nitrates as a function of RO<sub>2</sub> lifetime to constrain the equilibrium constants which describe the interconversion of the RO<sub>2</sub> isomers. We recommend these equilibrium constants here (Table 4.4).

equilibrium formula	$K$ ( $10^{-14}$ cm <sup>3</sup> molec <sup>-1</sup> )
$K_1 = [E-1-OH,4-OO-ISOP]/([trans-1-OH-ISOP][O_2])$	2
$K_2 = [1-OH,2-OO-ISOP]/([trans-1-OH-ISOP][O_2])$	49
$K_3 = [1-OH,2-OO-ISOP]/([cis-1-OH-ISOP][O_2])$	269
$K_4 = [Z-1-OH,4-OO-ISOP]/([cis-1-OH-ISOP][O_2])$	0.5
$K_5 = [E-4-OH,1-OO-ISOP]/([trans-4-OH-ISOP][O_2])$	13
$K_6 = [4-OH,3-OO-ISOP]/([trans-4-OH-ISOP][O_2])$	237
$K_7 = [4-OH,3-OO-ISOP]/([cis-4-OH-ISOP][O_2])$	507
$K_8 = [Z-4-OH,1-OO-ISOP]/([cis-4-OH-ISOP][O_2])$	2.1

Table 4.4: Equilibrium constants describing the RO<sub>2</sub> distribution from isoprene + OH at 297 K.

#### 4.3.2.4 Constraint on the absolute rates of O<sub>2</sub> loss from $\beta$ -ISOPOO

Synthesis of isoprene hydroxy hydroperoxide (ISOPOOH) isomers in pure form (Rivera-Rios *et al.*, 2014; St. Clair *et al.*, 2015) enabled an estimate of the absolute rate of O<sub>2</sub> loss from the  $\beta$ -hydroxy peroxy radical isomers (Teng *et al.*, 2017). As discussed in Section 4.7.3, OH reacts with (1-OH,2-OO) ISOPOOH (St. Clair *et al.*, 2015) to form (at ~10% yield)  $\beta$  RO<sub>2</sub> radicals *via* abstraction of the ROO-H hydrogen. This chemistry yields an isomerically pure source of a single isoprene RO<sub>2</sub> radical. By studying the nitrate distribution as a function of RO<sub>2</sub> lifetime, Teng *et al.* (2017) constrained the rate of O<sub>2</sub> loss from the (1-OH,2-OO) ISOPOO peroxy radicals to be  $\sim 2$  s<sup>-1</sup> at 297 K. This finding is consistent with an O<sub>2</sub> loss rate derived from the assumed bulk addition rate coefficient and the measured equilibrium constant Teng *et al.*, 2017.

#### 4.3.2.5 Modeling of ISOPOO isomer distribution

The complete list of reactions for the addition of OH to isoprene, the addition of O<sub>2</sub> to the isoprene-OH adduct, and the loss of oxygen from the resulting peroxy radicals can be found in the supplement. Incorporation of the complete RO<sub>2</sub> interconversion processes into a global chemical transport model requires the addition of a number of chemical species and reactions, and increases the computational load substantially. However, it has been shown theoretically by Peeters *et al.* (2014), and experimentally by Teng *et al.* (2017) that the RO<sub>2</sub> distribution can be approximately described using the equilibration constants, the forward O<sub>2</sub> + alkyl radical reaction rates, and the bimolecular RO<sub>2</sub> lifetime ( $k_{bimolecular} = k_{NO} \times [NO] + k_{HO_2} \times [HO_2] + k_{RO_2} \times [RO_2]$ ). To reduce the mechanism, we simplify the ten-species isoprene alkoxy and

peroxy radical system to two species, representing the steady-state peroxy radical distributions from the 1-OH and 4-OH additions. The full list of reactions used in the simplified model can be found in the Supplement. Isomer-specific bimolecular reactions and the isomerization of the  $\beta$  isomers can then be treated as second- and first-order processes of these peroxy radicals, scaled by the relative contributions of each isomer in steady state, while the isomerization of the  $Z$ - $\delta$  isomers requires a more complicated parameterization combining a first-order process from the peroxy radicals with a zeroth-order initial yield from isoprene + OH. These simplifications, which substantially reduce the numbers of species and reactions required to model the isomer distributions of isoprene's first-generation oxidation products, provide isomer and reaction pathway branching ratios within 5% of the full model for atmospheric conditions (*i.e.*  $k_{bimolecular} < 1 \text{ s}^{-1}$ ,  $T > 280 \text{ K}$  and  $P = 0.5\text{-}1 \text{ atm}$ ).

### 4.3.3 Reactions of ISOPOO

The peroxy radicals formed following addition of OH and O<sub>2</sub> to isoprene will react with NO (Figures 4.3-4.5), HO<sub>2</sub> (Figure 4.6), or other peroxy radicals. The  $Z$ - $\delta$  and  $\beta$  isomers also undergo intramolecular H-shift chemistry leading to hydroperoxy aldehydes and other products (Figures 4.7-4.9).

#### 4.3.3.1 Reaction of ISOPOO with NO

*Kinetics (Table 4.5)* - There have been many studies of the room temperature rate constant for the reaction of ISOPOO with NO (Chuong and Stevens, 2002; Ghosh *et al.*, 2010; Miller *et al.*, 2004; Park *et al.*, 2004; Reitz *et al.*, 2002; Stevens *et al.*, 1999; Zhang *et al.*, 2003b). Ghosh *et al.* (2010), Chuong and Stevens (2002), Reitz *et al.* (2002), Stevens *et al.* (1999), and Park *et al.* (2004) used LIF to detect the OH radical. Since OH is not produced in the nitrate pathway, this method measures only the rate of the alkoxy pathway, and the total rate includes errors in the nitrate branching ratios (Chuong and Stevens, 2002; Ghosh *et al.*, 2010; Park *et al.*, 2004; Reitz *et al.*, 2002; Stevens *et al.*, 1999). Zhang *et al.* (2003b) and Miller *et al.* (2004) found rates by measuring the decay of the isoprene peroxy radical with CIMS. Currently, IUPAC recommends a value of  $(8.8 \pm 1.2) \times 10^{-12} \text{ cm}^3 \text{ molec}^{-1} \text{ s}^{-1}$  (Atkinson *et al.*, 2006), which is equal to the value determined experimentally by Miller *et al.* (2004).

Only Ghosh *et al.* (2010) has measured an isomer-specific rate constant for the reaction of ISOPOO with NO. They synthesized a precursor whose photolysis forms

$k_{NO}$ ( $\times 10^{-12}$ cm <sup>3</sup> molec <sup>-1</sup> s <sup>-1</sup> )	T (K)	technique	citation
9(+9, -4.5)	298	DF-LIF	Stevens <i>et al.</i> (1999)
25 ± 5	295	PLP-LIF	Reitz <i>et al.</i> (2002)
11 ± 8	300	DF-LIF	Chuong and Stevens (2002)
9 ± 3	298	DF-CIMS	Zhang <i>et al.</i> (2003b)
8.8 ± 1.2	298	DF-CIMS	Miller <i>et al.</i> (2004)
9.0 ± 3.0	298	PLP-LIF	Park <i>et al.</i> (2004)
8.1(+3.4, -2.1)	298	PLP-LIF	Ghosh <i>et al.</i> (2010)
8.8 ± 1.25	298	-	IUPAC recommendation
$2.7 \times 10^{-12} \times e^{(350/T)}$	-	-	<b>our recommendation</b>

Table 4.5: Chronological measurements of rates of reaction of ISOPOO with NO.

only isomers with OH on carbon 1. Their value,  $8.1(+3.4, -2.1) \times 10^{-12}$  cm<sup>3</sup> molec<sup>-1</sup> s<sup>-1</sup>, is indistinguishable from the other studies. Miller *et al.* (2004) found  $k_{NO}$  for a large variety of simple alkenes, and all rate constants were within error of  $k_{NO}$  of isoprene, suggesting that small changes in the structure of the peroxy radical do not significantly affect  $k_{NO}$ . Thus, for all isomers of isoprene hydroxy peroxy radicals, we recommend the standard RO<sub>2</sub>+NO temperature dependent rate coefficient of  $k = 2.7 \times 10^{-12} \times \exp(350/T)$  cm<sup>3</sup> molec<sup>-1</sup> s<sup>-1</sup>.

*Mechanism (Figures 4.3-4.5; Tables 4.6 and 4.7)* - The reaction of ISOPOO with NO leads to the formation of organic nitrates (IHN) and alkoxy radicals (ISOPO).

*Mechanism - isoprene hydroxy nitrate (IHN) formation (Figures 4.3 and 4.4; Table 4.6)* - Formation of IHN represents a radical chain-terminating step and, therefore, acts as a significant local sink for both HO<sub>x</sub> and NO<sub>x</sub> (Ito *et al.*, 2007; Paulot *et al.*, 2012; Wu *et al.*, 2007). Laboratory estimates of the room temperature yield of IHN,  $Y_{IHN}$  vary from 0.04 (Chen *et al.*, 1998) to 0.15 (Chuong and Stevens, 2002). Table 4.6 lists laboratory studies and their methodology. Currently, the extent to which individual ISOPOO isomers have different branching ratios to form IHN is poorly constrained. Studies on saturated and monoalkenes show conflicting results (Arey *et al.*, 2001; Cassanelli *et al.*, 2007; Espada *et al.*, 2005; Teng *et al.*, 2015). Teng *et al.* (2017), however, suggest that the difference in yields between the  $\beta$  and  $\delta$  isomers is less than  $\pm 20\%$ . Paulot *et al.* (2009a) had suggested much larger differences based on the ratio of delta IHN to HC<sub>5</sub>. As discussed above, we now know that the HC<sub>5</sub> yield is much lower than assumed by Paulot *et al.* (2009a).

Recent results from Caltech suggest a branching fraction for hydroxynitrate for-

$\alpha$	T (K)	P (Torr)	technique	citation
$\sim 0.08-0.14$	298	740	chamber, FT-IR	Tuazon and Atkinson (1990)
$0.044 (\pm 0.008)$	298	743	chamber, GC-Pyrolysis-NO <sub>2</sub> detection	Chen <i>et al.</i> (1998)
$0.12 (\pm 0.07)$	297	750	flowtube, FT-IR	Sprengnether <i>et al.</i> (2002)
$0.08 (\pm 0.06)$	297	445	flowtube, FT-IR	Sprengnether <i>et al.</i> (2002)
$0.15 (\pm 0.10)$	300	150	flowtube, LIF-OH radical cycling	Chuong and Stevens (2002)
0.086	298	$\sim 760$	Structure Activity Relationship	Giacopelli <i>et al.</i> (2005)
0.07	298	100	flowtube, PTRMS/CIMS	Patchen <i>et al.</i> (2007)
$0.117 (\pm 0.03)$	296.5	$\sim 750$	chamber, CIMS and modeling	Paulot <i>et al.</i> (2009a)
$0.07 (+0.025/-0.015)$	295	$\sim 760$	chamber, GC-ECD with standards	Lockwood <i>et al.</i> (2010)
$0.1 (\pm 0.05)$	298	760	-	IUPAC recommendation
$0.09 (+0.04/-0.03)$	$\sim 297$	$\sim 760$	chamber, I <sup>-</sup> CIMS	Xiong <i>et al.</i> (2015)
$0.13 (\pm 0.02)$	297	745	chamber, CF <sub>3</sub> O <sup>-</sup> CIMS	Teng <i>et al.</i> (2017)
<b>0.13</b>	<b>297</b>	<b>745</b>	-	<b>our recommendation<sup>a</sup></b>

Table 4.6: Chronological estimates for  $\alpha$  of ISOPOO + NO to form IHN at 298 K and 1 atm (unless otherwise noted). <sup>a</sup>bulk yield at 297 K and 745 torr; for isomer-specific yields and T/P dependence, see Sections 4.3.3.1 and 4.2, respectively.

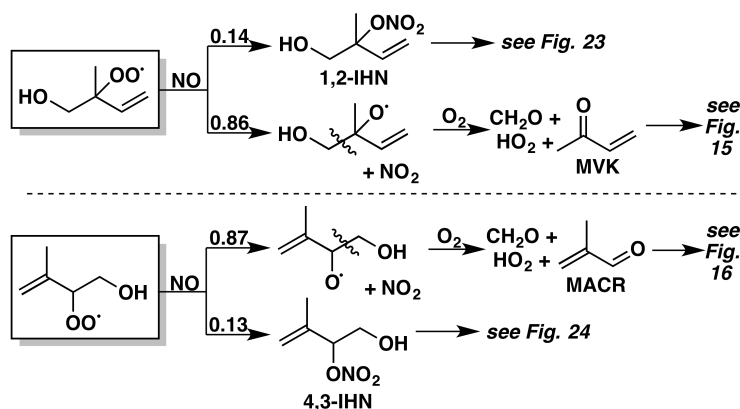


Figure 4.3: Reactions of the  $\beta$ -isoprene-OH-OO isomers with NO. Yields are for 298 K and 1 atm; the relative contributions of the nitrate and alkoxy pathways vary with both temperature and pressure.

mation of 0.13 at 297K, nearly independent of peroxy radical isomer (Teng *et al.*, 2017). Teng *et al.* (2017) note, however, that the ratio of 1-OH,2-ONO<sub>2</sub>-IHN to 4-OH,3-ONO<sub>2</sub>-IHN exceeded that of 1-OH,2-OOH-ISOPROOH to 4-OH,3-OOH-ISOPROOH by  $\sim 10\%$ , and that nitrate yields from  $\delta$ -ISOPROOH may be slightly lower than those from the  $\beta$ -ISOPROOH. Based on these findings, we recommend yields of 14%, 13%, and 12% for 1,2-IHN, 4,3-IHN, and the  $\delta$ -IHNs, respectively, at 297 K.

We recognize that our recommended IHN yield is at the high end of the laboratory studies (Table 4.6). As discussed by Xiong *et al.* (2015), the relatively low yield determinations made at Purdue before 2015 (Chen *et al.*, 1998; Lockwood *et al.*, 2010) were likely impacted by significant heterogeneous losses of the most abundant nitrate, the 1,2  $\beta$  isomer (Teng *et al.*, 2017). Lower yields were also reported by Sprengnether *et al.* (2002) (0.08) and Patchen *et al.* (2007) (0.07), but these were obtained at lower pressure (590 and 133 hPa, respectively). The yield reported by Xiong *et al.* (2015) (0.09 +0.04/-0.03) based on I<sup>-</sup> CIMS measurements is also somewhat lower. As discussed by Xiong *et al.* (2015), however, this yield estimate is sensitive to assumptions about the distribution of the IHN isomers and their rate of subsequent loss *via* OH chemistry. To estimate the isomer distribution, Xiong *et al.* (2015) used a model developed from the theoretical calculations of (Peeters *et al.*, 2014). Using the measured IHN distribution from Teng *et al.* (2017) for the conditions of the Purdue study, we calculate an updated yield for the Xiong *et al.* (2015) experiments of 0.115. Additionally, the recently measured rate constant for the reaction of OH with 1,2 IHN Xiong *et al.* (2015) is 50% faster than assumed (Teng *et al.*, 2017) – also leading to an underestimate of the reported yield in this

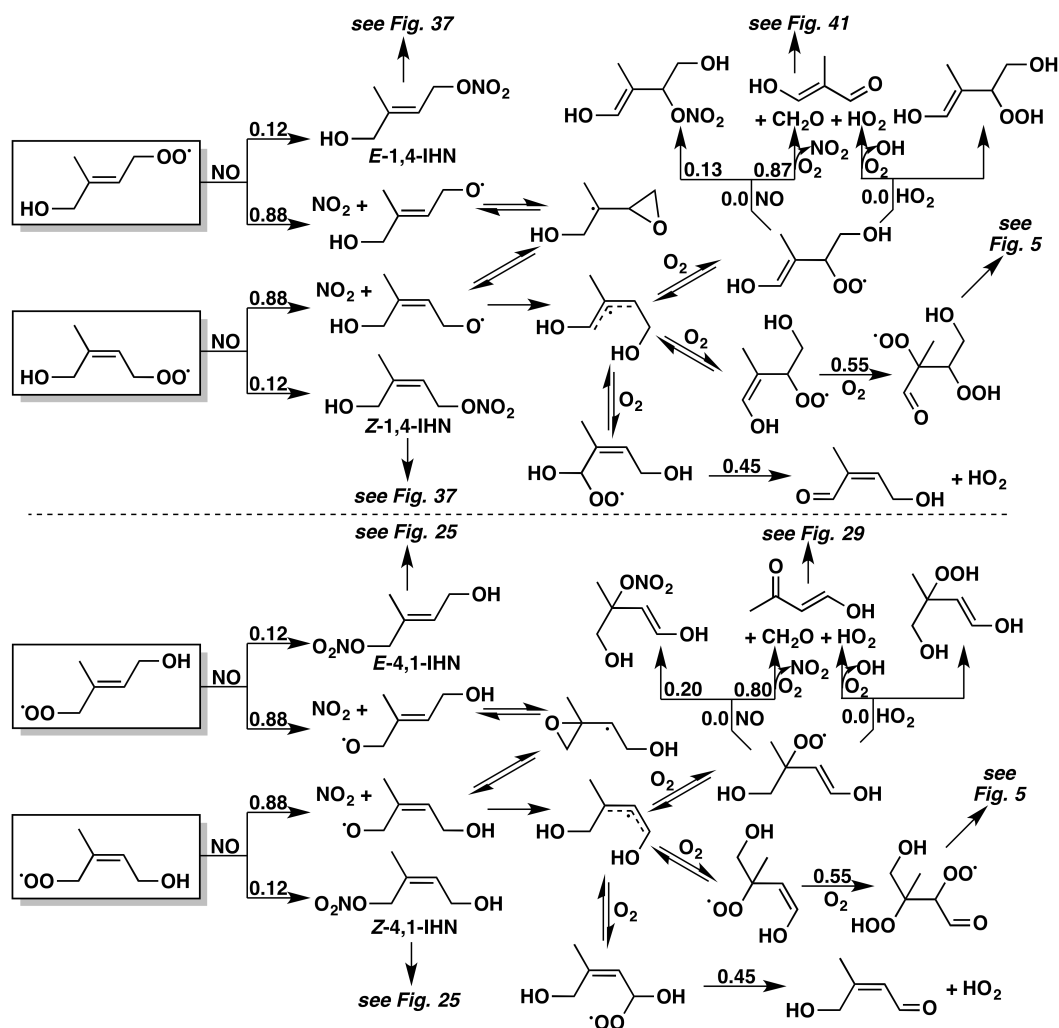


Figure 4.4: Reactions of the  $\delta$ -isoprene-OH-OO isomers with NO. Yields are for 298 K and 1 atm; the relative contributions of the nitrate and alkoxy pathways vary with both temperature and pressure. For the reduced mechanism, we ignore the  $Z$ - $\delta$  isomers.

study. We conclude that there is more consensus on the yield of IHN than the diversity of results listed in Table 4.6 would imply.

Finally, we recommend a temperature and pressure dependence of the isomer-specific IHN yields based on studies of Carter and Atkinson (1989) and Teng *et al.* (2017). Crouse *et al.* (2011) find that the temperature dependent parameterization is consistent with the change in the hydroxy nitrate yield with temperature. Error in the yield is estimated to be  $\pm 20\%$ .

*Mechanism - decomposition of ISOPO (Figures 4.3-4.5; Table 4.7)* - Methyl vinyl ketone (MVK), methacrolein (MACR), (and, following reaction with O<sub>2</sub>, formaldehyde (CH<sub>2</sub>O) and HO<sub>2</sub>) are believed to be the sole fate of the  $\beta$ -ISOPO radicals produced from the reaction of NO with the  $\beta$  ISOPOO (Figure 4.3). The -OH group  $\beta$  to the nascent alkoxy group lowers the barrier to decomposition substantially. In the structure activity relationship, Peeters *et al.* (2004) predict that the -OH group lowers the barrier to decomposition by a full 8 kcal mol<sup>-1</sup>, making decomposition much more favorable relative to the competing reaction with O<sub>2</sub> (Aschmann *et al.*, 2000; Dibble, 2001; Orlando *et al.*, 1998; Peeters *et al.*, 2004; Vereecken and Peeters, 1999). As detailed in Table 4.7) Yields determined experimentally under NO dominated conditions range from 30-45% for MVK and 20-30% for MACR. In the presence of oxygen, formaldehyde is produced in a yield equal to the combined yield of MVK and MACR (Miyoshi *et al.*, 1994; Sprengnether *et al.*, 2002; Tuazon and Atkinson, 1990).

Because the fraction of ISOPOO that are  $\beta$  isomers varies with peroxy radical lifetime, the yield of MVK and MACR from isoprene oxidation is not fixed. As shown in Table 4.7, the NO concentrations in many of the chamber experiments (except for those of Karl *et al.* (2006) and Liu *et al.* (2013)) are much higher than those typically found in the troposphere. As discussed in Section 4.3.2, in the atmosphere the ISOPOO isomer distribution favors the thermodynamically more stable  $\beta$ -substituted isomers. Since these isomers (that lead to MVK and MACR) are typically present at a lower fraction in chamber experiments than in the atmosphere, these experiments systematically underpredict MACR and, especially, MVK yields in the atmosphere. Liu *et al.* (2013) and Karl *et al.* (2006), who used NO concentrations comparable to the urban troposphere ( $2 \times 10^{10}$  and  $5 \times 10^9$  molec cm<sup>-3</sup>, respectively), found MVK and MACR yields higher than many other studies that employed higher NO concentrations (Table 4.7). The estimated MACR yield by

MVK yield	MACR yield	[NO] (molec cm <sup>-3</sup> )	citation
33 ± 7 <sup>a</sup>	24 ± 5 <sup>a</sup>	1.9 – 3.8 × 10 <sup>14</sup>	Tuazon and Atkinson (1990)
35.5 ± 4	25 ± 3	1.4 – 2.4 × 10 <sup>14</sup>	Paulson and Seinfeld (1992)
32 ± 5	22 ± 2	2 × 10 <sup>14</sup>	Miyoshi <i>et al.</i> (1994)
31 ± 3	20 ± 2	1.5 – 15 × 10 <sup>13</sup>	Ruppert and Heinz Becker (2000)
44 ± 6	28 ± 4	7.8 × 10 <sup>14</sup>	Sprengnether <i>et al.</i> (2002)
41 ± 3	27 ± 3 <sup>b</sup>	5 × 10 <sup>9</sup>	Karl <i>et al.</i> (2006)
30.4 ± 1.3	22.01 ± 0.62	6 – 12 × 10 <sup>12</sup>	Galloway <i>et al.</i> (2011)
44.5 ± 5.5 <sup>c</sup>	31.8 ± 4.2 <sup>c</sup>	2 × 10 <sup>10</sup>	Liu <i>et al.</i> (2013)
<b>40</b>	<b>23</b>	-	<b>our recommendation<sup>d</sup></b>

Table 4.7: MVK and MACR yields (%) from isoprene *via* RO<sub>2</sub> + NO. <sup>a</sup>corrected for O<sup>3</sup>P reaction as communicated to Paulson and Seinfeld (1992). <sup>b</sup>Karl *et al.* (2006) did not account for isomerization; at [NO] ≈ 0.2 ppb (RO<sub>2</sub> lifetime 25 s), isomerization would account for ~10% of peroxy radical reactivity, which would imply a corrected yield of MACR from NO + RO<sub>2</sub> of 35%. <sup>c</sup>assumes that 93% of the peroxy radicals react with NO (Liu *et al.*, 2013). <sup>d</sup>at the kinetic limit RO<sub>2</sub> distribution, as in Table 4.3.

Karl *et al.* (2006) is likely a lower limit as they were unaware that a significant fraction of the hydroxy peroxy radicals from the 4-OH system were undergoing 1,6 H-shift isomerization. In addition, subsequent studies have illustrated that MVK and MACR measurements can often be impacted by analytical challenges when ISOPOOH is present (Rivera-Rios *et al.*, 2014). Here, for the β-ISOPOO + NO reactions, we take the yield of MACR/MVK to be (1-*Y*<sub>IHN</sub>).

1,4- and 4,1-δ ISOPOO react with NO to form δ-ISOPO radicals (Figure 4.4). The *Z*-δ-ISOPO radicals will undergo 1,5 hydrogen shift (Dibble, 2002). This isomerization is faster than that of simple alkanes due activation of the H-shift hydrogen by the –OH group (Atkinson, 2007; Orlando *et al.*, 2003b). While the *E* 4-1 ISOPO cannot undergo such chemistry due to the lack of an abstractable hydrogen, Peeters and Nguyen (2012) calculate that rapid isomerization between the *E* and *Z* isomers *via* an epoxide intermediate results in both alkoxy radicals exiting *via* 1,5 H-shift from the *Z* isomer. Indeed, they calculate that similar epoxide-isomerization and the much faster 1,5 H-shift from the hydrogen α to the OH group vis-a-vis H-shift from the methyl group leads to both 1,4 isomers following similar chemistry. Here, we follow this recommendation.

Following the 1,5 H-shift, O<sub>2</sub> adds to the allylic radical either β or γ to C1 (C4). Addition β yields two 5-carbon hydroxy carbonyl species (HC<sub>5</sub>). Teng *et al.* (2017) determine the yield to be 45 ± 10% in both the 1-OH and 4-OH systems

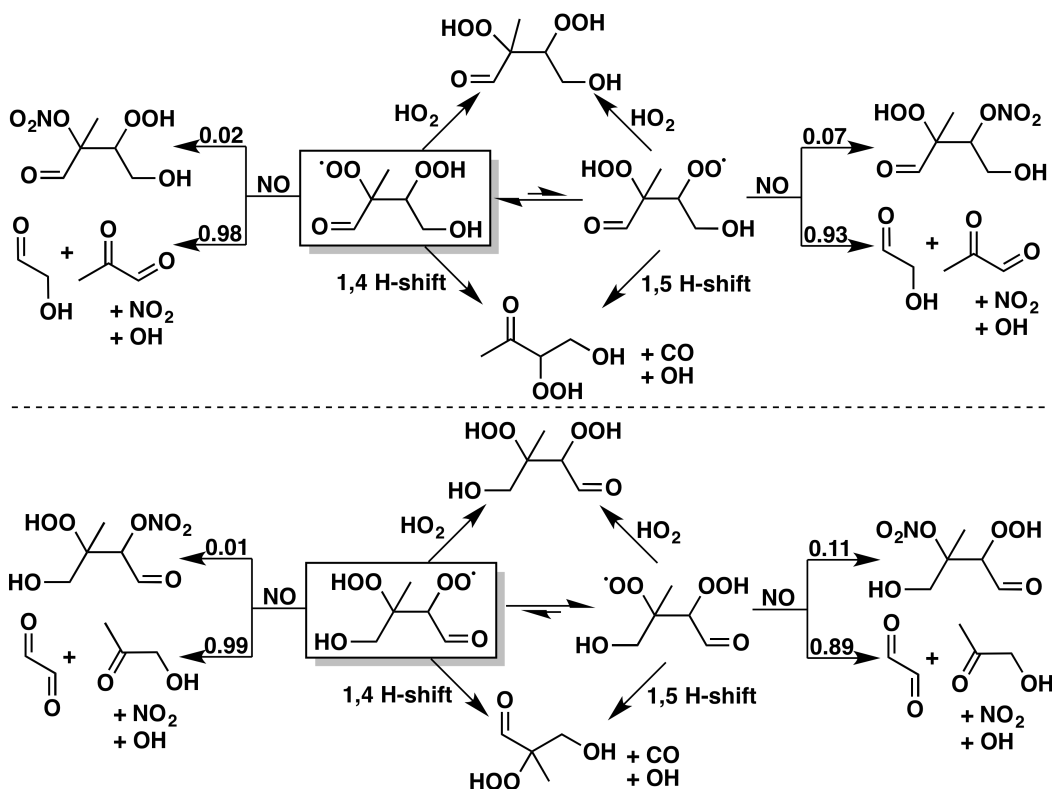


Figure 4.5: Reactions of the isoprene-CO-OH-OOH-OO isomers produced by  $\delta$ -isoprene-OH-OO + NO. Yields are for 298 K and 1 atm; the relative contributions of the nitrate and alkoxy pathways vary with both temperature and pressure. For the reduced mechanism, we assume that the 1,5 and 1,6 H-shift from the aldehyde outcompetes all bimolecular chemistry.

suggesting that approximately 55% undergoes  $O_2$  addition  $\gamma$  leading to formation of a ketene peroxy radical. The subsequent fate of these peroxy radicals is unknown, but based on studies by Galloway *et al.* (2011), Sprengnether *et al.* (2002) and Paulot *et al.* (2009a), we suggest that the products are likely hydroxyacetone, glyoxal, and glycoaldehyde (Figures 4.4 and 4.5).

#### 4.3.3.2 Reaction of ISOPOOH with $HO_2$

ISOPOOH has long been considered the likely product of isoprene  $RO_2 + HO_2$  reactions (Atkinson, 1997; Jenkin *et al.*, 1998; Madronich and Calvert, 1990). The first reported field measurements of ISOPOOH were over the Amazon basin in Suriname in 1998 (Crutzen *et al.*, 2000; Warneke *et al.*, 2001; Williams *et al.*, 2001) and over savannahs in Venezuela in 1999-2000 (Holzinger *et al.*, 2002) by proton transfer mass spectrometry, though recent laboratory investigations of PTR ion chemistry

with synthetic standards suggests that the  $m/z$  101 signal identified as ISOPOOH may instead be isoprene dihydroxy epoxides (IEPOX). Shortly thereafter, as its importance in the tropospheric chemistry of low-NO high-isoprene regions became clear, ISOPOOH began to receive attention in computational studies (Vereecken *et al.*, 2004), atmospheric chemical models (Kuhlmann *et al.*, 2004; Pfister *et al.*, 2008), and chamber studies (Paulot *et al.*, 2009b), where chemical ionization mass spectrometry (CIMS) demonstrated successful measurement of ISOPOOH (Paulot *et al.*, 2009b; St. Clair *et al.*, 2015).

*Kinetics* - The rate constant for the reaction of  $\text{HO}_2 + \text{RO}_2$  for the isoprene hydroxy peroxy radical has been measured only once, with  $k = 1.74 \pm 0.25 \times 10^{-11} \text{ cm}^3 \text{ molec}^{-1} \text{ s}^{-1}$  at 298 K (Boyd *et al.*, 2003). Most chemical mechanisms implement the parameterized recommendation of MCM (Equation 4.5), which varies with the number of carbons in the molecule (Jenkin *et al.*, 1997; Saunders *et al.*, 2003); for isoprene hydroxy peroxy +  $\text{HO}_2$ , this gives  $k = 2.06 \times 10^{-13} \times e^{(1300/T)}$  or  $k = 1.61 \times 10^{-11} \text{ cm}^3 \text{ molec}^{-1} \text{ s}^{-1}$  at 298 K. Using our alternate parameterization (Equation 4.6), which depends instead on the number of heavy atoms in the molecule (excluding the peroxy moiety), gives an improved fit and a value of  $k = 1.66 \times 10^{-11} \text{ cm}^3 \text{ molec}^{-1} \text{ s}^{-1}$  for isoprene hydroxy peroxy +  $\text{HO}_2$  at 298 K. To match the measured rate coefficient of (Boyd *et al.*, 2003), We scale our standard recommendation:

$$k = 2.12 \times 10^{-13} \times e^{(1300/T)} \text{ cm}^3 \text{ molec}^{-1} \text{ s}^{-1}$$

with an uncertainty of  $\pm 20\%$  from the experimental rate. Further measurements of this rate would be welcome.

*Mechanism* - (Figure 4.6; Table 4.8) - The main product of the reaction is the unsaturated hydroxy hydroperoxide, ISOPOOH, in yields estimated to be  $88 \pm 12\%$  (Paulot *et al.*, 2009b) or  $93.7 \pm 2.1\%$  (Liu *et al.*, 2013). Six possible isomers of ISOPOOH can be formed from this series of reactions, as shown in Figure 4.6, with their relative abundances determined by the distribution of their precursor  $\text{RO}_2$ . Under most atmospherically relevant conditions, the two  $\beta$  isomers – (1,2)- and (4,3)-ISOPOOH – comprise the majority ( $\sim 95\%$ ) of the total, with only  $\sim 5\%$  in the  $E \delta$  isomers (4,1) and (1,4). MVK and MACR have been suggested as minor products from isoprene  $\text{RO}_2 + \text{HO}_2$  for the (1,2)- $\text{RO}_2$  and (4,3)- $\text{RO}_2$ , respectively (Liu *et al.*, 2013; Paulot *et al.*, 2009b) (Dillon and Crowley, 2008; Hasson *et al.*, 2005). The 93.7% ISOPOOH yield was determined as (1-MVK-MACR) (Liu *et al.*, 2013). Liu *et al.* (2013) determined the yields of MVK ( $3.8 \pm 1.3\%$ ) and MACR

products	% yields			
	Liu <i>et al.</i> (2013) <sup>a</sup>		our recommendations	
	ISOPOO	1,2-ISOPOO	4,3-ISOPOO	$\delta$ -ISOPOO
ISOPOOH	93.7 $\pm$ 2.1	93.7	93.7	100
MVK + OH + HO <sub>2</sub> + CH <sub>2</sub> O	3.8 $\pm$ 1.3	6.3	0	0
MACR + OH + HO <sub>2</sub> + CH <sub>2</sub> O	2.5 $\pm$ 0.9	0	6.3	0

Table 4.8: Products of isoprene hydroxy peroxy RO<sub>2</sub> + HO<sub>2</sub>. <sup>a</sup>at RO<sub>2</sub> lifetime of  $\sim$ 4 s ([HO<sub>2</sub> = 1000 ppt]). MVK and MACR yields may be lower to the extent that the laboratory results may have been impacted by RO<sub>2</sub> + RO<sub>2</sub> chemistry.

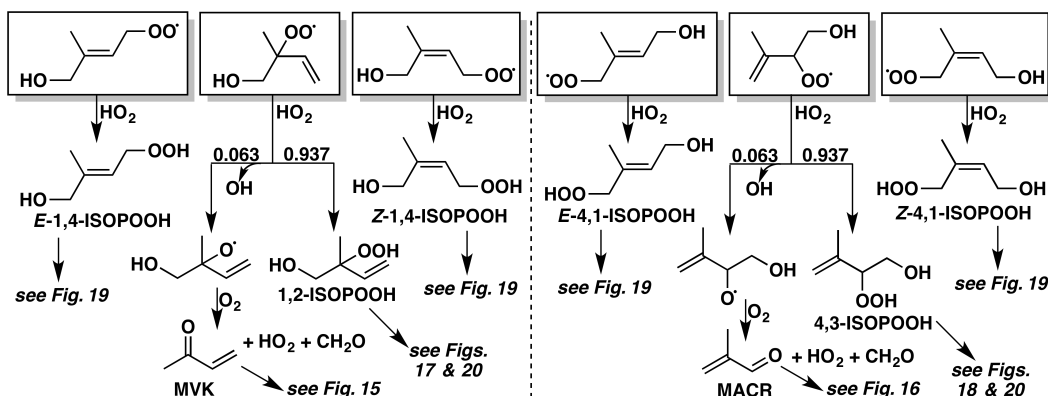


Figure 4.6: Reactions of the isoprene-OH-OO isomers with HO<sub>2</sub>. For the reduced mechanism, we ignore the *Z*- $\delta$  isomers, as they contribute less than 1% of the bimolecular chemistry for atmospheric conditions.

(2.5  $\pm$  0.9%) separately at RO<sub>2</sub> lifetime of  $\sim$ 4s (*e.g.* [HO<sub>2</sub>] = 1000 ppt). At this lifetime, Teng *et al.* (2017) find that the  $\sim$ 93% of the RO<sub>2</sub> are  $\beta$ -isomers. This result suggests that the MACR yield from 4,3-ISOPOO is slightly higher than MVK yield from 1,2-ISOPOO. This seems unlikely and suggests, perhaps, that some fraction of the MVK and MACR observed in the study may have been produced *via* RO<sub>2</sub> + RO<sub>2</sub>. Here, we recommend 1,2-ISOPOO + HO<sub>2</sub>  $\rightarrow$  MVK + OH + HO<sub>2</sub> + CH<sub>2</sub>O with a yield of 6.3% and, equivalently, 4,3-ISOPOO + HO<sub>2</sub>  $\rightarrow$  MACR + OH + HO<sub>2</sub> + CH<sub>2</sub>O with the same yield, 6.3%. The balance yields ISOPOOH.

#### 4.3.3.3 Reaction of ISOPOO with RO<sub>2</sub>

Peroxy radical self- and cross-reactions are important in low-NO<sub>x</sub> environments. A large body of work exists for the kinetics of prototypical organic peroxy radicals; these reactions have been the subject of several review papers (Kirchner and Stockwell, 1996; Lightfoot *et al.*, 1992; Orlando and Tyndall, 2012; Tyndall *et al.*, 2001;

Wallington *et al.*, 1992).

*Kinetics (Tables 4.9 and 4.10)* - Very few direct experimental measurements have been completed on the self- and cross-reactions for ISOPRO. Overall rate constants, as well as the accessible product channels, vary widely with the type of peroxy radical involved. The cocktail of ISOPRO formed during OH-initiated oxidation of isoprene makes deconvolution of the individual isomer-specific rates and branching ratios complex. Jenkin and Hayman (1995) used a structure-activity relationship (SAR) method to infer the self- and cross-reaction rates and branching fractions for ISOPRO radicals. The SAR results were improved later with OH-initiated oxidation experiments on 1,3-butadiene and 2,3-dimethyl-1,3-butadiene, which differ from isoprene only by the presence or absence of a methyl group on the carbon backbone, conducted at high radical concentrations ( $2.0\text{-}6.8 \times 10^{13}$  molec  $\text{cm}^{-3}$  of OH) in a small ( $\sim 175$   $\text{cm}^3$ ) quartz reaction cell (Jenkin *et al.*, 1998). The resulting experimental rate constants are much faster than those proposed with SAR arguments using smaller peroxy radicals, but appear to adequately describe the kinetics observed in isoprene oxidation experiments. MCM combines all peroxy radical rate constants into one value for each isomer by using a rate constant which is twice the geometric mean of the self-reaction rate constant for that isomer and the methyl peroxy self-reaction.

The overall reaction rate constants for all isomers are based on their structure (primary > secondary > tertiary peroxy radicals) and functionality ( $\beta$ -hydroxy peroxy radicals are significantly activated; allylic peroxy radicals are slightly activated). Here, we consider only the reactions of the two  $\beta$  peroxy radicals, as they comprise the large majority of the  $\text{RO}_2$  radical pool from isoprene. Table 4.9 compares the self-reaction rate constants inferred from SAR arguments for smaller peroxy radicals (Jenkin and Hayman, 1995) with those derived from 1,3-butadiene and 2,3-dimethyl-1,3-butadiene (Jenkin *et al.*, 1998) as well as our recommended rate constants. With the exception of the  $\beta$  4-OH 3-OO isomer, that we believe is mistakenly associated with a peroxy radical that is not allylic, our recommendations match those of MCM v3.3.1.

*Mechanism (Tables 4.10 and 4.11)* - Peroxy radicals ( $\text{RO}_2$ ) react *via* three channels:



isomer	Jenkin and Hayman (1995)	Jenkin <i>et al.</i> (1998)	our recommendations
$\beta$ 1-OH,2-OO	1.65	$6.92 \pm 1.38$	6.92
$\beta$ 4-OH,3-OO	139	$574 \pm 57$	574

Table 4.9: Self-reaction rate constants ( $\times 10^{-14}$  cm<sup>3</sup> molec<sup>-1</sup> s<sup>-1</sup>) for the two  $\beta$  isomers of isoprene hydroxy peroxy radicals.



The branching between these channels controls the contributions of each reaction to the formation of additional radical species, or in some cases low-volatility products. The alkoxy radicals (RO) formed in R1a undergo further reactions described in the "decomposition of ISOPO" subsection of Section 4.3.3.1, propagating the radical chain. R1b is a chain-terminating reaction that forms alcohol and aldehyde products through a hydrogen-bonded transition state involving a hydrogen atom  $\alpha$ - to the peroxy radical. This product channel does not occur for tertiary peroxy radicals. R1c has never been directly observed, but the ROOR product would likely have a low vapor pressure and would be important to the particle phase.

Similarly, the cross-reactions have been shown to undergo three channels (exclusive of the analogous ROOR channel) where R1O<sub>2</sub> and R2O<sub>2</sub> are different peroxy radicals:



Like the self-reaction, if either R1O<sub>2</sub> or R2O<sub>2</sub> are tertiary peroxy radicals, the corresponding aldehyde product channel is not accessible. Given the potential influence of R1a and R2a on radical propagation in low-NO environments, the chain branching of the self- and cross-reactions must be considered when developing an overall mechanism for ISOPOO.

In Table 4.11, we compare the findings of Jenkin and Hayman (1995) and Jenkin *et al.* (1998) for the branching fraction to form alkoxy radicals by Reaction R1a. The yield of R1c (formation of ROOR) is assumed to be zero and the branching fraction for channel R1b is the remainder of the rate constant. The tertiary peroxy radical  $\beta$  1-OH 2-OO cannot undergo reaction R1b, so the branching fraction is 1, by definition. As discussed previously, the alkoxy radicals will likely instantaneously decompose to either MVK or MACR.

The treatment of cross-reactions is complex in the case of ISOPOO. Individual

reaction	parameter	Jenkin and Hayman (1995)	Jenkin <i>et al.</i> (1998)	our recommendation
$\beta$ 1-OH,2-OO + $\beta$ 4-OH,3-OO	Rate ( $\times 10^{-14}$ cm <sup>3</sup> molec <sup>-1</sup> s <sup>-1</sup> ) Yield: MVK + MACR + 2HO <sub>2</sub> + 2CH <sub>2</sub> O Yield: ISOP3CO4OH + ISOP1OH2OH	15.1 0.875 0.125	308 0.9 0.1	308 0.9 0.1
All isomers + CH <sub>3</sub> O <sub>2</sub>	Rate ( $\times 10^{-14}$ cm <sup>3</sup> molec <sup>-1</sup> s <sup>-1</sup> )		200	200
$\beta$ 1-OH,2-OO + CH <sub>3</sub> O <sub>2</sub>	Yield: MVK + CH <sub>3</sub> O + HO <sub>2</sub> + CH <sub>2</sub> O Yield: ISOP1OH2OH + CH <sub>2</sub> O		0.5 0.5	0.5 0.5
$\beta$ 4-OH,3-OO + CH <sub>3</sub> O <sub>2</sub>	Yield: MACR + CH <sub>3</sub> O + HO <sub>2</sub> + CH <sub>2</sub> O Yield: ISOP3OH4OH + CH <sub>2</sub> O Yield: ISOP3CO4OH + CH <sub>3</sub> OH		0.5 0.25 0.25	0.5 0.25 0.25

Table 4.10: RO<sub>2</sub>-RO<sub>2</sub> cross-reaction rate constants and branching fractions. Individual rate constants and expected product branching rates are indicated for each radical pair ( $\times 10^{-14}$  cm<sup>3</sup> molec<sup>-1</sup> s<sup>-1</sup>).

isomer	Jenkin and Hayman (1995)	Jenkin <i>et al.</i> (1998)	our recommendations	products
$\beta$ 1-OH,2-OO	1	1	1	2MVK + 2HO <sub>2</sub> + 2CH <sub>2</sub> O
$\beta$ 4-OH,3-OO	0.75	0.8	0.8	2MACR + 2HO <sub>2</sub> + 2CH <sub>2</sub> O
	0.25	0.2	0.2	ISOP3CO4OH + ISOP3OH4OH

Table 4.11: Product yields from the self-reactions of the two  $\beta$  isomers of isoprene hydroxy peroxy radicals.

isomers are expected to react with any available peroxy radical, including the methyl peroxy radical. We have again presented the rate constants and branching fractions for only the  $\beta$  isomers in Table 4.10; a more detailed treatment of the cross-reactions can be found in the Supplement. In the case of primary or secondary peroxy radicals, channels R2a and R2b are assumed to make up equal portions of the remaining rate constant. We also list the rate constant for ISOPOO reactions with CH<sub>3</sub>O<sub>2</sub>, which is assumed to be the same for all isomers.

#### 4.3.3.4 H-Shift Isomerization of ISOPOO

Based on theoretical calculations, two novel HO<sub>x</sub> recycling pathways involving H-shift isomerizations of the ISOPOO radicals have been proposed (Peeters *et al.*, 2014, 2009; Silva *et al.*, 2010).

*1,6 H-shift* - Following a 1,6 H-shift to the *Z*- $\delta$  hydroxy peroxy radicals of isoprene, reaction with O<sub>2</sub> and elimination of HO<sub>2</sub> to form unsaturated hydroperoxy aldehydes (HPALDs) can occur. Peeters *et al.* (2009) suggested that these HPALD compounds photolyze rapidly to reform OH, sustaining HO<sub>x</sub>, even in the face of high levels of isoprene and low levels of NO<sub>x</sub>.

*Kinetics* - Laboratory studies by Crouse *et al.* (2011) determined that the bulk HPALD formation rate is substantially slower than predicted by Peeters *et al.* (2009), but still fast enough to have importance for atmospheric isoprene chemistry. Improved calculations of the isoprene RO<sub>2</sub> equilibrium constants (Section 4.3.2) and H-shift rates (Peeters *et al.*, 2014), along with the recognition that the HPALD yield following the 1,6 H-shift is likely not unity (Crouse *et al.*, 2011; Teng *et al.*, 2017), bring the laboratory and theoretical determinations for the individual peroxy radical isomerization rates well within their combined uncertainties.

Here, we recommend the 1,6 H-shift rates of the *Z*- $\delta$  isoprene peroxy radicals calculated by Teng *et al.* (2017). These calculations assumed 1,5 H-shift rates of  $\beta$  hydroxy peroxy radicals (see below) and tunneling temperature dependences

( $e^{1 \times 10^8/T^3}$ ) reported in Peeters *et al.* (2014).

$$k_{(1,6-H),z-1-OH-4-OO} = 5.47 \times 10^{15} \times e^{(-12200/T)} \times e^{(1 \times 10^8/T^3)} s^{-1} \quad (4.7)$$

$$k_{(1,6-H),z-4-OH-1-OO} = 2.40 \times 10^9 \times e^{(-7160/T)} \times e^{(1 \times 10^8/T^3)} s^{-1} \quad (4.8)$$

Teng *et al.* (2017) estimate that these rates are only certain within a factor of 3.5, which puts their values at ambient temperatures ( $0.36 s^{-1}$  and  $3.7 s^{-1}$ , respectively, at 297 K) well within the range of those calculated by Peeters *et al.* (2014) ( $0.49 \pm 0.32 s^{-1}$  and  $5.4 \pm 3.3 s^{-1}$ , respectively). Although the absolute rate for 1,6 H-shift to the Z- $\delta$  hydroxy peroxy radicals is highly uncertain due to large uncertainty in the fraction of ISOPOO present in this isomer, uncertainty in the bulk rate coefficient within each system (OH addition at C1 or C4) is much smaller (see Teng *et al.*, 2017) provided self-consistent application of the thermochemistry is employed.

*Mechanism (Figures 4.7 and 4.8)* - Teng *et al.* (2017) also estimated the yields of HPALDs and other products from the 1,6 H-shifts of the Z- $\delta$  isoprene peroxy radicals, and proposed a tentative mechanism for the formation of the observed products, which we modify slightly for our own recommendations. There remains considerable uncertainty in the yields of HPALDs and other products from the 1,6 H-shifts. Currently, from experimental (Crouse *et al.*, 2011; Teng *et al.*, 2017) and theoretical (Peeters *et al.*, 2014) work we recommend that the HPALD yield from each 1,6 H-shift channel is 0.33. We arrive at this estimate by combining the measurement of HPALD with an additional isomerization product identified by Teng *et al.* (2017) with the same mass. The balance of the isomerization products remain uncertain. (Crouse *et al.*, 2011; Teng *et al.*, 2017) observed approximately half of the non-HPALD products produced *via* the 1,6 H-shift chemistry at masses consistent with products of hydroperoxy acetone and hydroperoxy ethanal. Here, we recommend that these products are formed *via* bimolecular chemistry and accompanied by HO<sub>x</sub> recycling. The remainder of the carbon is routed to the C<sub>4</sub> dihydroperoxy carbonyls (3-OOH,4-OOH MVK and 2-OOH,3-OOH MACR) proposed by Peeters *et al.* (2014). These products may be rapidly lost to walls of chambers or tubing, and/or too fragile to detect at specific product masses with the CF<sub>3</sub>O<sup>-</sup> ion chemistry used in the Teng *et al.* (2017) study. In the atmosphere, they may undergo rapid photolysis (Peeters *et al.*, 2014; Praske *et al.*, 2015), leading to further HO<sub>x</sub> regeneration. Other experimental evidence for HO<sub>x</sub> recycling (Fuchs *et al.*, 2013) and HPALD formation (Berndt, 2012; Crouse *et al.*, 2011) is consis-

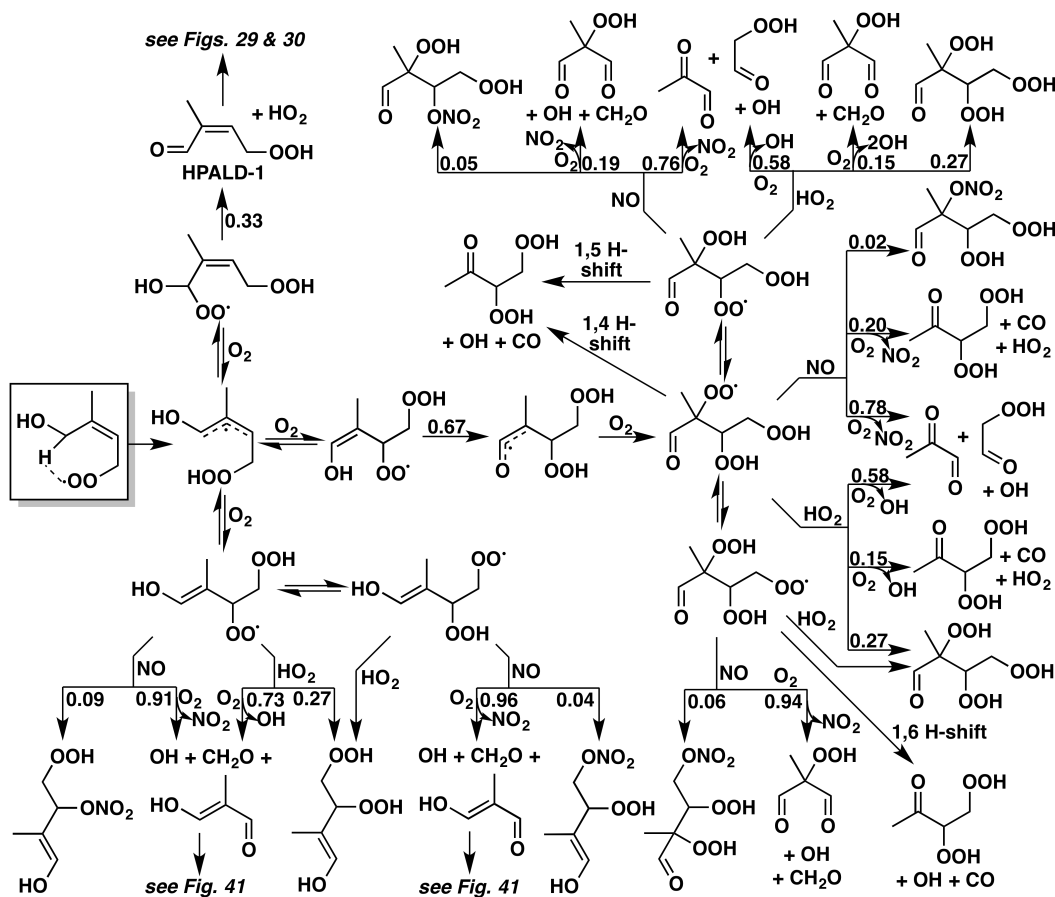


Figure 4.7: Reactions and products following the 1,6 H-shift of the Z-1-OO,4-OH-isoprene-hydroxy-peroxy radical. Yields are for 298 K and 1 atm; in reactions of peroxy radicals with NO, the relative contributions of the nitrate and alkoxy pathways vary with both temperature and pressure. Although we show the possible bimolecular reactions of the *E*-enol peroxy radicals (lower left) for completeness, we assume the initial addition and removal of oxygen occurs quickly enough to route all the non-HPALD products *via* the Z-enol peroxy radical (center). For the reduced mechanism, we represent the pool of hydroperoxy-peroxy radicals as a single species, and we assume the C<sub>4</sub> dihydroperoxycarbonyl compounds decompose immediately to form 2×OH + methylglyoxal + CH<sub>2</sub>O.

tent with the determinations of Teng *et al.* (2017), though they do not reduce the uncertainty in the isomerization rates or product yields.

*1,5-H-shift* (Figure 4.9) - The 1,5-H-shift of the O-H hydrogen in the major  $\beta$  hydroxy peroxy radicals has been calculated by several groups (Peeters *et al.*, 2014, 2009; Silva *et al.*, 2010) to have only minor importance in the atmospheric oxidation of isoprene. The products include MVK, MACR, HCHO, and OH. Here, we use the



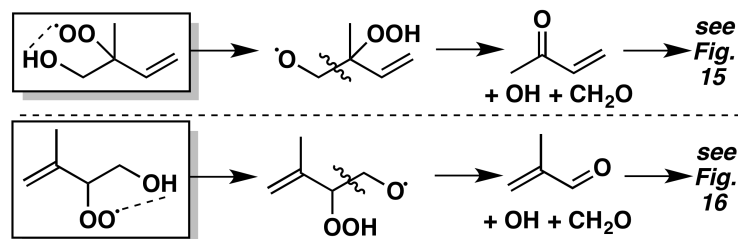


Figure 4.9: Reactions and products following the 1,5 H-shift of the  $\beta$ -isoprene-OH-OO isomers.

rates coefficients reported in Peeters *et al.* (2014), consistent with the experimental constraints of Crouse *et al.* (2011):

$$k_{(1,5-H),1-OH-2-OO} = 1.04 \times 10^{-11} \times e^{(-9746/T)} \text{ s}^{-1}$$

$$k_{(1,5-H),4-OH-3-OO} = 1.88 \times 10^{-11} \times e^{(-9752/T)} \text{ s}^{-1}$$

#### 4.4 isoprene + O<sub>3</sub>

Although reaction with OH constitutes the dominant isoprene loss process, reaction with ozone is estimated to account for approximately 10% of isoprene removal in the atmosphere (Atkinson *et al.*, 2006; Isidorov, 1990). Through a complex series of reactions and intermediates, ozonolysis of isoprene provides a source of OH radicals, organic peroxy radicals, and secondary organic aerosols (SOA) precursors to the atmosphere (*e.g.*, Biesenthal *et al.*, 1998; Kamens *et al.*, 1982; Nguyen *et al.*, 2010). In isoprene-rich regions, ozonolysis of isoprene can also represent an important ozone loss mechanism (Fiore *et al.*, 2005).

*Kinetics (Table 4.12)* - A number of studies have reported the rate coefficients for the reaction of ozone with isoprene. Most (Table 4.12) utilized environmental chambers and included addition of compounds such as cyclohexane, *n*-octane or carbon monoxide to remove the OH generated from ozonolysis. The measured reaction rate constants are generally in good agreement. Adeniji *et al.* (1981) reported an abnormally high value, likely because they did not use any OH scavenger (Klawatsch-Carrasco *et al.*, 2004). The causes of other smaller discrepancies are unclear. The IUPAC preferred value of  $k_{isop+O_3} = 1.1 \times 10^{-14} \times e^{-2000/T} \text{ cm}^3 \text{ molec}^{-1} \text{ s}^{-1}$  is adopted here.

*Mechanism (Figure 4.10)* - The mechanism of isoprene ozonolysis has also been the subject of numerous investigations, with more widely varying results. Here, we outline a reaction scheme developed from that compiled in Nguyen *et al.* (2016).

methodology	T (K)	rate constant ( $\times 10^{-17}$ $\text{cm}^3 \text{ molec}^{-1} \text{ s}^{-1}$ )	citation
chamber, excess reactant, no scavenger	295 $\pm$ 1	1.27	Arnts and Jr (1979)
chamber, excess reactant, no scavenger	294 $\pm$ 2	1.65	Adeniji <i>et al.</i> (1981)
chamber, excess reactant, no scavenger	296 $\pm$ 2	1.17 $\pm$ 0.19	Atkinson <i>et al.</i> (1982)
outdoor chamber, no scavenger	291	1.1	Kamens <i>et al.</i> (1982)
relative rate technique, n-octane scavenger	296 $\pm$ 2	1.16 $\pm$ 0.02	Greene and Atkinson (1992)
chamber, excess reactant, no scavenger	298	1.28 $\pm$ 0.12	Treacy <i>et al.</i> (1992)
chamber, cyclohexane scavenger	293 $\pm$ 2	0.895 $\pm$ 0.025	Grosjean <i>et al.</i> (1993b)
chamber, cyclohexane scavenger	291 $\pm$ 2	1.13 $\pm$ 0.32	Grosjean and Grosjean (1996)
relative rate technique, He diluent gas	298	1.3 $\pm$ 0.08	Khamaganov and Hites (2001)
theoretical study	300	1.58	Zhang and Zhang (2002)
relative rate technique, trimethylbenzene scavenger	298	1.22 $\pm$ 0.03	Avzianova and Ariya (2002)
chamber, CO scavenger	293 $\pm$ 2 K	1.19 $\pm$ 0.09	Klawatsch-Carrasco <i>et al.</i> (2004)
chamber, no scavenger	286 K	0.96 $\pm$ 0.07	Karl <i>et al.</i> (2004)
<b>IUPAC / our recommendation</b>	<b>240-360</b>	$1030 \times e^{(-1995/T)}$	<b>Atkinson <i>et al.</i> (2006)</b>

Table 4.12: Chronological estimates of isoprene + O<sub>3</sub> reaction rate constants.

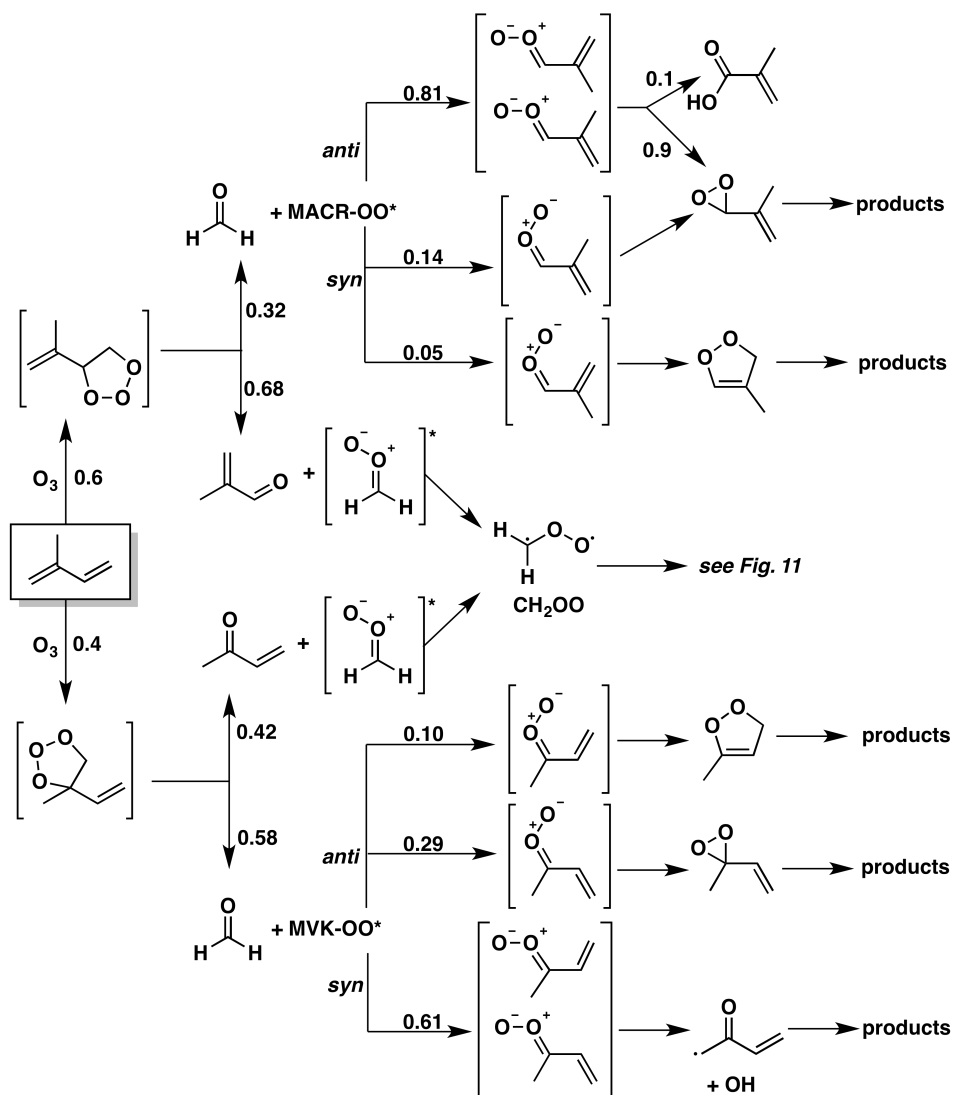


Figure 4.10: Reactions and products following the ozonolysis of isoprene. Many of the Criegee decomposition products remain unidentified; we therefore generally assume that they decompose to small, stable products. Our full and reduced recommended mechanisms can be found in the supplemental tables. For a more detailed treatment of the complete ozonolysis mechanism, see Nguyen *et al.* (2016).

Because of their uncertainty and minor yields, a number of C<sub>3</sub>-C<sub>4</sub> stable products of the C<sub>4</sub> Criegee intermediates are not treated discretely here; instead, to ensure mass balance, they are assumed to decompose to smaller products.

The generally accepted first step of ozonolysis involves the cycloaddition of ozone at either double bond in isoprene to form one of two possible primary ozonides (POZ) (*e.g.*, Zhang and Zhang, 2002). In our mechanism, we use the POZ branching ratio from Aschmann and Atkinson (1994), which suggests that the electron donating

effects of the methyl group are outweighed by its steric hindrance, leading to a 60% yield of the 3,4-addition POZ and a 40% yield of the 1,2-addition POZ.

Decomposition of the POZ yields MACR or formaldehyde in the major branch and MVK or formaldehyde for 1,2-addition. Both branches also yield a highly reactive C<sub>1</sub> or C<sub>4</sub> carbonyl oxide, also known as the activated Criegee intermediate (CI\*, where the asterisk denotes the unstable, activated state) (Criegee, 1975; Criegee and Wenner, 1949).

The zwitterionic C<sub>4</sub> CI\* has a number of distinct conformations – four each for MVK-OO\* and MACR-OO\*, either *syn* or *anti* to their methyl or vinyl groups – for which the barriers to interconversion are expected to be large (Anglada *et al.*, 1996; Hull, 1978; Taatjes *et al.*, 2013). We recommend the isomer branching ratios in Nguyen *et al.* (2016), derived in turn from Kuwata and Valin (2008) and Kuwata *et al.* (2010). The CI\* undergoes unimolecular decomposition, forming OH and a  $\beta$ -oxy alkyl radical (Kroll *et al.*, 2001), or is thermally stabilized to form a stabilized Criegee intermediate (SCI).

#### 4.4.1 Reactions of the stabilized Criegee intermediate

The C<sub>1</sub> SCI (CH<sub>2</sub>OO) is formed from the ozonolysis of all terminal alkenes, and has therefore been studied in much greater detail than the C<sub>4</sub> SCIs. Because CH<sub>2</sub>OO lacks substituents and cannot have a *syn* conformation, it has low unimolecular reactivity (Anglada *et al.*, 2011). Instead, CH<sub>2</sub>OO reacts with a number of gaseous molecules, the most relevant of which are shown in Figure 4.11.

*Kinetics* - We recommend reaction rate constants for the SCIs from Nguyen *et al.* (2016). The principal reaction partners of CH<sub>2</sub>OO in the atmosphere are water and its dimer, (H<sub>2</sub>O)<sub>2</sub>. At relative humidity below 60%, reaction with the water monomer dominates, with a rate constant of  $k_{H_2O} = 9 \times 10^{-16} \text{ cm}^3 \text{ molec}^{-1} \text{ s}^{-1}$ , consistent with previous estimates (Welz *et al.*, 2012). At RH > 60%, reaction of CH<sub>2</sub>OO with the water dimer dominates, with a rate constant of  $k_{(H_2O)_2} = 8 \times 10^{-13} \text{ cm}^3 \text{ molec}^{-1} \text{ s}^{-1}$  – much faster than that with the water monomer, and consistent with some (Leather *et al.*, 2012; Newland *et al.*, 2015) but slower than other estimates (Berndt *et al.*, 2014; Chao *et al.*, 2015; Lewis *et al.*, 2015).

Despite the dominance of reaction with water and its dimer in determining the fate of the C<sub>1</sub> SCI, other pathways may be important. In our mechanism, we include the reactions of CH<sub>2</sub>OO with SO<sub>2</sub> and formic acid, that while minor, can contribute to the local loss of those reactants. For reaction with SO<sub>2</sub>, we suggest a relative

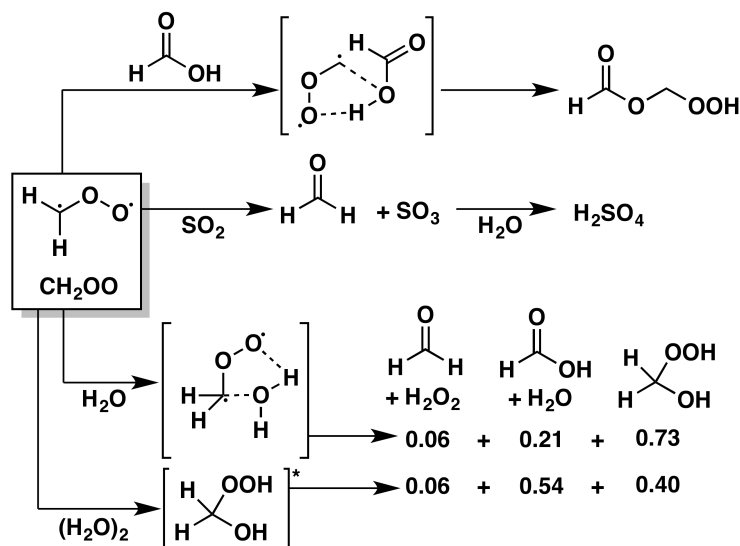


Figure 4.11: Reactions and products of the stabilized C<sub>1</sub> Criegee produced in the ozonolysis of isoprene. For the reduced mechanism, we remove the reactions with SO<sub>2</sub> and HCOOH.

rate constant of  $k_{SO_2}/(k_{H_2O} + k_{(H_2O)_2}) = 2.2(\pm 0.3) \times 10^4$  (Nguyen *et al.*, 2016), consistent with previous estimates (Atkinson and Lloyd, 1984; Newland *et al.*, 2015; Welz *et al.*, 2012). For reaction with formic acid, we use a relative rate constant of  $k_{HCOOH}/k_{SO_2} = 2.8$  (Sipilä *et al.*, 2014). Reactions of CH<sub>2</sub>OO with isoprene and RO<sub>2</sub> radicals ( $k_{isop} = 1.78 \times 10^{-13} \text{ cm}^3 \text{ molec}^{-1} \text{ s}^{-1}$  and  $k_{RO_2} = 5 \times 10^{-12} \text{ cm}^3 \text{ molec}^{-1} \text{ s}^{-1}$  respectively; Vereecken *et al.*, 2012) are not included in our mechanism. These may be relevant in chamber experiments performed with high isoprene loadings.

*Mechanism (Figure 4.11)* - We use recommendations from Nguyen *et al.* (2016) for products of the various reactions of the C<sub>1</sub> SCI. The reactions of CH<sub>2</sub>OO with water and the water dimer both follow three product channels – forming hydroxymethyl hydroperoxide (HMHP), formic acid and water, or formaldehyde and hydrogen peroxide – with differing branching ratios, shown in Figure 4.11. The subsequent chemistry of HMHP is described in Section 4.7.8. The reaction of CH<sub>2</sub>OO with SO<sub>2</sub> produces formaldehyde and SO<sub>3</sub>, which goes on to form sulfuric acid, while its reactions with formic acid produces hydroperoxy methylformate (HPMF).

The fates of the C<sub>4</sub> CI\* and SCI products are significantly less certain. Unlike CH<sub>2</sub>OO, the C<sub>4</sub> Criegees are most likely to undergo unimolecular decomposition

(either before or after stabilization), the rate and products of which depend on the conformation of the CI (Gutbrod *et al.*, 1997; Nguyen *et al.*, 2016); proposed pathways are shown in Figure 4.10. *Syn*-MVK-OO\* Criegees are expected to form a vinyl hydroperoxide, which will subsequently decompose to form OH and a  $\beta$ -oxy alkyl radical (Aschmann and Atkinson, 1994; Donahue *et al.*, 2011; Gutbrod *et al.*, 1997; Kuwata *et al.*, 2010; Paulson *et al.*, 1992). The other C<sub>4</sub> Criegees are presumed to decompose primarily *via* 5-member dioxole or 3-member dioxirane intermediates (Kuwata *et al.*, 2010; Kuwata and Valin, 2008; Vereecken *et al.*, 2012). As stated previously, our mechanism does not treat their stable products individually; for a more detailed treatment of the decomposition products of C<sub>4</sub> Criegee intermediates, see Nguyen *et al.* (2016).

#### 4.5 The reaction of NO<sub>3</sub> with isoprene

NO<sub>3</sub> represents a minor sink for isoprene in the atmosphere. As NO<sub>3</sub> readily photolyzes during the day, this chemistry is generally important only at night. When photolysis rates are reduced, however, such as below dense forest canopies or clouds, NO<sub>3</sub> oxidation can also be important during the day. Although isoprene emissions are typically low at night, many field studies demonstrate that isoprene can accumulate in the early evening. Sharp declines in isoprene concentration after sunset have been credited to NO<sub>3</sub> oxidation (Brown *et al.*, 2009; Starn *et al.*, 1998; Stroud *et al.*, 2002). Formation of isoprene NO<sub>3</sub> oxidation products (*e.g.*, organic nitrates) have been observed at night (Beaver *et al.*, 2012; Grossenbacher *et al.*, 2004). Horowitz *et al.* (2007) and Xie *et al.* (2013) using global chemical transport models predicted a considerable proportion (~40-50%) of isoprene derived nitrates are produced from NO<sub>3</sub> oxidation even though this chemistry represents a rather minor sink for isoprene (~5-6%; Horowitz *et al.*, 2007; Ng *et al.*, 2008).

*Kinetics (Table 4.13)* - NO<sub>3</sub> reacts with isoprene much like OH, by adding to a double bond. A number of studies have reported rate constants for the reaction of isoprene with NO<sub>3</sub>; a summary of measured rate coefficients from kinetic studies can be found in Table 4.13, along with the rates used in various models and those recommended by IUPAC (Atkinson *et al.*, 2006) and JPL (Burkholder *et al.*, 2015). Our mechanism uses the IUPAC value of  $2.95 \times 10^{-12} \times e^{(-450/T)} \text{ cm}^3 \text{ molec}^{-1} \text{ s}^{-1}$ .

*Mechanism (Figure 4.12; Tables 4.14 and 4.15)* - C1 addition of NO<sub>3</sub> is favored over C4 addition (Berndt and Boge, 1997; Schwantes *et al.*, 2015; Skov *et al.*, 1992), and a *cis:trans* ratio of 1:1 is assumed as calculated by Peeters *et al.* (2009) for OH

methodology <sup>a</sup>	T (K)	rate constant (cm <sup>3</sup> molec <sup>-1</sup> s <sup>-1</sup> )	citation
relative rate, GC-FID, N <sub>2</sub> O <sub>5</sub> ⇌ NO <sub>2</sub> + NO <sub>3</sub>	295 ± 1	(5.94 ± 0.16) × 10 <sup>-13</sup>	Atkinson <i>et al.</i> (1984)
flow tube, DF-MS, F + HNO <sub>3</sub> → HF + NO <sub>3</sub>	298	(1.3 ± 0.14) × 10 <sup>-12</sup>	Benter and Schindler (1988)
flow tube, LIF, N <sub>2</sub> O <sub>5</sub> ⇌ NO <sub>2</sub> + NO <sub>3</sub>	297	(6.52 ± 0.78) × 10 <sup>-13</sup>	Dlugokencky and Howard (1989)
relative rate, FTIR, N <sub>2</sub> O <sub>5</sub> ⇌ NO <sub>2</sub> + NO <sub>3</sub>	298 ± 2	(1.21 ± 0.20) × 10 <sup>-12</sup>	Barnes <i>et al.</i> (1990)
flow tube, DF-MS, F + HNO <sub>3</sub> → HF + NO <sub>3</sub>	298	(7.30 ± 0.44) × 10 <sup>-13</sup>	Wille <i>et al.</i> (1991)
flow tube, DF-MS, F + HNO <sub>3</sub> → HF + NO <sub>3</sub>	298	(8.26 ± 0.60) × 10 <sup>-13</sup>	Lancar <i>et al.</i> (1991)
UV-VIS, F + HNO <sub>3</sub> → HF + NO <sub>3</sub>	295 ± 2	(1.07 ± 0.20) × 10 <sup>-12</sup>	Ellermann <i>et al.</i> (1992)
relative rate, FTIR, N <sub>2</sub> O <sub>5</sub> ⇌ NO <sub>2</sub> + NO <sub>3</sub>	298	(6.86 ± 0.55) × 10 <sup>-13</sup>	Berndt and Boge (1997)
flow tube, CIMS, N <sub>2</sub> O <sub>5</sub> ⇌ NO <sub>2</sub> + NO <sub>3</sub>	298 ± 2	(7.3 ± 0.2) × 10 <sup>-13</sup>	Suh <i>et al.</i> (2001)
relative rate, FTIR, N <sub>2</sub> O <sub>5</sub> ⇌ NO <sub>2</sub> + NO <sub>3</sub>	296 ± 2	(7.0 ± 0.6) × 10 <sup>-13</sup>	Stabel <i>et al.</i> (2005)
relative rate, CIMS, N <sub>2</sub> O <sub>5</sub> ⇌ NO <sub>2</sub> + NO <sub>3</sub>	295 ± 2	(6.13 ± 0.12) × 10 <sup>-13</sup>	Zhao <i>et al.</i> (2011)
model: CMAQ	-	3.03 × 10 <sup>-12</sup> × e <sup>(-448/T)</sup>	Xie <i>et al.</i> (2013)
model: GEOS-Chem	-	3.3 × 10 <sup>-12</sup> × e <sup>(-450/T)</sup>	Mao <i>et al.</i> (2013)
model: MCM v3.3.1	-	3.15 × 10 <sup>-12</sup> × e <sup>(-450/T)</sup>	Jenkin <i>et al.</i> (2015)
JPL recommendation	251-381	3.5 × 10 <sup>-12</sup> × e <sup>(-450/T)</sup>	Burkholder <i>et al.</i> (2015)
<b>IUPAC / our recommendation</b>	<b>250-390</b>	2.95 × 10 <sup>-12</sup> × e <sup>(-450/T)</sup>	Atkinson <i>et al.</i> (2006)

Table 4.13: Chronological estimates of isoprene + NO<sub>3</sub> reaction rate constants, and those used in models. <sup>a</sup>studies employed a chamber technique unless otherwise noted.

nitrate yield	instrument for detection	chamber method	citation
~ 80%	In situ FTIR <sup>a</sup>	$\text{N}_2\text{O}_5 \rightleftharpoons \text{NO}_2 + \text{NO}_3$	Barnes <i>et al.</i> (1990)
~ 90%	In situ FTIR <sup>a</sup>	$\text{N}_2\text{O}_5 \rightleftharpoons \text{NO}_2 + \text{NO}_3$	Berndt and Boge (1997)
$70 \pm 8\%$	TD-LIF <sup>b</sup>	$\text{NO}_2 + \text{O}_3 \rightarrow \text{NO}_3 + \text{O}_2$	Rollins <i>et al.</i> (2009)
$65 \pm 12\%$	TD-LIF <sup>b</sup> and PTRMS <sup>c</sup>	$\text{NO}_2 + \text{O}_3 \rightarrow \text{NO}_3 + \text{O}_2$	Perring <i>et al.</i> (2009)
~ 80%	$\text{CF}_3\text{O}^-$ CIMS <sup>d</sup>	$\text{N}_2\text{O}_5 \rightleftharpoons \text{NO}_2 + \text{NO}_3$	Kwan <i>et al.</i> (2012)
$76 \pm 15\%^e$	$\text{CF}_3\text{O}^-$ CIMS <sup>d</sup>	$\text{NO}_2 + \text{O}_3 \rightarrow \text{NO}_3 + \text{O}_2$ , $\text{NO}_3 + \text{CH}_2\text{O} \rightarrow \text{HO}_2 + \text{HNO}_3$	Schwantes <i>et al.</i> (2015)

Table 4.14: Chronological estimates of overall molar nitrate yield from isoprene  $\text{NO}_3$  oxidation. Abbreviations: <sup>a</sup>Fourier transform infrared spectrometer; <sup>b</sup>thermal dissociation-laser induced fluorescence; <sup>c</sup>proton transfer reaction mass spectrometer; <sup>d</sup>chemical ionization mass spectrometer. <sup>e</sup>Reported nitrate yield is a lower bound. Isoprene also reacts to some extent with  $\text{O}_3$ , which is unlikely to form nitrates.

addition to C1 of isoprene.

Following addition of  $\text{NO}_3$ , nitrooxy peroxy radicals are formed *via* addition of oxygen. The nitrooxy peroxy radical ( $\text{INO}_2$ ) isomers and subsequent chemistry are displayed in Figure 4.12. The  $\delta$ - $\text{INO}_2$  exist in either the *Z*- or *E*-isomers. In our mechanism, these are combined with the exception of the *Z* and *E* isomers of IHN that are considered separately to be consistent with the OH-generated counterparts.

The  $\text{INO}_2$  distribution used here (Table 4.15) is not as well characterized as the ISOPOO distribution presented in Section 4.3.2. This distribution is the average distribution estimated by Schwantes *et al.* (2015) at an  $\text{RO}_2$  lifetime of  $\sim 30$  s based on products detected from the  $\text{INO}_2 + \text{HO}_2$  reaction including IPN isomers. To estimate this distribution, a number of assumptions were made, including that all isomers of  $\text{INO}_2$  react with  $\text{HO}_2$  at the same rate (see Schwantes *et al.* (2015) for more details). The  $\delta$ - $\text{INO}_2$  abundance is slightly higher than that of  $\beta$ - $\text{INO}_2$  - opposite to the ISOPOO isomer ratio in the OH oxidation at similar  $\text{RO}_2$  lifetimes (Section 4.3.2). This suggests that peroxy radicals produced from  $\text{NO}_3$  oxidation have different thermodynamic and kinetic properties. Future experimental and theoretical studies are recommended to better understand how the  $\text{RO}_2$  lifetime influences the  $\text{INO}_2$  isomer distribution.

#### 4.5.1 $\text{INO}_2$ reaction with $\text{HO}_2$

*Kinetics* - As discussed in Section 4.2, we use a relationship between the number of heavy atoms in  $\text{INO}_2$  to estimate the rate coefficient for the reaction of  $\text{INO}_2$  with  $\text{HO}_2$ ; this parameterization gives a rate coefficient of  $2.47 \times 10^{-13} \times \exp(1300/T)$



isomer	fraction <sup>a</sup>
$\beta$ -(1-ONO <sub>2</sub> ,2-OO)-INO <sub>2</sub>	0.42
$\beta$ -(4-ONO <sub>2</sub> ,3-OO)-INO <sub>2</sub>	0.045 ± 0.015 <sup>b</sup>
$\delta$ -(1-ONO <sub>2</sub> ,4-OO)-INO <sub>2</sub>	0.45 ± 0.01 <sup>b</sup>
$\delta$ -(4-ONO <sub>2</sub> ,1-OO)-INO <sub>2</sub>	0.085 ± 0.005 <sup>b</sup>

Table 4.15: Nitrooxy peroxy radical distribution at RO<sub>2</sub> lifetime of ~30 s. <sup>a</sup>Fraction reported by (Schwantes *et al.*, 2015). <sup>b</sup>Only a range of fractions was reported by (Schwantes *et al.*, 2015). The average is used in the mechanism, and the range is included above for reference.

isomer	products	yield, % <sup>a</sup>
$\beta$ -(1-ONO <sub>2</sub> ,2-OO)-INO <sub>2</sub>	MVK, CH <sub>2</sub> O, OH, NO <sub>2</sub>	53
	$\beta$ -(1-ONO <sub>2</sub> ,2-OOH)-IPN	47
$\beta$ -(4-ONO <sub>2</sub> ,3-OO)-INO <sub>2</sub>	MACR, CH <sub>2</sub> O, OH, NO <sub>2</sub>	26.5 ± 26.5 <sup>b</sup>
	$\beta$ -(4-ONO <sub>2</sub> ,3-OOH)-IPN	73.5 ± 26.5 <sup>b</sup>
$\delta$ -(1-ONO <sub>2</sub> ,4-OO)-INO <sub>2</sub>	$\delta$ -(1-ONO <sub>2</sub> ,4-OOH)-IPN	100
$\delta$ -(4-ONO <sub>2</sub> ,1-OO)-INO <sub>2</sub>	$\delta$ -(4-ONO <sub>2</sub> ,1-OOH)-IPN	100

Table 4.16: Estimated products from the reaction of INO<sub>2</sub> + HO<sub>2</sub>. <sup>a</sup>Yield reported by (Schwantes *et al.*, 2015). <sup>b</sup>Only a range of yields was reported by (Schwantes *et al.*, 2015). The average is used in the mechanism, and the range is included above for reference.

cm<sup>3</sup> molec<sup>-1</sup> s<sup>-1</sup>.

*Mechanism (Table 4.16)* - Traditionally, peroxy radicals are assumed to react with HO<sub>2</sub> to produce a hydroperoxide (in this case, IPN) in near unity yield. Recent studies have shown, however, that other pathways are important (Orlando and Tyndall, 2012, and references therein). Rollins *et al.* (2009) first proposed that INO<sub>2</sub> + HO<sub>2</sub> reactions yields OH. Kwan *et al.* (2012) constrained the OH producing pathway to 38-58%, somewhat higher than Schwantes *et al.* (2015), who estimated the yield of OH to be 22-25% at RO<sub>2</sub> lifetimes of ~30 s. The OH yield of the INO<sub>2</sub> + HO<sub>2</sub> reaction is expected to be isomer specific and so will depend on this lifetime (Schwantes *et al.*, 2015). The recommended products from the INO<sub>2</sub> + HO<sub>2</sub> reaction for each INO<sub>2</sub> isomer as estimated by Schwantes *et al.* (2015) are shown in Table 4.16.

#### 4.5.2 INO<sub>2</sub> reaction with NO/NO<sub>3</sub>

*Kinetics* - The reaction rate coefficients of INO<sub>2</sub> with NO and NO<sub>3</sub> are assumed to be  $2.7 \times 10^{-12} \times e^{(350/T)}$  and  $2.3 \times 10^{-12} \text{ cm}^3 \text{ molec}^{-1} \text{ s}^{-1}$ , respectively. These are generic RO<sub>2</sub> + NO and RO<sub>2</sub> + NO<sub>3</sub> rate coefficients used by MCM v3.3.1 (Jenkin *et al.*, 2015).

*Mechanism* - The nitrate yield from INO<sub>2</sub> + NO has not been measured, but chamber studies have detected the formation of a dinitrate (Ng *et al.*, 2008; Schwantes *et al.*, 2015). We use the formula presented in Equation 4.3 to calculate individual dinitrate yields for each INO<sub>2</sub> isomer, shown in Figure 4.12. The remaining products are assumed to be NO<sub>2</sub> and an alkoxy radical, the fate of which is discussed in Section 4.5.4. INO<sub>2</sub> + NO<sub>3</sub> reactions are assumed to only form an alkoxy radical and NO<sub>2</sub>.

#### 4.5.3 INO<sub>2</sub> reaction with RO<sub>2</sub>

*Kinetics* - RO<sub>2</sub> + RO<sub>2</sub> reaction rate constants for RO<sub>2</sub> radicals containing a nitrate functional group have not been well constrained. MCM v3.3.1 recommends the rate constant for RO<sub>2</sub> reactions with INO<sub>2</sub> to be  $1.3 \times 10^{-12} \text{ cm}^3 \text{ molec}^{-1} \text{ s}^{-1}$ . Experiments suggest, however, that the RO<sub>2</sub> + RO<sub>2</sub> reaction rate constants for INO<sub>2</sub> are actually much faster (Kwan *et al.*, 2012; Schwantes *et al.*, 2015). The faster INO<sub>2</sub> + INO<sub>2</sub> reaction rate constants estimated by Kwan *et al.* (2012) and Schwantes *et al.* (2015) are consistent with estimates for other electron withdrawing groups such as  $\beta$ -chloro,  $\beta$ -bromo, and  $\beta$ -hydroxy groups (Crowley and Moortgat, 1992; Jenkin and Hayman, 1995; Murrells *et al.*, 1991). Although Schwantes *et al.* (2015) estimated the self-reaction rate constants, they did not address potential cross-reactions as has been done for the OH system by Jenkin *et al.* (1998). Thus, the hydroxy peroxy radical reaction rate constants measured by Jenkin *et al.* (1998) are recommended to be used for the nitrooxy peroxy radical self- and cross-reactions (Table 4.10). The reaction rate constants for cross-reactions between nitrooxy peroxy radicals with methyl peroxy radicals are estimated by calculating the geometric mean of the individual self-reaction rate constants. Additional experimental studies are recommended to determine how nitrate groups influence RO<sub>2</sub> + RO<sub>2</sub> reactions.

*Mechanism* - Kwan *et al.* (2012) proposed that INO<sub>2</sub> + INO<sub>2</sub> leads to the following products: IHN + ICN (59-77%), ROOR (3-4%), and 2 INO (19-38%). Somewhat different yields - IHN + ICN (77%), ROOR (3.5%), and 2 INO (19.5%) - are

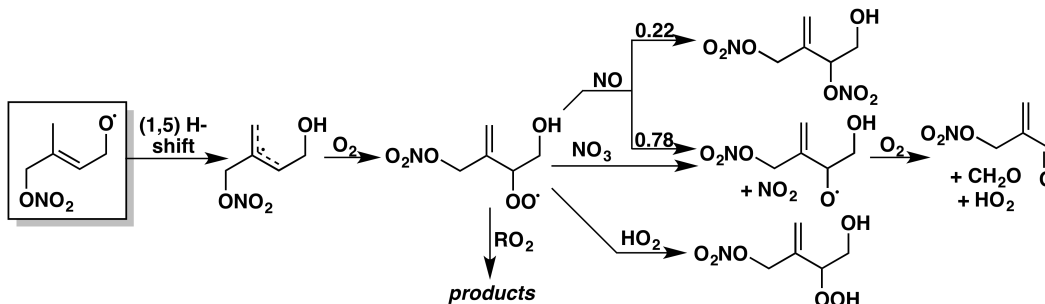


Figure 4.13: Reactions and products following the 1,5 H-shift of [1,4]-*E*- $\delta$ -INO, based on the mechanism proposed by Kwan *et al.* (2012). Yields are for 298 K and 1 atm; in reactions of peroxy radicals with NO, the relative contributions of the nitrate and alkoxy pathways vary with both temperature and pressure.  $\text{RO}_2 + \text{RO}_2$  reactions may be important peroxy radical sinks at night; for a discussion of the expected products, see Section 4.5.3.

recommended here, as these best matched experimental results for individual IHN isomers in the study of Schwantes *et al.* (2015). All cross-reactions are assumed to have the same product yields as the self-reactions. The ROOR product is assumed to only form from  $\text{INO}_2 + \text{INO}_2$  reactions.

#### 4.5.4 INO radical fate

The alkoxy radical isomers are assumed to decompose or react with  $\text{O}_2$  to form MVK, MACR, or ICN. [4,3]- $\beta$ -INO is assumed to form only MACR as no [4,3]- $\beta$ -ICN was detected in the work by Schwantes *et al.* (2015). In our mechanism, these reactions are generally included with the previous steps, except in the case of [1,4]- $\delta$ -*E*-INO, for which reaction with  $\text{O}_2$  competes with isomerization.

##### 4.5.4.1 H-shift isomerization reactions of INO and $\text{INO}_2$

Kwan *et al.* (2012) proposed that [1,4]- $\delta$ -*E*-INO would undergo a 1,5 H-shift to form the products shown in Figure 4.13. Schwantes *et al.* (2015) estimated this rate constant to be  $3 \times 10^5 \text{ s}^{-1}$ . Following Peeters and Nguyen (2012), it is expected that the *E* and *Z* isomers will interconvert; deactivation by  $\text{ONO}_2$  suggests that the H abstraction will be primarily from the *E* isomer as shown. This is in contrast to the OH system, in which the OH group is activating, leading most of the H-shift to occur from the *Z* isomer (Peeters and Nguyen, 2012).

The  $\text{INO}_2$  isomers, similar to the peroxy radicals produced from isoprene + OH oxidation (Section 4.3.3.4), may also undergo 1,6 H-shift isomerization but *via* the

E rather than the Z isomer. For example, Schwantes *et al.* (2015) detected products that suggest that the E-[1,4]- $\delta$ -INO<sub>2</sub> isomer undergoes a 1,6 H-shift. The lifetime of the INO<sub>2</sub> radical is particularly long at night suggesting this chemistry may be important in the atmosphere. Too little information is known about this pathway to incorporate it into the chemical mechanism at this time. Future theoretical and experimental studies addressing the potential isomerization of INO<sub>2</sub> isomers are needed.

#### 4.6 isoprene + Cl

Oxidation by chlorine radicals serves as a minor sink of isoprene. While the globally averaged concentration of Cl is estimated to have an upper limit of 10<sup>3</sup> atoms cm<sup>-3</sup> (Rudolph *et al.*, 1996), concentrations peaking at 10<sup>5</sup> atoms cm<sup>-3</sup> have been inferred for the marine boundary layer (Singh *et al.*, 1996). Recent observations of chlorine precursors in Boulder, Colorado have further suggested the importance of chlorine chemistry in mid-continental urban regions (Thornton *et al.*, 2010). Chlorine chemistry is thus expected to have the greatest impact on isoprene in coastal urban areas. In particular, unique products predicted in the oxidation of isoprene by Cl have been observed in Houston, Texas (Riemer *et al.*, 2008). Assuming [OH] ~10<sup>6</sup> molec cm<sup>-3</sup> and a peak [Cl] ~10<sup>5</sup> atoms cm<sup>-3</sup>, we estimate a relative reaction rate of  $k_{Cl}[Cl]/k_{OH}[OH] \sim 0.43$  to represent an upper bound on the importance of Cl oxidation in isoprene chemistry.

Sources of Cl atoms in the troposphere include photochemical degradation of gaseous halocarbons emitted both naturally and anthropogenically (Seinfeld and Pandis, 2006). In the marine boundary layer, multiphase and heterogeneous reactions of sea salt spray are known to yield photolabile precursors (Behnke *et al.*, 1997; Finlayson-Pitts *et al.*, 1989; Roberts *et al.*, 2008; Schroeder and Urone, 1974). Recent laboratory work has also shown the potential for chlorine activation through surface catalyzed chemistry of HCl with nitrogen oxides (Raff *et al.*, 2009). Many of these reactions do not require sunlight, suggesting the nighttime buildup of precursors which rapidly photolyze in the morning to yield reactive Cl (Ravishankara, 2009).

*Kinetics* - There have been many experimental and theoretical studies on the rate constant for the reaction of Cl with isoprene. The NASA JPL data evaluation recommends a rate constant of  $4.1 \times 10^{-10} \text{ cm}^3 \text{ molec}^{-1} \text{ s}^{-1}$  at 298 K, which is an average of the values found in experimental studies (Burkholder *et al.*, 2015).

The recommended temperature-dependent rate constant is  $7.6 \times 10^{-11} \times \exp(500/T)$   $\text{cm}^3 \text{ molec}^{-1} \text{ s}^{-1}$ , which is scaled from the value reported in the sole temperature-dependent study to match the recommended value at 298 K (Bedjanian *et al.*, 1998). The reaction of isoprene with Cl is approximately four times faster than its reaction with OH at 298 K.

*Mechanism (Figure 4.14)* - Our recommended mechanism for Cl oxidation of isoprene, carried out to first generation products, is presented in Figure 4.14. While we expect both *E* and *Z* stereoisomers of  $\delta$ -chloro peroxy radicals to form, we only show the *E* isomers for brevity (the chemistry of the *Z* isomers is expected to be similar). Isoprene reacts with Cl predominantly through an addition mechanism. The branching fractions for the Cl-isoprene adducts formed from the addition channel have been determined in a theoretical study as 0.40:0.02:0.08:0.50 for 1:2:3:4-addition at 300 K (Lei *et al.*, 2002b). Unlike OH addition, 4-addition of Cl is predicted to exceed 1-addition. Experimental measurements have shown that abstraction of a methyl hydrogen to yield HCl and an allylic radical also occurs at atmospheric temperatures, with measured branching fractions in the range of 0.13 – 0.17 (Bedjanian *et al.*, 1998; Fantechi *et al.*, 1998; Ragains and Finlayson-Pitts, 1997; Suh and Zhang, 2000; Xing *et al.*, 2009). No pressure dependence is observed despite the range of pressures used in the various experiments. The NASA JPL data evaluation recommends a branching fraction to form HCl of 0.15 at 298 K, which is an average of the values found in those studies (Burkholder *et al.*, 2015). The recommended temperature-dependent branching fraction is  $1.1 \times \exp(-595/T)$ , which is scaled from the value reported in the sole temperature-dependent study to match the recommended value at 298 K (Bedjanian *et al.*, 1998). Comparison of Cl oxidation rate constants for isoprene and isoprene- $\text{d}_8$  at low pressures has suggested that the abstraction pathway is not concerted, but instead occurs through an addition mechanism with subsequent elimination of HCl (Ragains and Finlayson-Pitts, 1997). Indeed, theoretical work has predicted the formation of a weakly bound complex between chlorine and isoprene, resembling a long-range interaction between HCl and the allylic  $\text{C}_5\text{H}_7$  radical, which undergoes elimination (Braña and Sordo, 2001). The existence of this complex may influence branching between the four Cl-isoprene adducts. Our recommended branching fractions for the reaction of Cl with isoprene are 0.15:0.38:0.47 for abstraction:1-addition:4-addition at 298 K. These values are derived by scaling the outer addition branching fractions to assume the inner addition branching fractions are negligible, and then scaling the result to

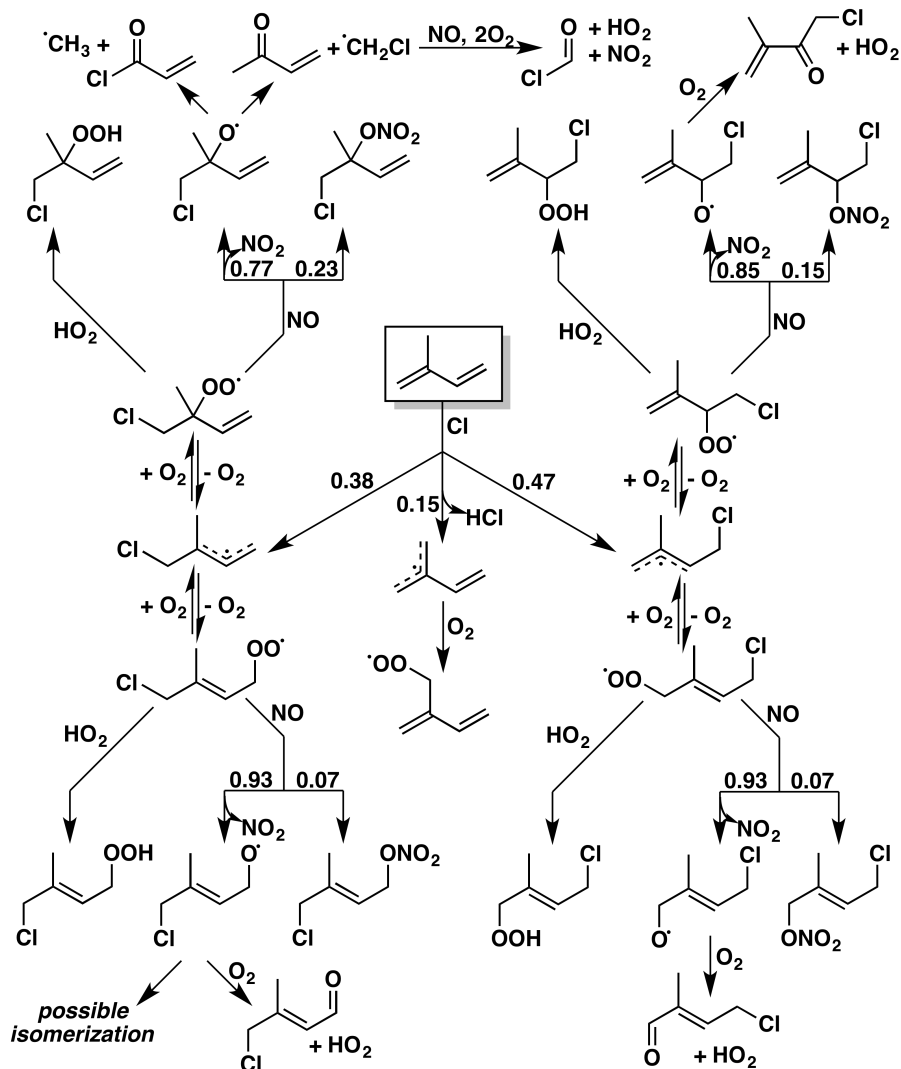


Figure 4.14: Reactions and products following the Cl-initiated oxidation of isoprene. While  $\delta$ -chloro peroxy radicals are assumed to form as equal mixtures of *E* and *Z* isomers, we only show the *E* isomers for brevity (bottom half). The chemistry of the *Z* isomers is expected to be similar. Branching fraction recommendations are for 298 K and 1 atm. As discussed in the text, the possibility that certain stereoisomers of the  $\delta$ -chloro alkoxy radicals could isomerize has not been previously studied.

account for the abstraction channel.

The carbon-centered radicals formed from Cl oxidation will immediately add  $O_2$  to form peroxy radicals (IClOO). No work has been done on the distribution of peroxy radicals from the abstraction channel. For the Cl-addition channel, rates of  $O_2$  addition have been computed in one theoretical study (Lei *et al.*, 2002a), which determined branching fractions of 0.44:0.56 for the [1,2]:[1,4] isomers and 0.60:0.40

for the [4,3]:[4,1] isomers at the kinetic limit. While the calculated energy difference between the  $\beta$ -chloro-peroxy radicals and  $E$ - $\delta$ -chloro-peroxy radicals from Lei *et al.* (2002a) are broadly consistent with those measured in the OH system by Teng *et al.* (2017), we note that the  $Z$ - $\delta$ -chloro-peroxy radicals were not considered in (Lei *et al.*, 2002a), and that even higher-level theoretical calculations were unable to provide an accurate assessment of the kinetic distribution in the OH system. We recommend, therefore, that the reversible O<sub>2</sub> addition kinetics from the OH system be used in the Cl system until such time that isomer specific data is available.

#### 4.6.1 Reactions of ICIOO

*Kinetics* - We do not present a recommendation for the fates of the dialkenylperoxy radicals due to a lack of studies on the organic products from the abstraction channel. Nevertheless, 2-methylene-3-butenal, which is a possible product, has been tentatively identified (Nordmeyer *et al.*, 1997). Even for the major Cl addition products, rate constants for the subsequent reactions of the chloroalkenylperoxy radicals remain largely unexplored. A bulk rate constant (with no isomer specificity) has been measured for the reaction between the chloroalkenylperoxy radicals and NO using a turbulent flow reactor and chemical ionization mass spectrometry (Patchen *et al.*, 2005). This study directly measured the loss of chloroalkenylperoxy radicals under pseudo-first-order conditions to determine a rate constant of  $(11.5 \pm 1.1) \times 10^{-12} \text{ cm}^3 \text{ molec}^{-1} \text{ s}^{-1}$  for 298 K, which we adopt as our recommended value. A rate constant for the reaction of hydroxyalkenylperoxy radicals with NO of  $(8.8 \pm 1.2) \times 10^{-12} \text{ cm}^3 \text{ molec}^{-1} \text{ s}^{-1}$  was measured in a separate study using the same apparatus (Miller *et al.*, 2004). Cl-substitution is slightly activating for this reaction relative to OH-substitution. To our knowledge, no measurements of the reaction between these chloroalkenylperoxy radicals with RO<sub>2</sub> or HO<sub>2</sub> have been reported in the literature. Such studies would provide further information on how the reactivity of atmospherically relevant peroxy radicals is influenced by substituents. We do not include RO<sub>2</sub> chemistry due to its minor importance in the atmosphere.

*Mechanism* - We assume the only product of the reaction with HO<sub>2</sub> is the corresponding hydroperoxide. We expect that the reaction with NO will produce both alkoxy radicals and organic nitrates, and use the nitrate yield parameterization in Equation 4.3 to calculate branching ratios; we note that the electron-withdrawing effect might serve to decrease the nitrate yield from  $\beta$ -chloro peroxy radicals, akin to the effect of a  $\beta$ -carbonyl peroxy radical (Praske *et al.*, 2015), but do not account

for this due to lack of experimental evidence.

Our recommended fates for the alkoxy radicals are guided by several theoretical and product studies. Observed products include methyl vinyl ketone (MVK), chloromethyl vinyl ketone (Cl-MVK), formyl chloride, several chloromethylbutenal (CMBA) isomers, and a chloromethylbutenone (CMBO). Product studies using a variety of techniques (FTIR, GC-MS, API-MS) have consistently measured small yields of MVK (~9% or less) and negligible yields of methacrolein (MACR) (Fantechi *et al.*, 1998; Nordmeyer *et al.*, 1997; Orlando *et al.*, 2003a; Ragains and Finlayson-Pitts, 1997). The observation of Cl-MVK and small yields of MVK suggests that there are two competing decomposition pathways for the [1,2] isomer. The lack of MACR suggests that decomposition is unimportant for the [4,3] isomer. The small measured yields of formyl chloride, a coproduct of both MVK and MACR production, range 4.7–8% (Fantechi *et al.*, 1998; Orlando *et al.*, 2003a; Ragains and Finlayson-Pitts, 1997) and agree with the MVK yield to further indicate that MACR is not a significant product of Cl oxidation. Instead, it is believed that reaction of primary and secondary alkoxy radicals with O<sub>2</sub> dominates to form the CMBA and CMBO isomers as the principal products. A chamber study using GC-MS and API-MS indeed detected at least four CMBA and CMBO isomers as products of Cl-initiated isoprene oxidation (Nordmeyer *et al.*, 1997). However, absolute yields were unable to be quantified. Theoretical calculations on C-C bond decomposition of the chloroalkenylalkoxy radicals predict that decomposition proceeds slowly with a high barrier, and that reaction with O<sub>2</sub> is the major channel under atmospheric conditions (Zhang *et al.*, 2003a). This work is consistent with findings of the experimental studies, further suggesting that CMBA and CMBO are the dominant products. CMBA and CMBO act as useful tracers of chlorine chemistry since they have no known direct anthropogenic or natural emissions (Nordmeyer *et al.*, 1997). Field observations of these compounds have successfully been used to identify episodes of chlorine chemistry in Houston, Texas (Riemer *et al.*, 2008). Nevertheless, the utility of these species as tracers is limited by the lack of absolute yield measurements.

We recommend that future product studies on the Cl-initiated oxidation of isoprene focus on determining absolute yields of CMBA and CMBO. This would directly validate the current evidence that the dominant fate of the primary and secondary alkoxy radicals is reaction with O<sub>2</sub>. These measurements should also be performed at a variety of NO<sub>x</sub> concentrations. The aforementioned product studies

(Fantechi *et al.*, 1998; Nordmeyer *et al.*, 1997; Orlando *et al.*, 2003a; Ragains and Finlayson-Pitts, 1997) were all performed under NO-free or low-NO conditions, and relied on RO<sub>2</sub> chemistry to produce the alkoxy radicals. Alkoxy radicals produced from NO chemistry typically possess greater amounts of vibrational energy than alkoxy radical produced from RO<sub>2</sub> chemistry. While the decomposition barriers of the alkoxy radicals are predicted to be greater than the exothermicity of the RO<sub>2</sub> + NO reaction (Zhang *et al.*, 2003a), experimental evidence that CMBA and CMBO are the dominant products in the presence of NO<sub>x</sub> is desirable. Finally, to our knowledge, the possibility that certain stereoisomers of the  $\delta$ -chloro alkoxy radicals could isomerize has not been previously considered. Alkoxy radical isomerization occurs in OH and NO<sub>3</sub> oxidation of isoprene and could also be occurring in Cl oxidation. Both theoretical and experimental studies to address this possibility would be useful.

## 4.7 Photochemistry of Major Oxidation Products of isoprene

### 4.7.1 Methyl Vinyl Ketone (MVK)

Methyl vinyl ketone (MVK) is a major first-generation product from OH-, O<sub>3</sub>-, and NO<sub>3</sub>-initiated oxidation of isoprene. The dominant fate of MVK is loss *via* reaction with OH (Gierczak *et al.*, 1997; Tuazon and Atkinson, 1990). For typical ambient concentrations of OH and O<sub>3</sub>, *i.e.*,  $2 \times 10^6$  molec cm<sup>-3</sup> (12 h average) and 30 ppb (24 h average), respectively, the lifetimes of MVK with respect to oxidation by OH and O<sub>3</sub> at room temperature are approximately 7 and 80 h, respectively. The reaction of MVK with NO<sub>3</sub> reaction is not competitive (Canosa-Mas *et al.*, 1999a; Kwok *et al.*, 1996; Rudich *et al.*, 1996).

*Kinetics (Table 4.17)* - A number of studies have measured the effective bimolecular reaction rate constant,  $k_{MVK+OH}$ , over a wide range of pressure and temperature (Atkinson *et al.*, 1983; Chuong and Stevens, 2003, 2004; Edney *et al.*, 1986; Gierczak *et al.*, 1997; Grosjean *et al.*, 1993b; Holloway *et al.*, 2005; Kleindienst *et al.*, 1982). A negative temperature dependence of  $k_{MVK+OH}$  was widely observed over a pressure range of 5 to 300 Torr (Chuong and Stevens, 2003; Gierczak *et al.*, 1997; Kleindienst *et al.*, 1982). Dependence of  $k_{MVK+OH}$  on pressure at 2 – 5 Torr was both observed and predicted in the temperature range of 300 – 425 K (Chuong and Stevens, 2003; Ochando-Pardo *et al.*, 2007). The reported values of  $k_{MVK+OH}$  at room temperature are in good agreement, falling into the range of  $(1-2) \times 10^{-11}$  cm<sup>3</sup> molec<sup>-1</sup> s<sup>-1</sup>, regardless of the pressure at which the measurements were conducted. Here, we use the IUPAC recommendation of  $2.6 \times 10^{-12} \times e^{(610/T)}$  cm<sup>3</sup> molec<sup>-1</sup> s<sup>-1</sup>.

oxidant	$k$ (cm <sup>3</sup> molec <sup>-1</sup> s <sup>-1</sup> )	$T$ (K)	citation
OH	$1.48 \times 10^{-11}$	300	Cox <i>et al.</i> (1980)
OH	$3.85 \times 10^{-12} \times e^{[(456 \pm 73)/T]}$	298-424	Kleindienst <i>et al.</i> (1982)
OH	$(1.96 \pm 0.15) \times 10^{-11}$	$299 \pm 2$	Atkinson <i>et al.</i> (1983)
OH	$(2.67 \pm 0.45) \times 10^{-12} \times e^{[(612 \pm 49)/T]}$	232-378	Gierczak <i>et al.</i> (1997)
OH	$(1.73 \pm 0.21) \times 10^{-11}$	300	Chuong and Stevens (2003)
OH	$(1.78 \pm 0.08) \times 10^{-11}$	300	Chuong and Stevens (2004)
OH	$(1.86 \pm 0.12) \times 10^{-11}$	$298 \pm 2$	Holloway <i>et al.</i> (2005)
<b>OH</b>	$2.6 \times 10^{-12} \times e^{(610/T)}$	<b>230-380</b>	<b>IUPAC / our recommendation</b>
O <sub>3</sub>	$(4.77 \pm 0.59) \times 10^{-18}$	$296 \pm 2$	Atkinson <i>et al.</i> (1981)
O <sub>3</sub>	$4.0 \times 10^{-18}$	~ 294	Kamens <i>et al.</i> (1982)
O <sub>3</sub>	$6.9 \times 10^{-16} \times e^{[(-1521 \pm 78)/T]}$	240-324	Treacy <i>et al.</i> (1992)
O <sub>3</sub>	$(4.72 \pm 0.09) \times 10^{-18}$	$291 \pm 2$	Grosjean <i>et al.</i> (1993b)
O <sub>3</sub>	$(5.84 \pm 0.39) \times 10^{-18}$	$291 \pm 1$	Grosjean and Grosjean (1998)
O <sub>3</sub>	$(5.4 \pm 0.6) \times 10^{-18}$	$296 \pm 2$	Neeb <i>et al.</i> (1998)
O <sub>3</sub>	$8.5 \times 10^{-16} \times e^{(-1520/T)}$	240-330	IUPAC recommendation
NO <sub>3</sub>	$< 6 \times 10^{-16}$	$296 \pm 2$	Kwok <i>et al.</i> (1996)
NO <sub>3</sub>	$\leq 1.2 \times 10^{-16}$	298	Rudich <i>et al.</i> (1996)
NO <sub>3</sub>	$(5.0 \pm 1.2) \times 10^{-16}$	$296 \pm 2$	Canosa-Mas <i>et al.</i> (1999a)
NO <sub>3</sub>	$< 6 \times 10^{-16}$	298	IUPAC recommendation

Table 4.17: Chronological estimates of the reaction rate constants for OH-, O<sub>3</sub>-, and NO<sub>3</sub>-initiated oxidation of MVK.

MVK reacts slowly with O<sub>3</sub> -  $k_{MVK+O_3} = (4 - 6) \times 10^{-18}$  cm<sup>3</sup> molec<sup>-1</sup> s<sup>-1</sup> at room temperature (Atkinson *et al.*, 1981; Cox *et al.*, 1980; Grosjean *et al.*, 1993b; Neeb *et al.*, 1998; Treacy *et al.*, 1992). A positive temperature dependence of  $k_{MVK+O_3}$  was observed by Treacy *et al.* (1992). Due to its minor importance, we do not include the reaction of MVK with O<sub>3</sub> in our mechanism.

*Mechanism (Figure 4.15; Tables 4.18 and 4.19)* - The OH-initiated oxidation of MVK occurs *via* OH addition to the double bond, forming two distinct RO<sub>2</sub>. The branching ratio, as shown in Table 4.18, has been reported (Praske *et al.*, 2015; Tuazon and Atkinson, 1989). The reaction of MVK-derived RO<sub>2</sub> and NO has been studied extensively (Galloway *et al.*, 2011; Paulot *et al.*, 2009b; Praske *et al.*, 2015; Tuazon and Atkinson, 1989). Glycolaldehyde, methylglyoxal, formaldehyde, and organic nitrates have been quantified as the primary first generation products. The organic nitrates, hereafter denoted MVKN and MVKN' for the internal and external nitrate, have respective atmospheric lifetimes of 4.3 and 6.6 h due to photolysis (Müller *et al.*, 2014). A comprehensive overview of the product yields reported in the literature is shown in Table 4.19. Reactions arising from the HO<sub>2</sub>-dominated regime, however, have only recently been reported (Praske *et al.*, 2015). Reaction of

citation	internal OH addition (%)	external OH addition (%)
Tuazon and Atkinson (1989)	28 ± 9	72 ± 21
Praske <i>et al.</i> (2015)	24 ± 14	76 ± 14

Table 4.18: OH addition branching for MVK.

citation	glycolaldehyde	methylglyoxal	MVKN	MVKN'
Tuazon and Atkinson (1989)	64 ± 8	25 ± 4		
Paulot <i>et al.</i> (2009a)	62.5			
Galloway <i>et al.</i> (2011)	67.4 ± 3	24.12 ± 0.14		
Praske <i>et al.</i> (2015)	74 ± 6		2.4 ± 0.4	1.6 ± 0.4
<b>our recommendation</b>	<b>74</b>	<b>22</b>	<b>2.3</b>	<b>1.7</b>

Table 4.19: Measured product yields (%) for the high-NO oxidation of MVK.

the internal RO<sub>2</sub> with HO<sub>2</sub> has been shown to follow three reaction channels, shown with their respective yields in Figure 4.15. Both the fragmentation and dicarbonyl pathways were found to be very efficient in the recycling of HO<sub>x</sub>. The fragmentation route is analogous to the reactions of acetyl RO<sub>2</sub> previously reported (Dillon and Crowley, 2008; Hasson *et al.*, 2005, 2004; Jenkin *et al.*, 2008). Formation of the dicarbonyl, however, was previously thought to occur only in halogenated peroxy systems (Hou *et al.*, 2005a,b; Hou and Wang, 2005). The hydroperoxide pathway, although radical terminating, promptly photolyzes with an atmospheric lifetime on the order of a few hours (Praske *et al.*, 2015). Assuming photolytic cleavage of the O-OH bond, this channel also serves to propagate the radical chain. Overall, the low NO chemistry of MVK was found to be much less HO<sub>x</sub> consuming than previously thought. Future work should identify the reaction routes arising from HO<sub>2</sub> reaction with the external RO<sub>2</sub>, as the current literature is largely speculative (Praske *et al.*, 2015). In this channel, a modest yield of methylglyoxal has been observed with the remaining assumed to form a hydroperoxide.

#### 4.7.2 Methacrolein

Methacrolein (MACR) is a major first-generation product from both OH- and O<sub>3</sub>-initiated oxidation of isoprene. The dominant fate of MACR is loss *via* reaction with OH (Gierczak *et al.*, 1997; Tuazon and Atkinson, 1990), but oxidation by O<sub>3</sub> and NO<sub>3</sub> is also considered.

*Kinetics (Table 4.20) - OH:* The reaction rate constant of MACR with OH has been closely studied, (Atkinson *et al.*, 1983; Chuong and Stevens, 2003, 2004;

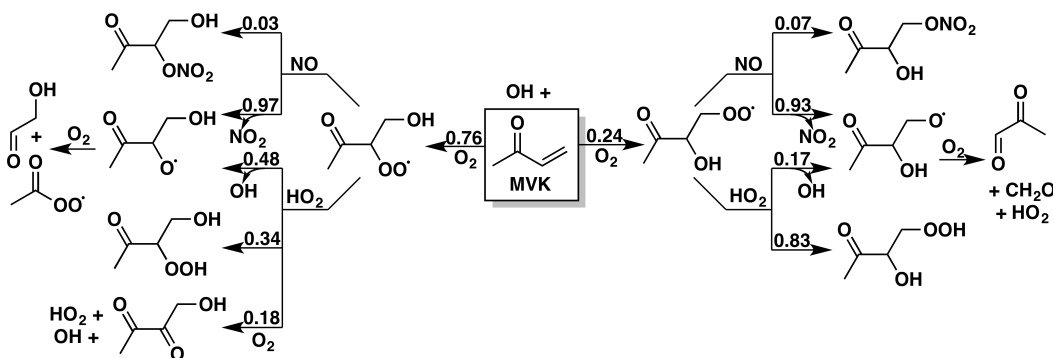


Figure 4.15: Reactions and products following the addition of OH to methyl vinyl ketone (MVK). Yields are for 298 K and 1 atm; in reactions of peroxy radicals with NO, the relative contributions of the nitrate and alkoxy pathways vary with both temperature and pressure. For the reduced mechanism, we treat (3-OO,4-OH)- and (3-OH,4-OO)-MVK as a single peroxy radical species, and scale the product yields of its reactions with NO and HO<sub>2</sub> according to the relative contributions of the two isomers.

Edney *et al.*, 1986; Gierczak *et al.*, 1997; Grosjean *et al.*, 1993b; Kleindienst *et al.*, 1982). The MACR + OH reaction exhibits a negative temperature dependence at pressure of 5 to 300 Torr (Chuong and Stevens, 2003; Gierczak *et al.*, 1997; Kleindienst *et al.*, 1982). Unlike the MVK + OH reaction, no strong pressure dependence is observed over a temperature range of 300 to 425 K, indicating the importance of the pressure-independent hydrogen abstraction reaction. The reported values of  $k_{MACR+OH}$  at room temperature are in good agreement, in the range of  $(3 - 4) \times 10^{-11} \text{ cm}^3 \text{ molec}^{-1} \text{ s}^{-1}$ . Here, we recommend separate addition and abstraction rate coefficients, as shown in Table 4.20.

*O*<sub>3</sub>: The ozonolysis of MACR proceeds *via* the O<sub>3</sub> addition to the C=C double bond to produce a primary ozonide which rapidly decomposes to methyoglyoxal or formaldehyde. The reaction rate constants,  $k_{MACR+O_3}$ , at room temperature have been measured within a range of  $(1.0 - 1.5) \times 10^{-18} \text{ cm}^3 \text{ molec}^{-1} \text{ s}^{-1}$  (Atkinson *et al.*, 1981; Grosjean *et al.*, 1993b; Neeb *et al.*, 1998; Treacy *et al.*, 1992).

*NO*<sub>3</sub>: The rate constant of the NO<sub>3</sub> reaction with MACR has only been measured at room temperature (Canosa-Mas *et al.*, 1999a; Kwok *et al.*, 1996; Rudich *et al.*, 1996). We therefore estimate the temperature dependence based on acrolein, a chemical proxy. The temperature dependence of the OH kinetics for these two  $\alpha,\beta$ -unsaturated aldehydes has been observed to be similar (Atkinson *et al.*, 2006; Magneron *et al.*, 2002; Vega-Rodriguez and Alvarez-Idaboy, 2009).

oxidant	$k$ (cm <sup>3</sup> molec <sup>-1</sup> s <sup>-1</sup> )	$T$ (K)	citation
OH	$1.77 \times 10^{-11} \times e^{[(175 \pm 52)/T]}$	300-423	Kleindienst <i>et al.</i> (1982)
OH	$(2.96 \pm 0.24) \times 10^{-11}$	$299 \pm 2$	Atkinson <i>et al.</i> (1983)
OH	$(3.90 \pm 0.31) \times 10^{-11}$	$298 \pm 2$	Edney <i>et al.</i> (1986)
OH	$(7.73 \pm 0.65) \times 10^{-12} \times e^{[(379 \pm 46)/T]}$	234-273	Gierczak <i>et al.</i> (1997)
OH	$(9.8 \pm 3.8) \times 10^{-13} \times e^{[(1050 \pm 120)/T]}$	300-422	Chuong and Stevens (2003)
OH	$(3.22 \pm 0.10) \times 10^{-11}$	300	Chuong and Stevens (2003)
OH	$8.0 \times 10^{-12} \times e^{(380/T)}$	230-380	IUPAC recommendation
<b>OH</b>	$4.4 \times 10^{-12} \times e^{(380/T)}$	-	<b>our recommendation: addition<sup>a</sup></b>
<b>OH</b>	$2.7 \times 10^{-12} \times e^{(470/T)}$	-	<b>our recommendation: abstraction<sup>b</sup></b>
O <sub>3</sub>	$(1.12 \pm 0.13) \times 10^{-18}$	$296 \pm 2$	Atkinson <i>et al.</i> (1981)
O <sub>3</sub>	$1.1 \times 10^{-18}$	$\sim 294$	Kamens <i>et al.</i> (1982)
O <sub>3</sub>	$1.3 \times 10^{-15} \times e^{[-(2112 \pm 131)/T]}$	240-324	Treacy <i>et al.</i> (1992)
O <sub>3</sub>	$(1.02 \pm 0.05) \times 10^{-18}$	$291 \pm 2$	Grosjean <i>et al.</i> (1993b)
O <sub>3</sub>	$(1.08 \pm 0.20) \times 10^{-18}$	$290 \pm 1$	Grosjean and Grosjean (1998)
O <sub>3</sub>	$(1.3 \pm 0.14) \times 10^{-18}$	$296 \pm 2$	Neeb <i>et al.</i> (1998)
<b>O<sub>3</sub></b>	$1.4 \times 10^{-15} \times e^{(-2100/T)}$	<b>240-330</b>	<b>IUPAC / our recommendation</b>
NO <sub>3</sub>	$(4.46 \pm 0.58) \times 10^{-15}$	$296 \pm 2$	Kwok <i>et al.</i> (1996)
NO <sub>3</sub>	$\leq 8 \times 10^{-15}$	298	Rudich <i>et al.</i> (1996)
NO <sub>3</sub>	$3.08 \pm 0.18$	$298 \pm 2$	Chew <i>et al.</i> (1998)
NO <sub>3</sub>	$(3.7 \pm 0.47) \times 10^{-15}$	$296 \pm 2$	Canosa-Mas <i>et al.</i> (1999a)
NO <sub>3</sub>	$3.4 \times 10^{-15}$	298	IUPAC recommendation
<b>NO<sub>3</sub></b>	$1.85 \times 10^{-13} \times e^{(-1190/T)}$	-	<b>our recommendation<sup>c</sup></b>

Table 4.20: Chronological estimates of the reaction rate constants for OH-, O<sub>3</sub>-, and NO<sub>3</sub>-initiated oxidation of MACR. <sup>a</sup>overall rate from Atkinson *et al.* (2006); scaling for addition from Orlando *et al.* (1999) and Tuazon and Atkinson (1990); <sup>b</sup>Ochando-Pardo *et al.* (2007); <sup>c</sup>overall rate from Atkinson *et al.* (2006); temperature dependence by analogy with acrolein (Salgado *et al.*, 2008).

*Mechanism (Figure 4.16; Table 4.21) - OH addition:* The addition of OH to the double bond occurs primarily at the external olefinic carbon, with a molar ratio estimated as  $\sim 85\%$  under the assumption that all the observed methylglyoxal (8%, see Table 4.21 (Galloway *et al.*, 2011; Tuazon and Atkinson, 1990)) is produced from the internal OH addition. Crouse *et al.* (2012) suggested that this ratio can be up to 96.5% based on the measured yields of <sup>18</sup>O labeled hydroperoxyacetone (HPAC-<sup>18</sup>O) and hydroxyacetone (HAC-<sup>18</sup>O).

The MACR-derived RO<sub>2</sub> radicals can react with NO or HO<sub>2</sub> but, under typical atmospheric conditions, most of the RO<sub>2</sub> radicals from external OH addition will undergo a fast 1,4-H-shift isomerization process (Crouse *et al.*, 2012). The product of this isomerization process, a hydroxy hydroperoxy carbonyl radical, decomposes rapidly, producing hydroxyacetone and re-forming OH. Similarly, RO<sub>2</sub> radicals from internal OH addition undergo a rapid 1,5-H-shift isomerization followed by decomposition and reaction with O<sub>2</sub> to form hydroperoxyacetone (HPAC), CO, and

citation	products (%)					experimental conditions (ppb)			
	CH <sub>2</sub> O	HAC	GLYX	MPAN		[NO] <sub>0</sub>	[NO <sub>2</sub> ] <sub>0</sub>	[MACR] <sub>0</sub>	OH source
Tuazon and Atkinson (1990)	28-67	41 ± 3	8.4 ± 1.6	10-24		6000-8000	-	10000	C <sub>2</sub> H <sub>5</sub> ONO
Orlando <i>et al.</i> (1999)	40-70	47 ± 5	<12	4-30		1970-2630		1316-3950	CH <sub>3</sub> ONO
Galloway <i>et al.</i> (2011)		39.5 ± 1.7	8.09 ± 0.45			231	437	42	HONO

Table 4.21: Molar yields of key products from OH-initiated oxidation of MACR in the presence of NO.

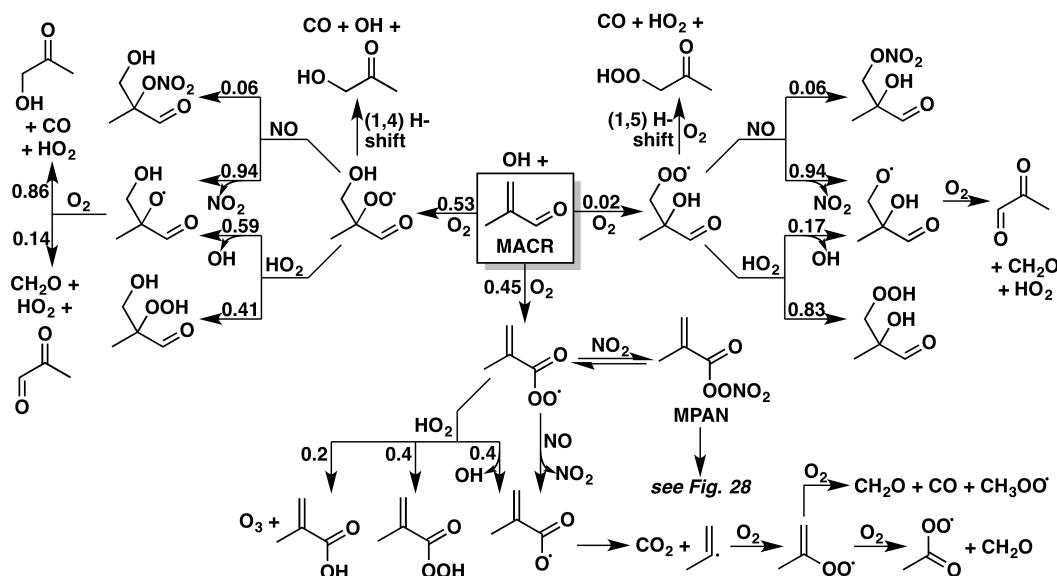


Figure 4.16: Reactions and products in the OH + methacrolein (MACR) system. Yields are for 298 K and 1 atm; the OH-abstraction and OH-addition pathways have different temperature dependences, and in reactions of peroxy radicals with NO, the relative contributions of the nitrate and alkoxy pathways vary with both temperature and pressure. For the reduced mechanism, we ignore the minor internal OH addition channel (combining it with the major addition channel and scaling the subsequent yields, as with MVK). We also assume that the peroxy radical formed from the external addition of OH proceeds entirely through the 1,4 H-shift isomerization channel.

## HO<sub>2</sub>.

The MACR-derived RO<sub>2</sub> radicals will react with NO yielding alkoxy radicals (RO) and organic nitrates, with a branching ratio of 94% and 6%, respectively (Unpublished, Caltech). The resulting RO radicals can undergo decomposition, isomerization and reaction with O<sub>2</sub>, although the last two reaction pathways are not considered to be important in the RO degradation (Park *et al.*, 2003). Decomposition of the RO radicals produces hydroxyacetone (HAC), methylglyoxal, formaldehyde, CO, and HO<sub>2</sub> (Orlando *et al.*, 1999). The reaction of MACR-derived RO<sub>2</sub> with HO<sub>2</sub> is not well constrained. Here we assume that the MACR-derived RO<sub>2</sub> radicals behave similar to the MVK-derived RO<sub>2</sub> radicals, producing both RO radicals and peroxides upon reaction with HO<sub>2</sub> (Praske *et al.*, 2015). The MACR-derived RO<sub>2</sub> self/cross reactions are not considered as a major pathway in the MACR photochemistry, based on the measured reaction rate constants for  $\beta$ -hydroxy peroxy radicals, which are at least an order of magnitude less than those measured for RO<sub>2</sub> + HO<sub>2</sub> and RO<sub>2</sub> + NO

reactions (Jenkin and Hayman, 1995).

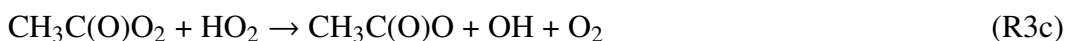
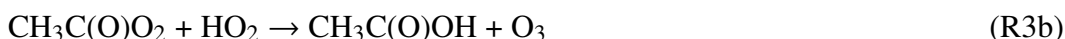
*Mechanism (Figure 4.16) - H abstraction:* The abstraction of the aldehydic hydrogen atom followed by O<sub>2</sub> addition leads to the peroxyacryl radical (C=C(CH<sub>3</sub>)C(O)O<sub>2</sub>, MACR1OO), which subsequently reacts with NO, NO<sub>2</sub>, and HO<sub>2</sub>.

#### 4.7.2.1 MACR1OO

*Kinetics* - The direct measurement of the rate constant for the MACR1OO + NO reaction was conducted by Gouw and Howard (1997) over the temperature range 240 – 360 K and at pressures of 1.3 – 3.9 Torr. Their measured value at 298 K is very close to the results from the analogous acetylperoxy radical (CH<sub>3</sub>C(O)O<sub>2</sub>) + NO reaction (Maricq and Szente, 1996; Sehested *et al.*, 1998; Villalta and Howard, 1996), indicating that the rate constant for RC(O)O<sub>2</sub> + NO reactions may not be sensitive to the structure of the R group.

*Mechanism* - The C=C(CH<sub>3</sub>)C(O)O radical produced from MACR1OO + NO reaction decomposes to CO<sub>2</sub> and the methyl vinyl radical (CH<sub>2</sub>=CCH<sub>3</sub>), which ultimately yields formaldehyde, CO, and CO<sub>2</sub> (Orlando *et al.*, 1999). We recommend that the MACR1OO + NO reaction proceeds exclusively to the products of C=C(CH<sub>3</sub>)C(O)O and NO<sub>2</sub>, by analogy with measured product yields from the CH<sub>3</sub>C(O)O<sub>2</sub> + NO reaction (Maricq and Szente, 1996).

The reaction of peroxyacryl radical with NO<sub>2</sub> produces methacryloyl peroxy nitrate (MPAN), which was directly observed by Orlando *et al.* (1999) *via* IR absorption spectroscopy. Kinetic data for this reaction are not available. Here we refer to the rate coefficients for the CH<sub>3</sub>C(O)O<sub>2</sub> + NO<sub>2</sub> + M reaction reviewed by Atkinson *et al.* (2006). At 298 K and 1 bar, the rate constant for MPAN formation is  $1 \times 10^{-11} \text{ cm}^3 \text{ molec}^{-1} \text{ s}^{-1}$ , while the decomposition occurs with a rate constant of  $3.3 \times 10^{-4} \text{ s}^{-1}$  at the same conditions. Subsequent chemistry of MPAN is described in Section 4.7.6. The chemical mechanism and kinetic data for the reaction of peroxyacryl radical with HO<sub>2</sub> are evaluated based on the CH<sub>3</sub>C(O)O<sub>2</sub> + HO<sub>2</sub> reaction, which yields peroxyacetic acid *via* channel R3a, acetic acid and ozone *via* channel R3b, and propagates OH radical *via* channel R3c:



The measured yield of OH radical from Reaction R3c is highly uncertain, ranging

from < 10% to 40%. (Hasson *et al.*, 2004; Horie and Moortgat, 1992; Jenkin *et al.*, 2007; Le Crane *et al.*, 2006; Niki *et al.*, 1985; Tomas *et al.*, 2001). Here we recommend an overall branching ratio of 0.4/0.2/0.4 obtained from the two most recent studies, Hasson *et al.* (2004) and Jenkin *et al.* (2007).

### 4.7.3 ISOPOOH

isoprene hydroxyhydroperoxide (ISOPOOH) is the major first-generation product of OH-initiated isoprene oxidation in regions with low NO concentrations, particularly remote forests, where HO<sub>2</sub> dominates the peroxy radical reactivity. The dominant sink of ISOPOOH in the atmosphere is reaction with OH, which leads primarily to the production of isoprene epoxydiols (IEPOX). Reaction with O<sub>3</sub> and NO<sub>3</sub> are not expected to contribute significantly to the fate of ISOPOOH. Photolysis is unlikely to be important given the very fast rate coefficient of OH with ISOPOOH.

*Kinetics (Table 4.22)* - The rate constants for ISOPOOH oxidation by OH were first inferred by Paulot *et al.* (2009b) from isoprene + OH chamber experiments. These experimental procedures precluded the separation of the individual isomer kinetic rates and reaction products. Recently, a synthetic route to the production of various ISOPOOH isomers has been developed that enables chamber experiments to achieve greater accuracy in measuring the rates of the specific isomers' oxidation, summarized in Table 4.22. St. Clair *et al.* (2015) performed chamber experiments at 297 K with (1,2)- and (4,3)-ISOPOOH, using both tandem-MS CF<sub>3</sub>O<sup>-</sup> CIMS and gas chromatography coupled to CF<sub>3</sub>O<sup>-</sup> CIMS to detect both ISOPOOH and its products (Crouse *et al.*, 2006; Paulot *et al.*, 2009b; St. Clair *et al.*, 2010). Experiments performed under high NO conditions were used to measure overall OH + ISOPOOH reaction rates, as well as to infer hydroperoxy-H-abstraction rates (by yields of isoprene hydroxynitrates) and the branching between non-IEPOX forming OH-addition (assumed only to yield hydroxyacetone, glycolaldehyde, hydroperoxyacetone, and hydroperoxyethanal) and IEPOX formation (by difference from unity). Experiments under HO<sub>2</sub>-dominated conditions were used to measure non-hydroperoxy H-abstraction rates and further product yields. St. Clair *et al.* (2015) found that (1,2)-ISOPOOH reacts with OH with an overall rate constant of  $7.5 \pm 1.2 \times 10^{-11} \text{ cm}^3 \text{ molec}^{-1} \text{ s}^{-1}$ , while (4,3)-ISOPOOH proceeds with a rate constant of  $1.18 \pm 0.19 \times 10^{-10} \text{ cm}^3 \text{ molec}^{-1} \text{ s}^{-1}$ .

*Mechanism (Figures 4.17-4.20; Table 4.23)* - Paulot *et al.* (2009b) were also the

$k$	(1,2)-ISOPOOH (cm <sup>3</sup> molec <sup>-1</sup> s <sup>-1</sup> )	(4,3)-ISOPOOH (cm <sup>3</sup> molec <sup>-1</sup> s <sup>-1</sup> )
$k_{total}$	$7.5 \pm 1.2 \times 10^{-11}$	$1.18 \pm 0.19 \times 10^{-10}$
$k_{OO-H}$	$9.0 \pm 1.4 \times 10^{-12}$	$4.2 \pm 0.7 \times 10^{-12}$
$k_{total-H}$	$1.2 \times 10^{-11}$	$8 \times 10^{-12}$

Table 4.22: Rate coefficients for ISOPOOH + OH (St. Clair *et al.*, 2015).

first to report product yields from the oxidation of ISOPOOH by OH, estimating that isoprene dihydroxy epoxides (IEPOX) comprised >75% of the products, with the remainder assumed to form ISOPOO radicals or C<sub>5</sub> hydroxycarbonyl compounds following H-abstraction. The isomer-specific studies of St. Clair *et al.* (2015) largely corroborated these estimates while providing greater precision of yields and identification of some minor products. Product yields measured by St. Clair *et al.* (2015) are shown in Table 4.23; we adopt similar yields, with slight modifications for potentially undetected highly functionalized products (*e.g.* hydroperoxynitrates and dihydroxydihydroperoxides), in our recommendations, shown in Figures 4.17-4.20.

OH addition to (1,2)- and (4,3)-ISOPOOH (Figures 4.17 and 4.18) occurs predominantly at the external position, and proceeds primarily by rapid fragmentation of the hydroperoxide and cyclization to form IEPOX. The two isomers of  $\beta$ -IEPOX (in a ratio of approximately 2:1 *trans:cis*) were found to account for 71% of products from (1,2)-ISOPOOH and 79% of products from (4,3)-ISOPOOH, in line with the estimate of 75% from Paulot *et al.* (2009b). This leaves 13% and 14% of the total ISOPOOH + OH reaction pathway (for (1,2)- and (4,3)-ISOPOOH, respective) that proceeds by addition but does not produce IEPOX; this fraction is assumed to add oxygen, forming a peroxy radical that can react with HO<sub>2</sub> to form a dihydroxydihydroperoxide or with NO, forming hydroperoxynitrates or fragmenting to glycolaldehyde, hydroxyacetone, and their hydroperoxide analogs.

Hydrogen abstraction from ISOPOOH (Figure 4.19) represents only a small fraction of its reactivity, but accounts for some of the minor products observed by St. Clair *et al.* (2015) at  $m/z$  185 and 201 using CF<sub>3</sub>O<sup>-</sup> CIMS. Abstraction of the hydroperoxy hydrogen represents 12% of overall (1,2)-ISOPOOH + OH reactivity and 4% of (4,3)-ISOPOOH + OH at 297 K and 745 Torr; this pathway regenerates the precursor ISOPOO, which will then follow the many reaction pathways discussed in Section 4.3.3. Abstraction of the  $\alpha$ -hydroxy hydrogen from (1,2)-ISOPOOH (4% of overall reactivity at the same conditions) forms an alkyl radical

<i>pathway/product</i>	% yield from 1,2-ISOPOOH	% yield from 4,3-ISOPOOH
<i>H-addition</i> → <i>IEPOX</i>	71	79
of which, <i>trans</i>	67 ± 1	68 ± 2
of which, <i>cis</i>	33 ± 1	32 ± 2
<i>H-addition</i> → <i>non-IEPOX</i> <sup>a</sup>	13	14
high-NO: glycolaldehyde	9 ± 1	14 ± 2
high-NO: hydroxyacetone	13 ± 2	13 ± 2
high-NO: hydroperoxyacetone	-	~2
high-NO: hydroperoxyethanal	3 ± 1	-
<i>OOH H-abstraction</i>	12	4
<i>other H-abstraction</i>	4	3
low-NO: <i>m/z</i> 201 <sup>b</sup>	2.0	2.3
low-NO: <i>m/z</i> 185 <sup>c</sup>	2.0	1.1
<i>unspecified</i>		
low-NO: <i>m/z</i> 189	3.4	3.2
low-NO: hydroxyacetone	1.3	4.4
low-NO: glycolic acid	<1	1.4
low-NO: <i>m/z</i> 93	1.4	<1
low-NO: <i>m/z</i> 161	1.1	<1
low-NO: glycolaldehyde	0.9	<1
low-NO: unidentified <sup>d</sup>	16.9	8.6

Table 4.23: Oxidation products of ISOPOOH + OH, as measured and inferred by (St. Clair *et al.*, 2015). <sup>a</sup>Inferred by difference from unity of high-NO products; <sup>b</sup>presumed to be a C<sub>5</sub> unsaturated hydroperoxy aldehyde; <sup>c</sup>presumed to be either a C<sub>5</sub> unsaturated hydroxy epoxide or, in the case of 4,3-ISOPOOH, a C<sub>5</sub> unsaturated hydroxy carbonyl; <sup>d</sup>inferred by difference from unity of low-NO products.

that can either isomerize to form a hydroxyepoxide or react with O<sub>2</sub> to form a hydroperoxycarbonyl, the masses of which were observed by St. Clair *et al.* (2015) in ~2% overall yield from (1,2)-ISOPOOH. Similarly, abstraction of the  $\alpha$ -hydroxy and  $\alpha$ -hydroperoxy hydrogens from (4,3)-ISOPOOH (3% of overall reactivity at the same conditions) can yield hydroperoxycarbonyl and hydroxycarbonyl species, respectively, the masses of which were observed by St. Clair *et al.* (2015) in ~2.3% and ~1.1% overall yields.

A few unresolved mechanistic details remain for the OH + ISOPOOH reaction. The rates and products of the  $\delta$ -ISOPOOH isomers have not yet been directly measured, though these isomers are likely only ~5% in total of the ISOPOOH formed from OH + isoprene in nature. Our recommendations for the  $\delta$ -ISOPOOH oxidation

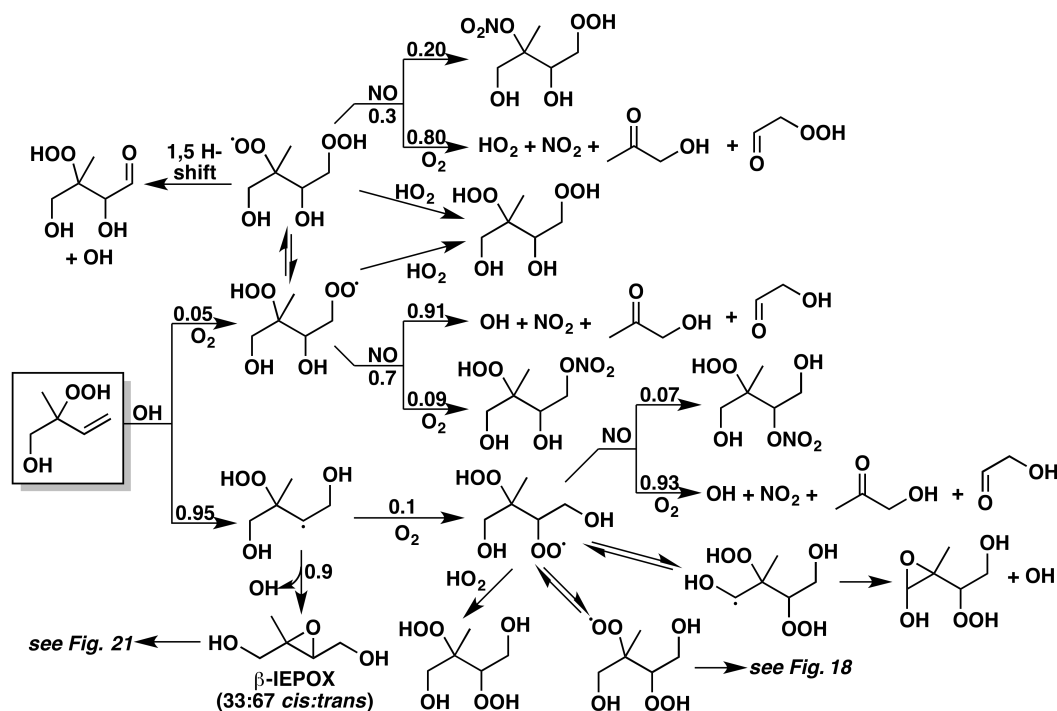


Figure 4.17: Reactions and products following the addition of OH to (1,2)- $\beta$ -ISOPOOH. Yields are for 298 K and 1 atm; in reactions of peroxy radicals with NO, the relative contributions of the nitrate and alkoxy pathways vary with both temperature and pressure, and the branching ratios between IEPOX formation and O<sub>2</sub> addition also vary with pressure. For the simplified mechanism, we combine all six dihydroxy-hydroperoxy-peroxy radicals into a single species, which isomerize or react with NO or HO<sub>2</sub> with product yields scaled by the relative contributions of each isomer.

channels are shown in Figure 4.20. While the internal addition of OH to the double bond of (4,3)-ISOPOOH is likely very small, the OH internal addition to (1,2)-ISOPOOH may be more important (St. Clair *et al.*, 2015). St. Clair *et al.* (2015) did not observe any products other than IEPOX with a yield above 4%, suggesting that either the reaction has multiple product channels, CF<sub>3</sub>O<sup>-</sup> CIMS is not sensitive to the product(s), or the product is lost to the chamber walls. One potential product from internal OH addition to (1,2)-ISOPOOH is a diperoxydiol (D'Ambro *et al.*, 2017a; Krechmer *et al.*, 2015; Liu *et al.*, 2016; Riva *et al.*, 2016b), which can also be formed from external addition; another recent study suggests that external addition followed by intramolecular hydrogen shifts can result in the prompt formation of dihydroxy-hydroperoxy-epoxide (D'Ambro *et al.*, 2017b). These functionalization pathways, shown with our recommendations in Figure 4.17, and other potential autoxidation products from the internal addition are likely to produce secondary

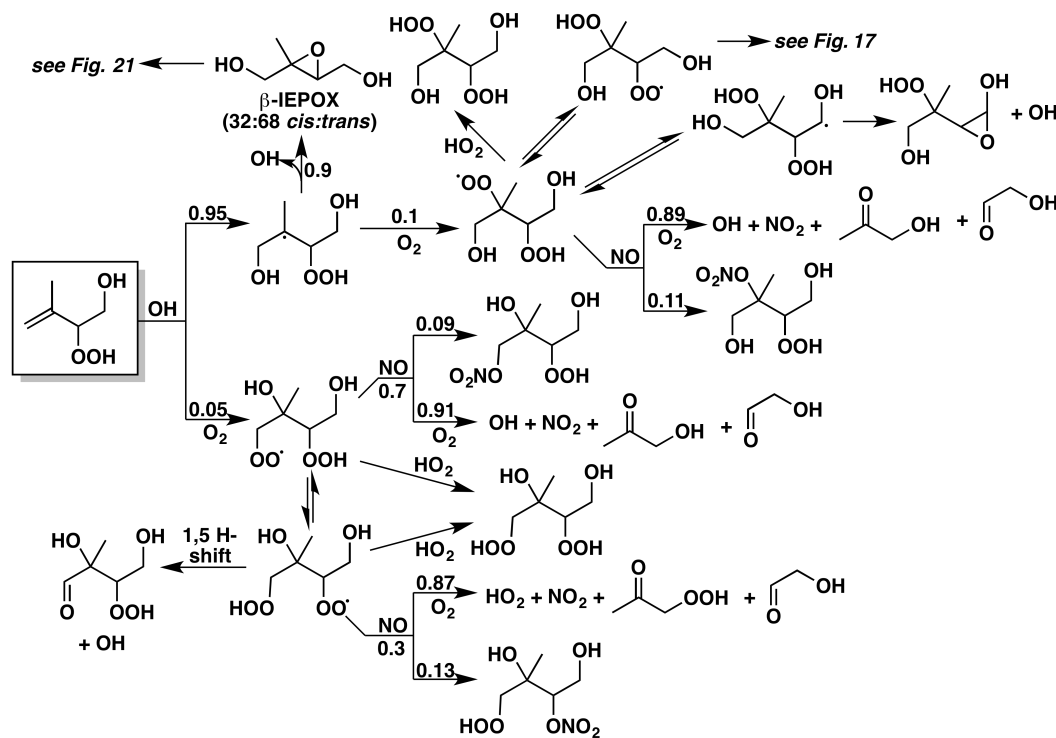


Figure 4.18: Reactions and products following the addition of OH to (4,3)- $\beta$ -ISOPOOH. Yields are for 298 K and 1 atm; in reactions of peroxy radicals with NO, the relative contributions of the nitrate and alkoxy pathways vary with both temperature and pressure, and the branching ratios between IEPOX formation and O<sub>2</sub> addition also vary with pressure. For the simplified mechanism, we combine all six dihydroxy-hydroperoxy-peroxy radicals into a single species, which isomerize or react with NO or HO<sub>2</sub> with product yields scaled by the relative contributions of each isomer.

organic aerosol (SOA). The O<sub>3</sub> and NO<sub>3</sub> chemistry of ISOPOOH has yet to be investigated but is expected to play only a small role in the atmospheric fate.

#### 4.7.4 IEPOX

isoprene epoxydiols (IEPOX) are the major product of the oxidation of ISOPOOH by OH (Paulot *et al.*, 2009b). Although four isomers of IEPOX can form following the addition of OH to the six ISOPOOH isomers, only two - *cis*- and *trans*- $\beta$ -IEPOX - account for nearly all (>97%) IEPOX formed from isoprene. Due to the high global abundance, along with the high reactivity and low volatility of IEPOX, a number of studies have focused on its reactive uptake onto particles and contribution to SOA formation (Budisulistiorini *et al.*, 2013; Chan *et al.*, 2010b; Eddingsaas *et al.*, 2010; Froyd *et al.*, 2011; Hatch *et al.*, 2011; Lin *et al.*, 2013a; McNeill *et al.*, 2012;

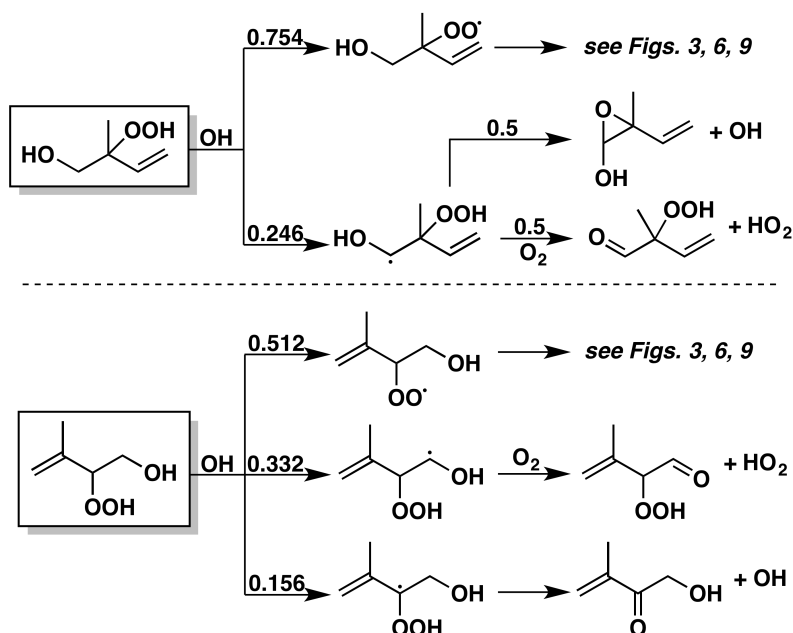


Figure 4.19: Reactions and products following the abstraction of a hydrogen from the two  $\beta$ -ISOPOOH isomers by OH. Branching ratios are for 298 K and 1 atm; the branching ratio between epoxide and hydroperoxy-aldehyde formation from (1-OH,2-OOH)-ISOPOOH varies with pressure.

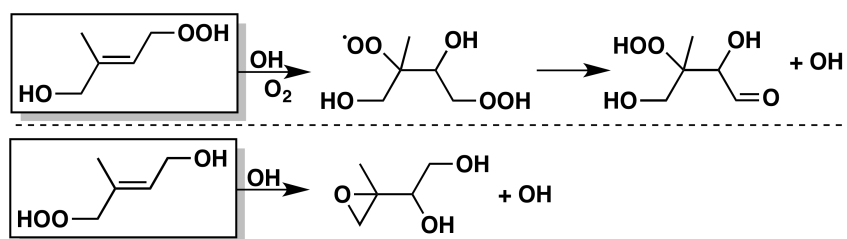


Figure 4.20: Reactions and products following the addition of OH to the  $\delta$ -ISOPOOH isomers. *E*- $\delta$  isomers are shown for the reduced mechanism, but for the full mechanism their *Z*- $\delta$  counterparts are suggested to follow the same mechanisms.

isomer	Jacobs <i>et al.</i> (2013)	Bates <i>et al.</i> (2014) <sup>a</sup>	our recommendations
<i>cis</i> - $\beta$	-	$1.52 \pm 0.07$	$5.82 \times e^{(-400/T)}$
<i>trans</i> - $\beta$	$3.60 \pm 0.76$	$0.98 \pm 0.05$	$3.75 \times e^{(-400/T)}$
$\delta 1$	-	$0.84 \pm 0.07$	$3.22 \times e^{(-400/T)}$
$\delta 4$	$3.52 \pm 0.72$	-	$3.22 \times e^{(-400/T)}$

Table 4.24: Rate coefficients for IEPOX oxidation by OH ( $\times 10^{-11}$  cm<sup>3</sup> molec<sup>-1</sup> s<sup>-1</sup>). <sup>a</sup>Error bounds do not include 15% error in propene standard rate.

Minerath *et al.*, 2008; Nguyen *et al.*, 2014a; Surratt *et al.*, 2007a), aided by the development of synthetic pathways to produce pure IEPOX standards (Zhang *et al.*, 2012). The compound's gas-phase chemistry, on the other hand, has received less attention. Only three studies have investigated rates and product yields of IEPOX oxidation by OH and the discrepancies in their results suggest that additional studies will be required (Bates *et al.*, 2014, 2016; Jacobs *et al.*, 2013).

*Kinetics (Table 4.24)* - Both Jacobs *et al.* (2013) and Bates *et al.* (2014) determined the rate coefficients of IEPOX oxidation by OH, with widely differing results (Table 4.24). Jacobs *et al.* (2013) obtained the rate coefficients using a flow tube by comparing the rate of IEPOX oxidative loss to that of competitor molecules (pentenols and butenols) as measured by CIMS. IEPOX rate coefficient values from Jacobs *et al.* (2013) imply an atmospheric lifetime of only 4 h under standard conditions ( $[OH] = 2 \times 10^6$  molec cm<sup>-3</sup>). Bates *et al.* (2014) found the rate coefficients to be lower than those measured by Jacobs *et al.* (2013) by factors of two to four (Table 4.24). The Bates *et al.* (2014) rate coefficient values were determined by CIMS detection of IEPOX loss to reaction with OH in an environmental chamber, measured relative to propene oxidative loss at 299 K. These smaller rate coefficients imply atmospheric lifetimes of 18 – 33 h under standard conditions, and are more consistent with those inferred by Paulot *et al.* (2009b), which used IEPOX generated from isoprene in chamber experiments at 298 K to estimate an upper limit of  $1.5 \times 10^{-11}$  cm<sup>3</sup> molec<sup>-1</sup> s<sup>-1</sup> for the rate constant of IEPOX oxidation by OH. Further experiments are needed to resolve the discrepancies in measured reaction rate constants; at present, we recommend use of the rate coefficients from Bates *et al.* (2014), and suggest extrapolation of the  $\delta 1$ -IEPOX coefficient for the  $\delta 4$  isomer.

*Mechanism (Figures 4.21-4.22; Table 4.25)* - Jacobs *et al.* (2013) and Bates *et al.* (2014) also measured the products of IEPOX oxidation by OH, and estimated the

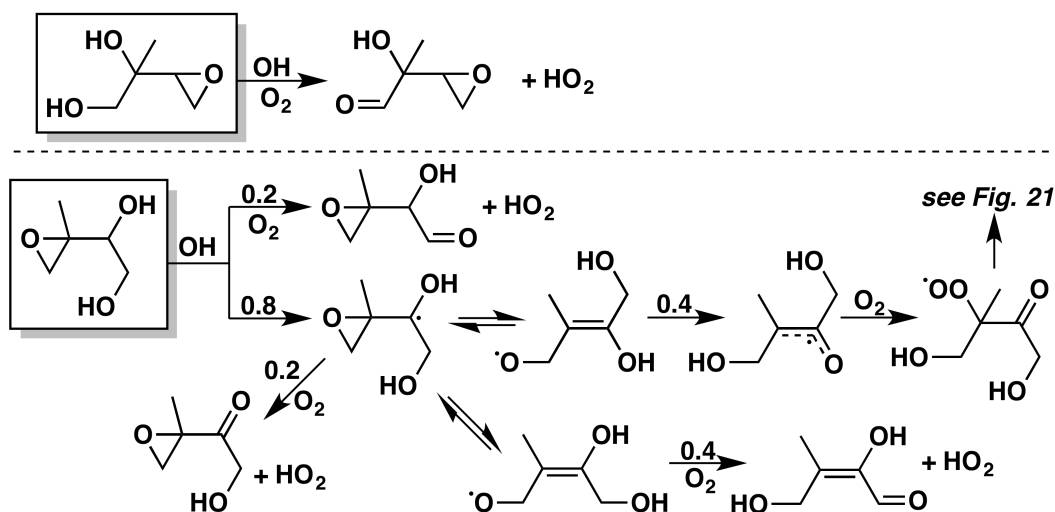


Figure 4.21: Reactions and products following the abstraction of a hydrogen from  $\delta$ -IEPOX. Due to a lack of experimental data, these mechanisms remain highly speculative. Yields are for 298 K and 1 atm; branching between isomerization reactions and reaction with  $O_2$  will vary with pressure. For the reduced mechanism, we ignore the  $\delta$ -IEPOX isomers.

first-generation yields of a number of these products, shown in Table 4.25 (Bates *et al.*, 2014; Jacobs *et al.*, 2013). Only Jacobs *et al.* (2013) investigated the products of  $\delta$ 4-IEPOX oxidation, and proposed that OH exclusively abstracted the  $\alpha$ -hydroxy hydrogens, leading either to formation of a  $C_5$  hydroxycarbonyl epoxide or fragmentation to form hydroxyacetone and glyoxal. We propose that the fragmentation occurs in a slightly different pattern, leading to higher yields of  $C_5$  hydroxycarbonyl epoxide, an isomeric  $C_5$  dihydroxy aldehyde, or a  $C_4$  hydroxydicarbonyl. Extrapolating this mechanism to  $\delta$ 1-IEPOX suggests that only the  $C_5$  hydroxycarbonyl epoxide can form, because the molecule has no  $\alpha$ -hydroxy  $\beta$ -epoxy hydrogen. These mechanisms for the  $\delta$ -IEPOX isomers are included in our recommendations at the bottom of Table 4.25, and in Figure 4.21.

Both Jacobs *et al.* (2013) and Bates *et al.* (2014) investigated the products of  $\beta$ -IEPOX oxidation by OH, which are shown in a combined format in Figure 4.22. These mechanisms share a number of pathways, and both suggest little dependence on NO concentrations. In each reaction scheme, the abstraction of a hydrogen in a position  $\alpha$  to a hydroxyl group can result in conversion of the hydroxyl substituent to a carbonyl. Both Jacobs *et al.* (2013) and Bates *et al.* (2014) found the resulting  $C_5$  hydroxyepoxycarbonyl to account for 10-20% of the first-generation products of every IEPOX isomer studied. Both mechanisms also show a substantial amount

citation	isomer	NO	hydroxy- acetone <sup>a,c</sup>	glycolal- dehyde <sup>b,c</sup>	C <sub>5</sub> H <sub>8</sub> O <sub>3</sub> <sup>d</sup>	C <sub>4</sub> H <sub>8</sub> O <sub>3</sub> <sup>c</sup> + CO	C <sub>4</sub> H <sub>6</sub> O <sub>3</sub> <sup>c</sup> + CH <sub>2</sub> O	other
Bates <i>et al.</i> (2014)		high	16.8 ± 0.3	11.8 ± 0.5	10.6 ± 0.7	46.4 ± 1.7	14.4 ± 0.6	20.1 ± 0.8
	<i>cis</i> -β	low	8.5 ± 0.5	2.5 ± 0.6	12.9 ± 1.0	37.1 ± 2.2	10.4 ± 0.6	35.6 ± 3.3
	<i>trans</i> -β	low	5.41 ± 0.17	4.55 ± 0.24	10.5 ± 0.27	21.7 ± 0.5	3.69 ± 0.15	11.5 ± 0.8
Jacobs <i>et al.</i> (2013)		high	25	14	22			39
	<i>trans</i> -β	low	24	12	16			48
		high	81		19			
	δ4	low	78		22			
Our recommendations (including Bates <i>et al.</i> (2016))	<i>cis</i> -β		8	17	21	46	8	
	<i>trans</i> -β		16	14	18	45	7	
	δ1				100			
	δ4				68		32	

Table 4.25: Product yields (%) from IEPOX. Coproducts: <sup>a</sup> glyoxal; <sup>b</sup> methylglyoxal; <sup>c</sup> OH; <sup>d</sup> HO<sub>2</sub>. <sup>e</sup> In Bates *et al.* (2014), other includes formic and acetic acids; in Jacobs *et al.* (2013), other includes products observed at *m/z* (MH<sup>+</sup>) = 89 (C<sub>4</sub>H<sub>8</sub>O<sub>2</sub> or C<sub>3</sub>H<sub>4</sub>O<sub>3</sub>), 133 (C<sub>5</sub>H<sub>8</sub>O<sub>4</sub>), and 151 (C<sub>5</sub>H<sub>10</sub>O<sub>5</sub>).

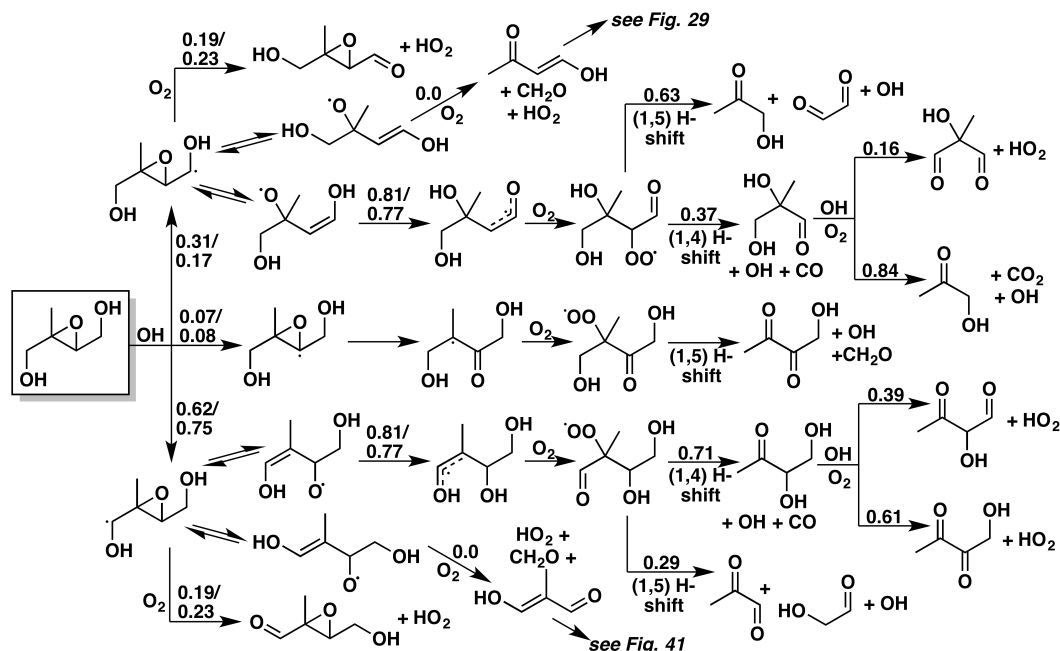


Figure 4.22: Reactions and products following the abstraction of a hydrogen from  $\beta$ -IEPOX. The oxidation mechanisms of the *cis* and *trans* isomers diverge only slightly in their branching ratios, which are denoted as "*trans/cis*" where they differ. Reactions labeled as 1,5 H-shifts could also proceed by reaction of the peroxy radical with NO, HO<sub>2</sub>, or RO<sub>2</sub> to form an alkoxy radical, which would subsequently decompose to the identical products (along with NO<sub>2</sub>, OH, or RO respectively).

of IEPOX fragmenting to a C<sub>2</sub> and a C<sub>3</sub> product, concurrently forming either hydroxyacetone and glyoxal or methylglyoxal and glycolaldehyde.

The remaining first-generation products differ between the two mechanisms, suggesting that further experimentation will be needed to constrain the products of IEPOX oxidation. Jacobs *et al.* (2013) detected large amounts of C<sub>5</sub> dihydroxy dicarbonyls and dihydroxy hydroperoxycarbonyls, in addition to an unidentified product postulated to be C<sub>4</sub>H<sub>8</sub>O<sub>2</sub> or C<sub>3</sub>H<sub>4</sub>O<sub>3</sub>, none of which were detected by Bates *et al.* (2014). In contrast, Bates *et al.* (2014) determined that C<sub>4</sub> dihydroxycarbonyls and hydroxydicarbonyls are the most abundant first-generation products in the OH-initiated oxidation of both *cis*- and *trans*- $\beta$ -IEPOX. In a subsequent study, Bates *et al.* (2016) refined the product yields from their 2014 study, and determined that the previously unidentified C<sub>4</sub> dihydroxycarbonyls consisted primarily of a single C<sub>4</sub>H<sub>8</sub>O<sub>3</sub> isomer, 1,2-dihydroxy-3-butanone, along with a minor contribution from 2,3-dihydroxy-2-methylpropanal. Our preliminary recommendations for product branching ratios can be found in Table 4.25, but additional efforts to identify and

quantify the products of IEPOX + OH oxidation and field measurements of these postulated products may be needed to reconcile the differences between the two postulated mechanisms and arrive at a more unified and comprehensive mechanism.

#### 4.7.5 isoprene Nitrates: IHN, ICN, and IPN

First generation isoprene-derived organonitrates are produced from two main channels: the reaction of isoprene-peroxy radicals with NO (section 4.3.3.1) and the reaction of isoprene directly with NO<sub>3</sub> (Section 4.5). The former mechanism produces primarily  $\beta$ -hydroxynitrates, with a small yield of  $\delta$ -hydroxynitrates, while the latter mechanism produces hydroxy-, carbonyl-, and hydroperoxy-nitrates depending on the fate of the peroxy radicals formed. Despite the importance of these products to local HO<sub>x</sub> and NO<sub>x</sub> budgets, their subsequent reactivities remain poorly constrained, and most estimates of their reaction rates and mechanisms have relied primarily on chemical intuition (Giacopelli *et al.*, 2005; Paulot *et al.*, 2009a; Rollins *et al.*, 2009). The recent development of synthetic routes to IHN has facilitated an improved understanding of their fates in the gas phase (Jacobs *et al.*, 2014; Lee *et al.*, 2014; Lockwood *et al.*, 2010; Teng *et al.*, 2017). Here, we recommend rate constants and products for the reactions of hydroxynitrate isomers with OH; we use these recommendations to provide guidance for the equivalent photochemistry of the other functionalized nitrates. Finally, we discuss other fates of the isoprene nitrates, including ozonolysis, photolysis, and reaction with NO<sub>3</sub>.

##### 4.7.5.1 Reactions of IHN, ICN, and IPN with OH

*Kinetics (Tables 4.26 and 4.27)* - Synthetic standards have enabled measurements of the rate constants for reactions of OH with all six isoprene hydroxynitrate (IHN) isomers produced following the reaction of isoprene with OH. Recommended values for these rate constants can be found in Table 4.26. The two main  $\beta$ -hydroxynitrates, which dominate the isomer distribution, exhibit similar rate constants; Teng *et al.* (2017) measured that of 1-OH,2-ONO<sub>2</sub> to be  $3.0 \pm 0.9 \times 10^{-11} \text{ cm}^3 \text{ molec}^{-1} \text{ s}^{-1}$ , while Lee *et al.* (2014) and Jacobs *et al.* (2014) report a slightly higher value for the 4-OH,3-ONO<sub>2</sub> isomer ( $4.2 \pm 0.7$  and  $3.6 \pm 0.8 \times 10^{-11} \text{ cm}^3 \text{ molec}^{-1} \text{ s}^{-1}$ ). The  $\delta$ -hydroxynitrates react faster with OH; Lee *et al.* (2014) measured the rate constant of 1-OH,4-ONO<sub>2</sub> + OH to be  $1.1 \pm 0.2 \times 10^{-10} \text{ cm}^3 \text{ molec}^{-1} \text{ s}^{-1}$ , and Teng *et al.* (2017) measured the rate constant of 4-OH,1-ONO<sub>2</sub>-IHN + OH to be  $8.0 \pm 2.4 \times 10^{-11} \text{ cm}^3 \text{ molec}^{-1} \text{ s}^{-1}$ . No differences were reported between reaction rates of *E* and *Z* isomers for the two  $\delta$ -hydroxynitrates.

isomer	$k_{OH} \times 10^{11}$	$k_{O_3} \times 10^{19}$	$k_{NO_3} \times 10^{14}$
1-OH, 2-ONO <sub>2</sub>	3.0 ± 0.9	2.8	5
4-OH, 3-ONO <sub>2</sub>	4.2 ± 0.7	5	5
<i>E</i> 1-OH, 4-ONO <sub>2</sub>	11 ± 2	270	80
<i>Z</i> 1-OH, 4-ONO <sub>2</sub>	11 ± 2	290	80
<i>E</i> 4-OH, 1-ONO <sub>2</sub>	8 ± 2.4	270	80
<i>Z</i> 4-OH, 1-ONO <sub>2</sub>	8 ± 2.4	280	80

Table 4.26: Recommended rate constants ( $\text{cm}^3 \text{ molec}^{-1} \text{ s}^{-1}$ ) at  $\sim 298 \text{ K}$  for the reactions of OH, O<sub>3</sub>, and NO<sub>3</sub> with isoprene hydroxynitrates formed following the reaction of isoprene with OH.

isomer	$k_{OH} \times 10^{11}$	$k_{O_3} \times 10^{19}$	$k_{NO_3} \times 10^{14}$
1-ONO <sub>2</sub> , 2-OH IHN	3.0	2.8	5
4-ONO <sub>2</sub> , 3-OH IHN	4.2	5	5
1-ONO <sub>2</sub> , 2-OOH IPN	3.7	2.8	5
1-ONO <sub>2</sub> , 4-OOH IPN	8.7	280	80
4-ONO <sub>2</sub> , 1-OOH IPN	11.7	280	80
4-ONO <sub>2</sub> , 3-OOH IPN	4.9	5	5
1-ONO <sub>2</sub> , 4-CO ICN	3.4	44	80
4-ONO <sub>2</sub> , 1-CO ICN	4.1	44	80
4-ONO <sub>2</sub> , 3-CO ICN	1.0	0.8	5

Table 4.27: Proposed rate constants ( $\text{cm}^3 \text{ molec}^{-1} \text{ s}^{-1}$ ) at  $\sim 298 \text{ K}$  for the reactions of OH, O<sub>3</sub>, and NO<sub>3</sub> with isoprene hydroxynitrates, hydroperoxynitrates, and carbonyl nitrates formed following the reaction of isoprene with NO<sub>3</sub>. *E* and *Z* isomers of the  $\delta$  reactants are treated together.

For most of the organic nitrates produced in the reaction of isoprene with NO<sub>3</sub>, no synthetic standards are available; we therefore use IHN as a model. Suggested rate constants are listed in Table 4.27. Briefly, we recommend the same rates of OH addition for 2-OH,1-ONO<sub>2</sub> as for 1-OH,2-ONO<sub>2</sub>, and the same for 4-OH,3-ONO<sub>2</sub> as for 3-OH,4-ONO<sub>2</sub>. For the isoprene hydroperoxynitrates (IPN), we recommend the same OH-addition rates as for their respective IHN isomers, but we also add a channel for abstraction of the hydroperoxy hydrogen, for which we use an average of the abstraction rate constants measured by St. Clair *et al.* (2015) for [1,2]- and [4,3]-ISOPOOH. Finally, for the carbonyl nitrates (ICN), we also recommend the same OH-addition rates as for their respective IHN isomers, but we include a channel for abstraction of the aldehydic hydrogen, as estimated from the SAR developed by Kwok and Atkinson (1995).

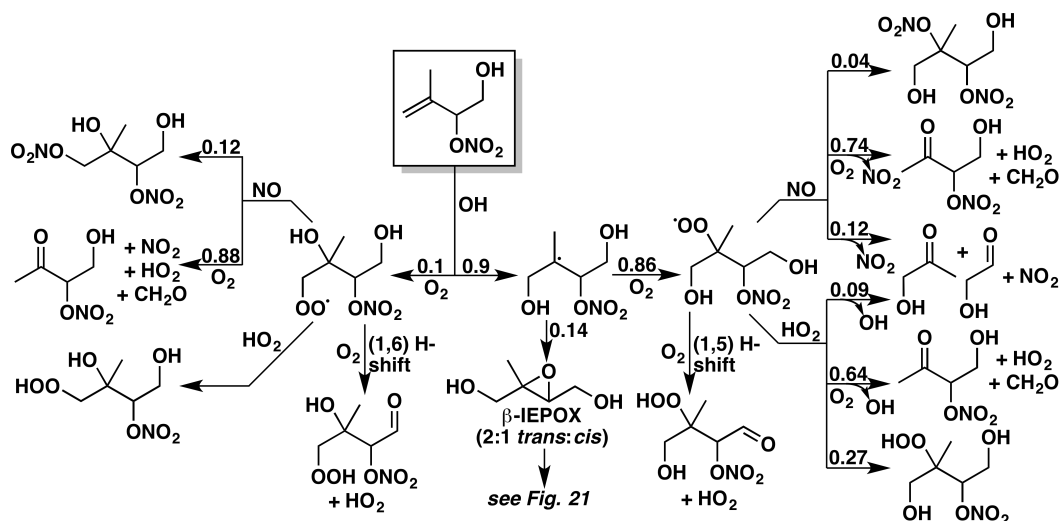


Figure 4.23: Reactions and products following the addition of OH to (4-OH,3-ONO<sub>2</sub>)-IHN. Yields are for 298 K and 1 atm; in reactions of peroxy radicals with NO, the relative contributions of the nitrate and alkoxy pathways vary with both temperature and pressure, and the branching ratio between IEPOX formation and O<sub>2</sub> addition also varies with pressure. For the reduced mechanism, we combine the various isomers of stable C<sub>5</sub> tetrafunctionalized products.

*Mechanism: OH +  $\beta$ -nitrates (Figures 4.23, 4.24, 4.31-4.33)* - The most comprehensively studied isoprene nitrate is the (4-OH,3-ONO<sub>2</sub>)-IHN, for which product studies have been carried out in bulk (Paulot *et al.*, 2009a) and with authentic standards (Jacobs *et al.*, 2014; Lee *et al.*, 2014), though only under NO-dominated conditions. Product yields from many other  $\beta$ -nitrates are inferred from these results. Our recommended OH + 4-OH,3-ONO<sub>2</sub>-IHN mechanism is shown in Figure 4.23. We suggest OH reaction branching ratios of 90% 1-addition and 10% 2-addition, although this ratio is poorly constrained due to the similarity of products between the two channels (Jacobs *et al.*, 2014; Lee *et al.*, 2014).

Following OH and O<sub>2</sub> addition, the resulting peroxy radicals are expected to react predominantly with HO<sub>2</sub> and NO. Reactions of the peroxy radicals with both HO<sub>2</sub> and NO are expected to produce mainly alkoxy radicals, which then go on to fragment, except in the case of external peroxy radicals reacting with HO<sub>2</sub>, which are expected to produce hydroperoxides in high yields. At atmospheric pressure, the main products of the fragmentation are formaldehyde and MVKN, although  $\beta$ -scission of the C2-C3 bond to yield NO<sub>2</sub>, glycolaldehyde, and hydroxacetone is also a minor channel (Jacobs *et al.*, 2014; Lee *et al.*, 2014; Paulot *et al.*, 2009a).

In addition to the fragmentation reactions, a number of functionalization channels

have been observed or proposed. OH addition at the outer carbons can result in prompt IEPOX formation, the yield of which is pressure-dependent (Jacobs *et al.*, 2014). Yields of IEPOX reported by Jacobs *et al.* (2014) at 50 Torr were as high as 71%, with an extrapolated yield (based on pressure dependence measurements up to 450 Torr) of 16% at atmospheric pressure, consistent with the yield reported by St. Clair *et al.* (2015) of 12%. Alternatively, the peroxy radicals can undergo 1,5 and 1,6 H-shifts with external  $\alpha$ -hydroxy hydrogens, which is followed rapidly by reaction with O<sub>2</sub> to form hydroxy-hydroperoxy-carbonyl-nitrates. Other functionalizations include reaction of the peroxy radicals with HO<sub>2</sub> and NO to produce dihydroxy-hydroperoxy-nitrates and dihydroxy-dinitrates respectively. Wall loss and/or aerosol formation make the measurement of these products difficult, but Lee *et al.* (2014) report a 3% dinitrate yield. The low yield requires a smaller branching ratio to form nitrates from RO<sub>2</sub> + NO when there are two electron withdrawing groups beta to RO<sub>2</sub>, as in the case of the branching ratios to yield organic nitrates from methacrolein and methyl vinyl ketone (Crouse *et al.*, 2012; Praske *et al.*, 2015), which our formula in Equation 4.3 provides. For the dihydroxy-hydroperoxy-nitrate formation from reaction of peroxy radicals with HO<sub>2</sub>, we assume a unity yield for primary peroxy radicals, and use yields for analogous hydroxynitrates assumed in Schwantes *et al.* (2015).

The recommended mechanism of the reaction of 1-OH,2-ONO<sub>2</sub>-IHN with OH is shown in Figure 4.24, and is similar to that of 4-OH,3-ONO<sub>2</sub>-IHN, with the main difference being the recommended branching ratios of 25% 3-OH-addition and 75% 4-OH-addition. Again, reactions of the resulting peroxy radicals with NO and HO<sub>2</sub> produce predominantly alkoxy radicals, which can then fragment to form either formaldehyde and MACRN or NO<sub>2</sub>, glycolaldehyde and hydroxyacetone. The estimated IEPOX yield from 1-OH,2-ONO<sub>2</sub>-IHN is inferred to be similar to that of 4-OH,3-ONO<sub>2</sub>-IHN (St. Clair *et al.*, 2015), as are the dinitrate yields Lee *et al.* (2014). However, the overall hydroperoxide yield from the reaction of the peroxy radicals with HO<sub>2</sub> is predicted to be substantially higher than that of 4-OH,3-ONO<sub>2</sub>-IHN, due to the larger fraction of primary peroxy radicals formed.

The oxidation mechanisms of  $\beta$ -functional nitrate isomers formed in the reaction of isoprene with NO<sub>3</sub> (Figure 4.31) are less well constrained; here, we apply a mechanism similar to that described in Schwantes *et al.* (2015), which draws upon both bulk chamber studies of isoprene + NO<sub>3</sub> and extrapolation from Lee *et al.* (2014) and Jacobs *et al.* (2014). Briefly, the positions of OH addition to the

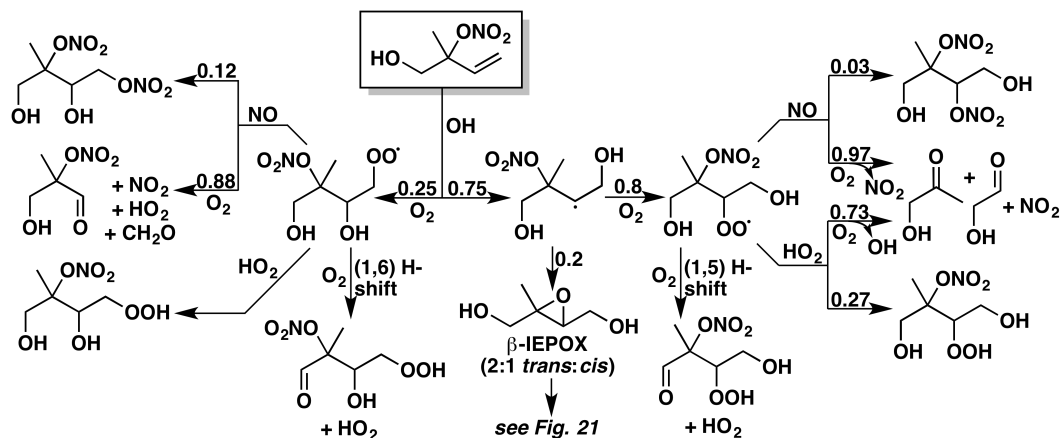


Figure 4.24: Reactions and products following the addition of OH to 1-OH,2-ONO<sub>2</sub>-IHN. Yields are for 298 K and 1 atm; in reactions of peroxy radicals with NO, the relative contributions of the nitrate and alkoxy pathways vary with both temperature and pressure, and the branching ratio between IEPOX formation and O<sub>2</sub> addition also varies with pressure. For the reduced mechanism, we combine the various isomers of stable C<sub>5</sub> tetrafunctionalized products.

1-ONO<sub>2</sub> and 4-ONO<sub>2</sub> β nitrates are assumed to match those of MVK (Praske *et al.*, 2015) and MACR (Crouse *et al.*, 2012), respectively. The positions of the nitrate moieties preclude IEPOX formation, so all 1-ONO<sub>2</sub> and 4-ONO<sub>2</sub> β-IHNs form peroxy radicals in 100% yield. The fates of these peroxy radicals are similar to those of the 4-OH,3-ONO<sub>2</sub> and 1-OH,2-ONO<sub>2</sub>-IHNs; reaction with NO can produce dinitrates, reaction with HO<sub>2</sub> can produce hydroperoxides, and reaction with either can cause fragmentation, forming smaller nitrates and carbonyl-containing compounds (PROPNN + GLYC or MACRN + CH<sub>2</sub>O for 1-ONO<sub>2</sub>,2-OH-IHN; ETHLN + HAC or MVKN + CH<sub>2</sub>O for 3-ONO<sub>2</sub>,4-OH-IHN). Recommended yields of these channels are calculated from Equation 4.3 or taken from Schwantes *et al.* (2015).

The 1-ONO<sub>2</sub> and 4-ONO<sub>2</sub> β-IPNs (Figures 4.32 and 4.33) follow the same OH oxidation mechanism as their corresponding IHNs, with two important exceptions. First, OH can abstract the hydroperoxy hydrogen, reforming the isoprene-nitrate-peroxy radical described in Section 4.5. Second, when OH adds at the terminal carbon, the hydroperoxide moieties on the IPNs can unimolecularly react in high yields (~50%) to form a nitroxy-hydroxy-epoxide (INHE) similar to IEPOX (Schwantes *et al.*, 2015). The recommended subsequent chemistry of INHE (Figures 4.34 - 4.36) is extrapolated from the IEPOX chemistry described in Section 4.7.4, using averages of the *cis*- and *trans*-β-IEPOX isomers' branching ratios for the β-INHE



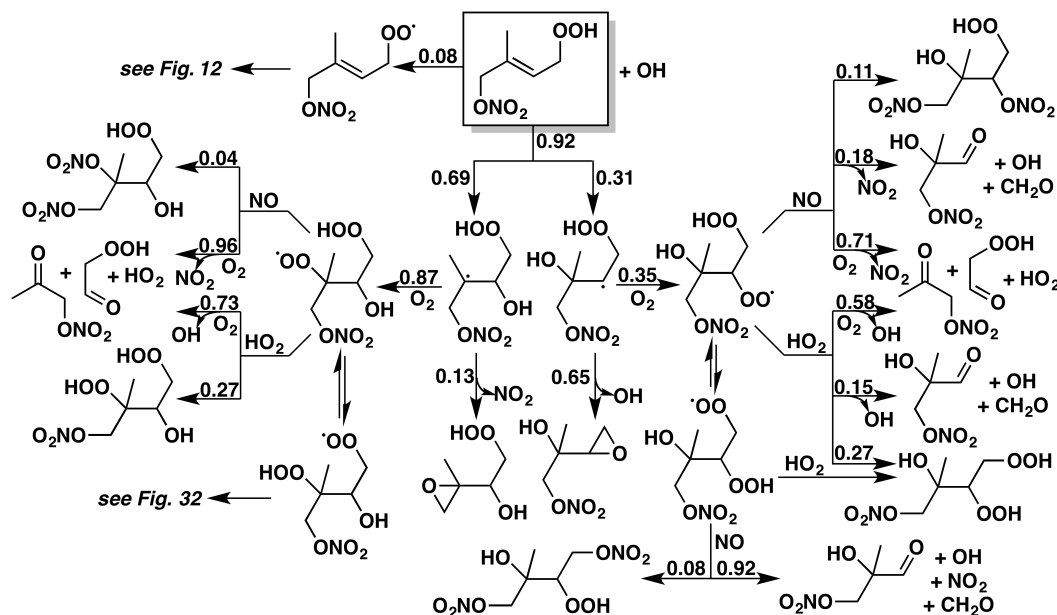


Figure 4.26: Mechanism of the reaction of OH with *E*-(1-ONO<sub>2</sub>,4-OOH)-IPN. *Z*-(1-ONO<sub>2</sub>,4-OOH)-IPN is expected to react identically. Yields are for 298 K and 1 atm; branching ratios between OH-addition and -abstraction, epoxide formation and O<sub>2</sub> addition, and nitrate and alkoxy formation all vary with temperature and/or pressure. For the reduced mechanism, we combine the  $\delta$ -IPN isomers into a single species, and scale the product yields of its subsequent reactions according to the relative contributions of the isomers. We also combine the various isomers of stable C<sub>5</sub> tetrafunctionalized products.

alkoxy radical, which, as with the  $\beta$  isomers, fragments to form smaller nitrates and carbonyl-containing compounds (PROPNN + GLYC or MACRN' + CH<sub>2</sub>O for 4-OH,1-ONO<sub>2</sub>; ETHLN + HAC or MVKN' + CH<sub>2</sub>O for 1-OH,4-ONO<sub>2</sub>). Additionally, reaction of the peroxy radicals with NO can form dinitrates in small yields, while reaction of the peroxy radicals with HO<sub>2</sub> forms hydroperoxides in only moderate (~27%) yields, as assumed in Schwantes *et al.* (2015).

The reactions of  $\delta$ -IPNs with OH follow similar channels to the  $\delta$ -IHNs, with two exceptions. First, OH can abstract the hydroperoxy hydrogen, reforming the isoprene-nitrate-peroxy radical described in Section 4.5. Second, OH addition at the  $\alpha$ -nitroxy position allows the hydroperoxide moiety to unimolecularly form OH + the epoxide INHE, for which we recommend yields from Schwantes *et al.* (2015). The remaining OH reaction products of  $\delta$ -IPNs are assumed to be similar to those formed from  $\delta$ -IHNs.

The  $\delta$ -ICNs also have unique channels in their reaction with OH, for which we use

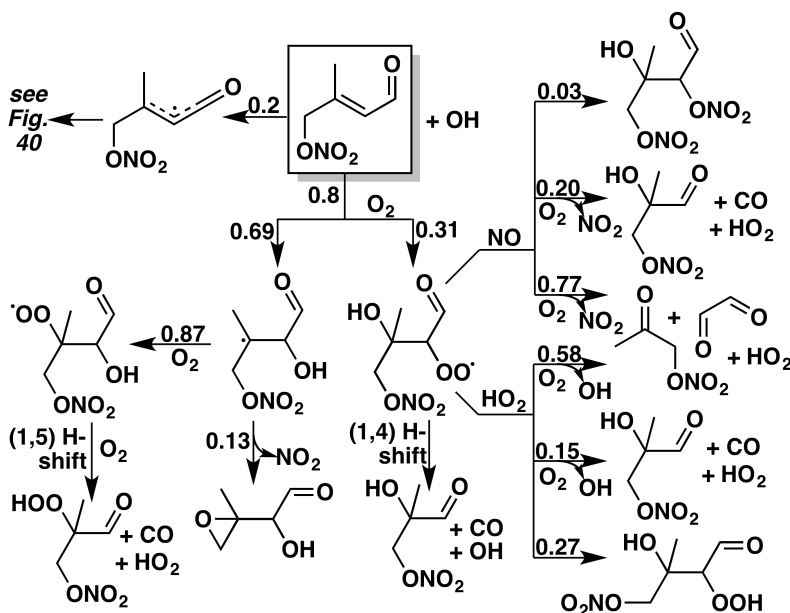


Figure 4.27: Mechanism of the reaction of OH with *E*-(1-ONO<sub>2</sub>,4-CO)-ICN. *Z*-(1-ONO<sub>2</sub>,4-CO)-ICN is expected to react identically. Yields are for 298 K and 1 atm; branching ratios between OH-addition and -abstraction, epoxide formation and O<sub>2</sub> addition, and nitrate and alkoxy formation all vary with temperature and/or pressure. For the reduced mechanism, we combine the four isomers of peroxy radicals derived from the addition of OH and O<sub>2</sub> to the  $\delta$ -ICN isomers, and scale the product yields of its subsequent reactions with NO and HO<sub>2</sub> according to the relative contributions of the isomers. We also combine the various isomers of stable C<sub>5</sub> tetrafunctionalized products.

branching ratios from Schwantes *et al.* (2015). Peroxy radicals formed following OH addition can undergo [1,4]- and [1,5]-H-shifts, similar to those described by Crouse *et al.* (2012) for MACR. Under high NO conditions, Xiong *et al.* (2016) measured 27% and 9% yields of MVKN and ETHLN, respectively, from the reaction of (4-ONO<sub>2</sub>,1-CO)-ICN with OH. This distribution suggests that the C-CHO bond on ICN is weaker than the C-CH<sub>2</sub>OH bond on IHN. Thus, based on the product distribution measured by Xiong *et al.* (2016), for  $\delta$ -ICN OH-addition products, we recommend that 75% of the alkyl radicals formed from RO<sub>2</sub> + NO and RO<sub>2</sub> + HO<sub>2</sub> reactions breaks at the C-CHO bond to form MVKN and MACRN. Additionally, products from OH hydrogen abstraction from the aldehyde group of ICN are estimated and included in the mechanism (Figure 4.40).

#### 4.7.5.2 Reactions of IHN, ICN, and IPN with O<sub>3</sub> and NO<sub>3</sub>

Published rate constants for the reactions of IHNs with O<sub>3</sub> based on authentic standards show significant disagreement. Lockwood *et al.* (2010) report ozone rate constants for the 1-OH,2-ONO<sub>2</sub>, 2-OH,1-ONO<sub>2</sub>, and *E*-1-OH,4-ONO<sub>2</sub> isomers that are two to three orders of magnitude faster than those reported by Lee *et al.* (2014) for the 4-OH,3-ONO<sub>2</sub> and *E*- and *Z*-1-OH,4-ONO<sub>2</sub>. Based on ambient measurements which show significant isoprene hydroxy nitrates at night (Beaver *et al.*, 2012), it is unlikely that the ozone rate constants are as large as reported by Lockwood *et al.* (2010) and therefore we recommend the Lee *et al.* (2014) ozone rate constants. Unpublished measurements at Caltech of the 1-OH,2-ONO<sub>2</sub> ozonolysis rate constant show similar order of magnitude rate constant to 4-OH,3-ONO<sub>2</sub>. Recommended rate constants for the reaction of ozone with the IHNs produced from isoprene + OH are listed in Table 4.26. Recommended rate constants for the reaction of ozone with the ICNs, IPNs, and IHNs produced from isoprene + NO<sub>3</sub> are listed in Table 4.27. Xiong *et al.* (2016) measured the ozone reaction rate constant for (4-ONO<sub>2</sub>,1-CO)-ICN to be  $4.4 \pm 0.3 \times 10^{-18} \text{ cm}^3 \text{ molec}^{-1} \text{ s}^{-1}$ . As with the OH oxidation of ICN, all other ICN isomer rate constants were directly extrapolated using the rate measured by Xiong *et al.* (2016) and the isomer-specific rate constants from IHN. Ozonolysis rate constants for IPNs and IHNs are directly extrapolated from those of the IHNs produced by isoprene + OH.

There is currently little measured data on NO<sub>3</sub> rate constants with isoprene nitrates. Lee *et al.* (2014) discuss various SAR estimates for the potential importance of loss by NO<sub>3</sub> radical and finds that this process is probably negligible (lifetime of 13 h at 10 pptv NO<sub>3</sub>, using a SAR estimate proposed by Pfrang *et al.*, 2008 and scaled by results for 1-hydroxy-2-butene by Zhao *et al.*, 2011) to completely negligible (lifetime of 130 h at similar conditions by Kerdouci *et al.* (2010)). In the absence of experimental data to provide guidance, we recommend a rate constant which is an average of the two revised SAR estimates from Lee *et al.* (2014) for the IHNs, and extend this directly to the ICNs and IPNs (see Tables 4.26 and 4.27).

#### 4.7.5.3 Photolysis of organic nitrates

The photolysis of organic nitrates is still poorly understood, with few measured cross-sections. Several recent studies suggest, however, that photolysis may be a dominant loss process for some of these compounds under typical ambient conditions. Previously compiled mechanisms have usually assumed slow photolysis

of nitrates, and in particular, have assigned low quantum yields for the carbonyl nitrates (Saunders *et al.*, 2003; Xie *et al.*, 2013), with some making an exception for  $\alpha$ -nitrooxy ketones, for which the neighboring functional groups demonstrably increase absorption cross-sections (Barnes *et al.*, 1993; Robert and Fajer, 1989). However, recent measurements of carbonyl nitrate photolysis by Suarez-Bertoa *et al.* (2012), along with analysis by Müller *et al.* (2014), suggest much faster photolysis for second-generation isoprene-derived nitrates, including PROPNN, ETHLN, MVKN, and MACRN. We include these increased photolysis rates in our mechanism.

In light of the recent studies on carbonyl nitrates, we recommend further research on the role of photolysis as a sink for the more complex organic nitrates formed in the isoprene oxidation mechanism. The photolysis of (4-ONO<sub>2</sub>,1-CO)-ICN has been measured ( $4.6 \times 10^{-4} \text{ s}^{-1}$  at solar zenith angle = 0°) to be quite fast (Xiong *et al.*, 2016). All ICN are assumed to photolyze at this same rate. Xiong *et al.* (2016) detected a number of products from the dissociation of both the C-CHO and O-NO<sub>2</sub> bonds, but unfortunately no yields were reported. Future studies should focus on identifying product yields from ICN photolysis, as photolysis represents an important atmospheric sink for ICN (Xiong *et al.*, 2016). Additionally, hydroperoxy nitrates formed in the reaction of isoprene with NO<sub>3</sub> may have significant photolysis rates, and should be investigated. There has also been some suggestion of higher photolysis rates of non-carbonyl nitrates, including the first-generation hydroxy isoprene nitrates themselves (Xiong *et al.*, 2015). Further study is suggested.

#### 4.7.6 MPAN

MPAN is formed from the reaction of methacryloyl peroxy radical (MACR1OO) with NO<sub>2</sub>. The amount of MPAN in the atmosphere is extremely sensitive to the NO<sub>2</sub> to NO ratio. At high NO to NO<sub>2</sub> ratio, MACR1OO is channeled toward irreversible reaction with NO. The lifetime of MPAN is also highly dependent on temperature as this compound (and other acylperoxynitrates) is labile to thermal decomposition. At 298 K, the thermal loss of MPAN occurs with an *e*-folding time of 4.5 h. Oxidation with OH is also competitive within the thermal timescale ( $\tau_{OH} = 4.8 \text{ h}$  at  $2 \times 10^6 \text{ molec cm}^{-3}$ ), and is considered below. The reactions of MPAN with O<sub>3</sub> and NO<sub>3</sub> are likely too slow to be competitive with thermal decomposition and OH reaction (see Table 4.28).

*Kinetics (Table 4.28)* - IUPAC recommends a rate constant for the reaction of MPAN with OH of  $2.9 \times 10^{-11} \text{ cm}^3 \text{ molec}^{-1}$  (at 298 K, adjusted based on OH +

oxidant	T (K)	$k$ (cm <sup>3</sup> molec <sup>-1</sup> )	citation
OH	298 ± 2	$3.6 \pm 0.4 \times 10^{-12}$	Grosjean <i>et al.</i> (1993c)
OH	275 ± 3	$3.2 \pm 0.8 \times 10^{-11}$	Orlando <i>et al.</i> (2002)
OH	298	$3.0 \times 10^{-11}$	our recommendation
O <sub>3</sub>	291-297	$8.2 \pm 2 \times 10^{-18}$	Grosjean <i>et al.</i> (1993a)
NO <sub>3</sub>	296 ± 2	$1.45 \pm 0.45 \times 10^{-16}$	Canosa-Mas <i>et al.</i> (1999b)

Table 4.28: Reaction rate constants for the oxidation of MPAN by OH, O<sub>3</sub>, and NO<sub>3</sub>.

propene temperature dependence). The rate constant determined by Grosjean *et al.* (1993c) is inexplicably 10 times lower than that determined by Orlando *et al.* (2002) (see Table 4.28), both by competitive rate techniques. The Orlando *et al.* (2002) rate constant is preferred by IUPAC based on analogy with the OH reaction of CH<sub>2</sub>=C(CH<sub>3</sub>)C(O)OONO<sub>2</sub> at 298 K (Saunders *et al.*, 1994). Recent determinations by Nguyen *et al.* (2015b) are also consistent with Orlando *et al.* (2002). The reaction of OH + MPAN may have a small (probably negative) temperature dependence by analogy with CH<sub>2</sub>=C(CH<sub>3</sub>)C(O)OONO<sub>2</sub>, but for our mechanism, we follow the recommendation of Orlando *et al.* (2002) and assume no temperature dependence.

*Mechanism (Figure 4.28)* - The mechanism of the OH reaction with MPAN, which is remarkable due to its propensity to produce secondary organic aerosol (*e.g.*, Surratt *et al.*, 2010), has been subject of debate. Experimental studies of MACR photooxidation in the presence of NO<sub>2</sub> suggested the formation of an epoxide stable product, called methacrylic acid epoxide (MAE), and NO<sub>3</sub> (Lin *et al.*, 2013b) or an unstable dioxo-ketone product and NO<sub>2</sub> (Chan *et al.*, 2010a). A theoretical study (Kjaergaard *et al.*, 2012) suggested the formation of an unstable product, a hydroxy methyl methyl- $\alpha$ -lactone (HMML) and NO<sub>3</sub>. The Kjaergaard *et al.* (2012) study proposes that 36% of HMML promptly decomposes to hydroxyacetone, while Lin *et al.* (2013b) proposes very low (~3%) hydroxyacetone formation. Compared to 60 ± 10% hydroxyacetone yield observations of Grosjean *et al.* (1993c), the suggestion of Kjaergaard *et al.* (2012) appears more favorable.

Recent laboratory work using synthesized and purified MPAN (Nguyen *et al.*, 2015b) confirms the formation of NO<sub>3</sub> in high yields. Yields of hydroxyacetone of approximately 30 ± 10% are in good agreement with theoretical predictions by Kjaergaard *et al.* (2012) but in poor agreement with experimental observations of Grosjean *et al.* (1993c). Further, the secondary organic aerosol yield was roughly equal to (1 - Y<sub>HAC</sub>) and Y<sub>NO<sub>3</sub></sub>. Notably, Nguyen *et al.* (2015b) did not observe MAE

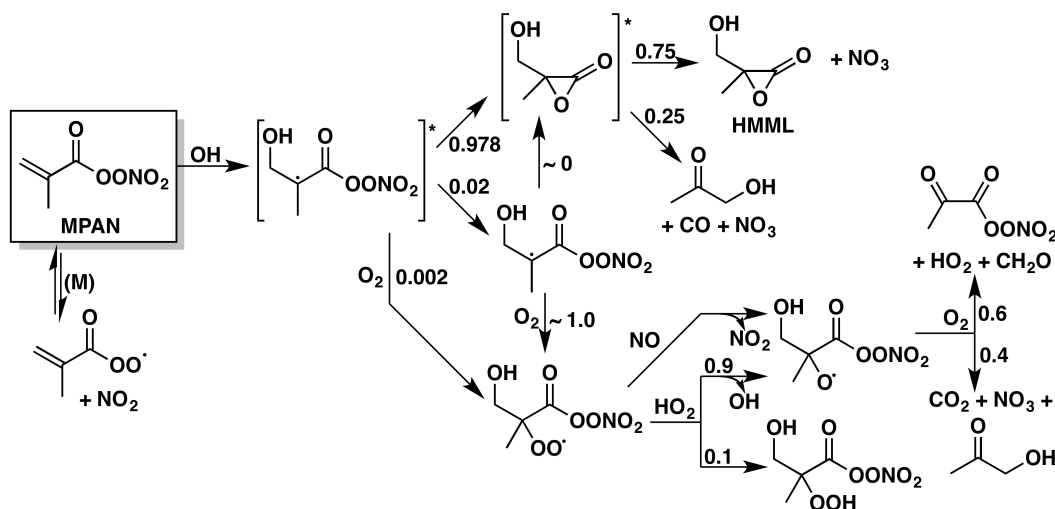


Figure 4.28: Reactions and products following the addition of OH to MPAN. Yields are for 298 K and 1 atm; in reactions of peroxy radicals with NO, the relative contributions of the nitrate and alkoxy pathways vary with both temperature and pressure. For the reduced mechanism, we ignore the low-yielding O<sub>2</sub>-addition channel, and instead recommend the prompt formation of 1.0×NO<sub>3</sub> + 0.25×(hydroxyacetone + CO) + 0.75×HMML.

formation from MPAN + OH, but did observe what appears to be MAE formation (~3%) from MACR + OH + NO<sub>2</sub>. Thus, based on experimental results from MPAN, we recommend the HMML formation mechanism and yields in Figure 4.28.

#### 4.7.7 HPALDs

Two isomers of isoprene hydroperoxy aldehydes (HPALDs) can be formed from the 1,6 H-shift isomerization of the *Z*- $\delta$  isoprene hydroxy peroxy radicals: (1-CO, 4-OOH)-HPALD (HPALD1) from the *Z*-1-OH-4-OO radical, and (1-OOH, 4-CO)-HPALD (HPALD2) from the *Z*-1-OO-4-OH radical. Both remain in the *Z* configuration through the formation process. While other hydroperoxy-carbonyl compounds may be formed at other stages of the isoprene oxidation mechanism, these two represent major first-generation products, and their subsequent chemistry is therefore of primary importance. However, few experimental constraints exist on the oxidation of HPALD; our recommendations here should therefore be updated liberally as new evidence is published.

*Kinetics - photolysis:* Loss of HPALDs was originally predicted to occur mainly by fast photolysis on the order of  $J = 10^{-4}$  to  $10^{-3}$  s<sup>-1</sup> by Peeters and Muller (2010) and Peeters *et al.* (2009). The weak hydroperoxide O–OH bond has a low

cross section, while the  $\alpha,\beta$ -enone has a high cross section in the 290–370 nm range and a stronger C–C bond. Fast internal conversion after absorption of a photon changes the molecule to a lower electronic but higher vibrational state which results in dissociation of the O–OH bond, resulting in a photolysis rate estimated to be some 2 orders of magnitude faster than for the chromophore moieties –O–OH or O=C–C=C– alone (Peeters and Muller, 2010). Experimental work using a synthetic C<sub>6</sub>-HPALD corroborated these hypotheses, demonstrating a near-unity ( $\pm 0.4$ ) quantum yield over the range 300–400 nm, and thus estimating an HPALD atmospheric lifetime of 30–180 minutes (Wolfe *et al.*, 2012). However, recent theoretical calculations place the quantum yields much lower, at 0.58 for HPALD1 and 0.55 for HPALD2 (Liu *et al.*, 2017). This would result in a near-doubling of the HPALD lifetime against photolysis, potentially bringing modeled mixing ratios into closer alignment with aircraft measurements (Travis *et al.*, 2016). Based on the primary O=C–C=C– chromophore in HPALDs, we suggest a cross-section equivalent to that of methacrolein (MACR), along with the quantum yields from Liu *et al.* (2017).

*Mechanism - photolysis (Figures 4.29 and 4.41):* Peeters *et al.* (2009) predicted that initial photolysis of the O–OH bond is followed by a 1,5-H-shift, O<sub>2</sub> addition, a 1,6-H-shift and abstraction of a hydrogen atom by O<sub>2</sub> to yield an HO<sub>2</sub> and a peroxy-acid-aldehyde (PACALD). However, PACALDs were not detected in experiments (Wolfe *et al.*, 2012), and a subsequent theoretical study identified a faster photolysis route that bypassed the PACALD mechanism (Peeters *et al.*, 2014). The latest calculations from this fast photolysis channel (Liu *et al.*, 2017) are in reasonable agreement with what little experimental data exist, and we therefore recommend the product yields from that computational study, as shown in Figures 4.29 and 4.41 for HPALD 1 and 2 respectively. Of particular note is the high radical recycling from the photolysis of HPALDS, which produces  $\sim 1.65$  equivalents of OH.

Briefly, for both HPALDs, photolysis of the aldehyde  $\pi$ -bond can either be followed by a rapid 1,5-H shift of an  $\alpha$ -hydroperoxy hydrogen and lose OH to form a resonance-stabilized carbonyl doublet radical (22% for HPALD1, 36% for HPALD2), or by a series of internal rearrangements and a loss of OH to form an alkoxy radical (78% for HPALD1, 64% for HPALD2). The carbonyl doublet radical intermediate is then expected to add oxygen; if it does so at the  $\alpha$ -hydroxy position, it will undergo a 1,4 H-shift and lose HO<sub>2</sub> to form 2-methylbut-2-ene-1,4-dial (50%), while oxygen addition at an internal carbon is followed by a series of re-

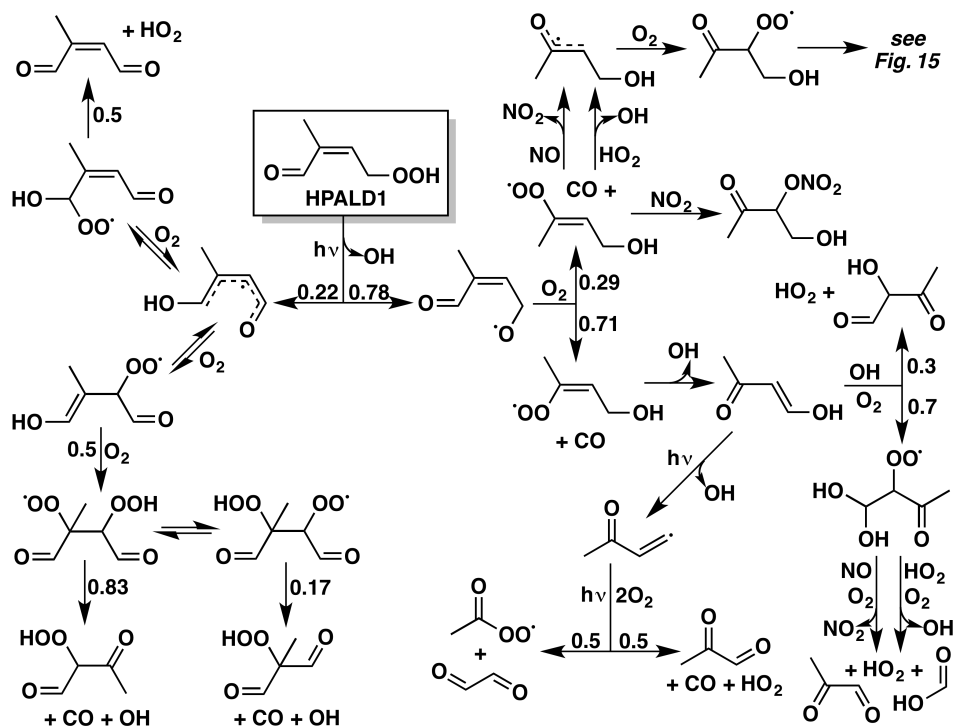


Figure 4.29: Reactions and products following the photolysis of the HPALD1.

arrangements, fragmentation, and further oxygen addition to form CO, OH, and a C<sub>4</sub>-hydroperoxy-dicarbonyl (50%). The major product (71%) of the alkoxy radical is a C<sub>4</sub> enol (hydroxy-MVK for HPALD1 and hydroxy-methacrolein for HPALD2), which is coproduced with CO and OH. The minor channel (29%) from the alkoxy radical produces CO and a C<sub>4</sub> vinyl peroxy radical, which can then react with NO or HO<sub>2</sub>. Liu *et al.* (2017) point out that another non-traditional but energetically favorable pathway for this peroxy radical is reaction with NO<sub>2</sub> followed by rearrangement to form (3-ONO<sub>2</sub>, 4-OH)-MVK (HPALD1) or 2-ONO<sub>2</sub>, 3-OH)-MACR (HPALD2). Some subsequent chemistry for the aforementioned products of HPALD photolysis is provided in the figures and the explicit mechanism (see Supporting Information), including the photolysis and reaction with OH of the enol products by extrapolation from Zhou *et al.* (2008), although we caution that these pathways are highly speculative.

*Kinetics - reaction with OH:* Loss of HPALDs also occurs by reaction with OH, though this is expected to be slower than photodissociation under most conditions (Wolfe *et al.*, 2012). Few direct constraints exist on the overall rate of reaction between OH and HPALD, let alone the rates of the individual reaction pathways.

Peeters and Muller (2010) estimated  $k_{OH+HPALD} = 5.2 \times 10^{-11} \text{ cm}^3 \text{ molec}^{-1} \text{ s}^{-1}$ , and Wolfe *et al.* (2012) measured the rate of reaction between OH and a C<sub>6</sub>-HPALD to be  $k_{OH+HPALD} = (5.1 \pm 1.8) \times 10^{-11} \text{ cm}^3 \text{ molec}^{-1} \text{ s}^{-1}$ . Based on this evidence, we recommend an overall rate coefficient of  $k_{OH+HPALD} = 5 \times 10^{-11} \text{ cm}^3 \text{ molec}^{-1} \text{ s}^{-1}$  for both HPALD isomers at 298 K, although we note that this is surprisingly low compared to rate coefficients of similarly structured molecules.

To apportion this recommended rate between the likely reaction pathways, we extrapolate H-abstraction rates from similar molecules, and assign the remaining fraction of the overall rate to OH addition, divided between the C2 and C3 positions based on the 2:1 relative stability of their resulting alkyl radicals. We assign rate coefficients for H-abstraction of the  $\alpha$ -carbonyl,  $\alpha$ -hydroperoxy, and ROO-H hydrogens to be  $k_{HCO} = 3.8 \times 10^{-12} \times e^{400/T}$ ,  $k_{H-ROOH} = 7.5 \times 10^{-12} \times e^{20/T}$ , and  $k_{H-OOR} = 2 \times 10^{-12} \times e^{200/T} \text{ cm}^3 \text{ molec}^{-1} \text{ s}^{-1}$  for both HPALD isomers. These are derived, respectively, from H-abstraction rates of methacrolein (with temperature dependence from acetaldehyde), ethanol (increased by 4× due to the hydroperoxy moiety and the allylic stability of the alkyl radical), and ISOPPOOH. By subtracting these abstraction rates from the overall rate, we derive OH addition rates at the C2 and C3 positions of  $k_{C2} = 1 \times 10^{-12} \times e^{650/T}$  and  $k_{C3} = 2 \times 10^{-12} \times e^{650/T} \text{ cm}^3 \text{ molec}^{-1} \text{ s}^{-1}$ , respectively, for both HPALD isomers.

*Mechanism - reaction with OH (Figures 4.30 and 4.42):* The products of the reactions of HPALDs with OH are even more poorly understood than the rates. Peeters and Muller (2010) predicted that photolabile peroxy-acid-aldehydes (PACALDs) would be a major product, but no PACALDs were detected by Wolfe *et al.* (2012). Without strong experimental or theoretical constraints, we formulate our recommended mechanisms – shown in Figure 4.30 for HPALD1 and Figure 4.42 for HPALD2 – based largely on extrapolation from similar compounds found elsewhere in the isoprene mechanism.

Addition of OH to either HPALD isomer - which accounts for 50% of the OH reaction channels at 298 K - can occur either at the  $\beta$ -hydroperoxy or  $\beta$ -aldehydic positions. Addition at the  $\beta$ -hydroperoxy position is followed by O<sub>2</sub> addition and an intramolecular H-shift, which leads to fragmentation, forming CO, OH, and a C<sub>4</sub>-hydroperoxy-hydroxy-carbonyl. Addition at the  $\beta$ -aldehydic position can follow a similar route, fragmenting instead to form CO, HO<sub>2</sub>, and a C<sub>4</sub>-dihydroperoxycarbonyl, but also enables the fragmentation of the hydroperoxide

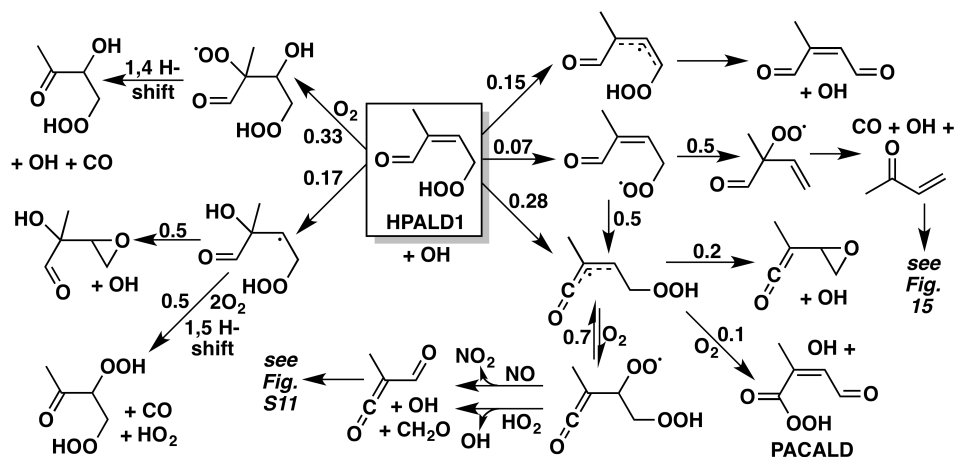


Figure 4.30: Reactions and products following the oxidation of HPALD1 by OH. Yields are for 298 K and 1 atm; the relative contributions of the H-abstraction and OH-addition pathways vary with both temperature, and the branching ratio between epoxide formation and O<sub>2</sub> addition varies with pressure.

followed by cyclization to form an epoxide and OH. We estimate that these two pathways each comprise 50% of the  $\beta$ -aldehydic OH addition mechanism.

Abstraction of the  $\alpha$ -aldehydic hydrogen is both the dominant and most complex abstraction pathway, as it forms a vinyllic radical with ketene properties. We estimate that this radical will form an epoxy-ketene in 20% yield from the fragmentation and cyclization of the hydroperoxide; a C<sub>5</sub> PACALD in 10% yield from O<sub>2</sub> addition at the  $\alpha$ -aldehydic position, followed by a 1,6 H-shift; and a hydroperoxy-ketene-peroxy radical in 70% yield from O<sub>2</sub> addition at the  $\beta$ -hydroperoxy position, which can then react either with HO<sub>2</sub> or NO and fragment to form CH<sub>2</sub>O and a C<sub>4</sub> carbonyl-ketene. In each of the three pathways, OH is recycled as a coproduct of the stable organic products.

Abstraction of the hydroperoxy hydrogen (H-OOR) yields a peroxy radical that can follow two channels: an intramolecular 1,6 H-shift, forming the same vinyllic radical discussed in the preceding paragraph, or loss of O<sub>2</sub> and re-addition at the  $\beta$ -aldehydic position. The latter pathway is likely followed by a rapid 1,4 H-shift, producing CO, OH, and either MVK (from HPALD1) or MACR (from HPALD2). We recommend that each channel represent 50% of the total hydroperoxy H-abstraction. Finally, abstraction of the  $\alpha$ -hydroperoxy hydrogen yields an alkyl radical that rapidly fragments to form OH and an unsaturated dialdehyde, which presumably photolyzes readily.

### 4.7.8 HMHP

HMHP is explicitly produced in our mechanism in contrast to most current atmospheric chemistry models. Thus, we also propose a reduced mechanism for its loss *via* OH chemistry and photolysis. We recommend an OH rate coefficient of  $k_{HMHP+OH} = 4.3 \times 10^{-12} \times e^{190/T} \text{ cm}^3 \text{ molec}^{-1} \text{ s}^{-1}$  with equal yields of  $\text{CH}_2\text{O} + \text{HO}_2$  and formic acid + OH (Allen, et al., in prep.). Recommended photolysis rates, based on cross sections from Roehl *et al.* (2007) are also included. Products of the photolysis are 2OH and formaldehyde (Roehl *et al.*, 2007).

## 4.8 Model

A semi-explicit mechanism for isoprene is included in the Supplement comprising the reactions described in this paper along with rate constants and product distributions. The mechanism is in a format suitable for use with the Kinetic Preprocessor (KPP) tool. Table I.2 in Appendix I gives the names of the species in the mechanism according to our naming convention along with the corresponding MCM name (where available). Terminal species with no subsequent chemistry are shown in bold font, while radical species are shown in italic font.

### 4.8.1 Naming Scheme

Names of most species are based on precursor names (ISOP for isoprene, MVK for methyl vinyl ketone, MACR for methacrolein, etc.) that have the same carbon structure. Attached to the precursor name are any additional functional groups, each functional group immediately preceded by the carbon number that the functional group is attached to, in order of ascending location (*i.e.* functional groups attached to C1 precede functional groups attached to C2). Carbon numbers are those assigned to isoprene. E or Z or c (*cis*) or t (*trans*) are attached to the end of the name when appropriate to designate stereoisomers. A Stabilized Criegee Intermediate (SCI) is designated by "ci" before the precursor name and "OO" following. An energetically hot radical is designated by a lowercase "x" at the end of the name, and an alkyl radical is denoted by an "r" at the radical position. Any functional groups included within the precursor molecule (*e.g.*, ISOP) are not included within the name. Abbreviations for different functional groups are shown in Table I.1 in Appendix I.

Abbreviations for common species that do not follow this naming convention (such as GLYX for glyoxal) are also given in Table I.2 in Appendix I.

As an example of the naming scheme, an isoprene hydroxyhydroperoxide with

the peroxide group attached to C3 and the alcohol group attached to C4 would be named ISOP3OOH4OH. The double bond is not included in the name because this double bond is present in isoprene (the precursor molecule).

#### 4.8.2 Temperature and pressure dependence of rate coefficients

Most rate coefficients in our mechanism are formulated with the traditional Arrhenius exponential parameterization for temperature dependence ( $k = A \times e^{-r/T}$ ). However, our mechanism also includes four alternative forms of rate coefficients: (1) the 1,6 H-shift isomerizations with an extra tunneling factor, (2) the pressure- and temperature-dependent Troe modification of a Lindemann-Hinshelwood rate expression (Troe, 1983), (3) the pressure-dependent expression for epoxide formation rates formulated by Jacobs *et al.* (2014), and (4) the temperature- and pressure-dependent nitrate yields from  $\text{RO}_2 + \text{NO}$  reactions formulated by Arey *et al.* (2001) (and earlier by Carter and Atkinson (1985) and Carter and Atkinson (1989)), as described in Section 4.2. These parameterizations are described in greater detail below.

The 1,6 H-shift isomerization reactions described in Section 4.3.3.4 are modeled with a strongly negative T-dependent tunneling factor, best expressed as an Arrhenius rate parameterization with an additional exponential term that includes  $T^{-3}$  in the argument. We denote these rates with "k\_tunneling[A,B,C]" in place of a typical rate coefficient formula, where A, B, and C can then be applied in the following formula:

$$k_{\text{tunneling}} = A \times e^{B/T} \times e^{C/T^3} \quad (4.9)$$

The modified Lindemann-Hinshelwood rate coefficient (Troe, 1983) is only applied in two reactions within our mechanism: the formation and decomposition of MPAN. These rates are denoted with "k\_troe[A,B,C]", where A, B, and C, respectively, signify  $k_0$ ,  $k_\infty$ , and  $F_c$  in the equation:

$$k_{\text{troe}} = \frac{k_0 \times [M]}{1 + \frac{k_0 \times [M]}{k_\infty}} \times F_c^{(1 + [\log_{10}(\frac{k_0 \times [M]}{k_\infty})]^2)^{-1}} \quad (4.10)$$

The pressure dependence of epoxide yields can simply be understood as a means of including the  $\text{O}_2$  concentration in the rate coefficient to skip a step and remove an intermediate compound from the mechanism. In the full explicit mechanism, OH addition to a double bond forms an alkyl radical, which can then either add  $\text{O}_2$  or form an epoxide from an  $\alpha$ -hydroperoxy or -nitrooxy group. Thus, the branching ratios

of O<sub>2</sub> addition and epoxide formation are dependent upon the O<sub>2</sub> concentration. Alternatively, the reaction can be written in a single step (OH addition to directly form an epoxide) if the O<sub>2</sub> concentration is included in the rate coefficient, in the form  $k = k_0 \times 1 / (A \times [O_2] + 1)$ . This parameterization allows for the removal of a species from the mechanism (the intermediate alkyl radical), which may benefit models limited by computational capacity, but at the cost of making the rate formulations more complicated. We provide both parameterizations, such that either can be used depending on the priorities and limitations of the modeling platform. The primary explicit mechanism in the Supplement includes the intermediate alkoxy species and their relevant reactions for every epoxide-forming step in the mechanism (including those of ISOPPOOH, isoprene hydroxynitrates, and other functionalized nitrates formed from NO<sub>3</sub> chemistry). A separate table is also included in the Supplement with the reactions required for the [O<sub>2</sub>]-dependent rate coefficient parameterization, as well as a list of reactions to remove from the full mechanism.

Finally, the temperature- and pressure-dependent yields of organic nitrates from reactions of peroxy radicals with NO are described in Section 4.2, and we incorporate these dependences into the rate coefficients of all RO<sub>2</sub> + NO reactions in the explicit and reduced mechanism. We denote the rate coefficients of nitrate-forming reactions with "k\_nitrate[X,Y,Z,n]", where X and Y are the preexponential and exponential factors in the Arrhenius equation for the overall reaction rate, Z is the normalization term for the nitrate yield (equal to  $A_0(n) \times (1 - \alpha_0) / \alpha_0$  in Equation 4.3, and n is the number of heavy atoms excluding the peroxy moiety. Thus, as in Equation 4.3, the nitrate formation rate coefficient is given by the equation:

$$k_{nitrate} = \left( X \times e^{-Y/T} \right) \times \left( \frac{A(T, [M], n)}{A(T, [M], n) + Z} \right) \quad (4.11)$$

where A refers to the Arey *et al.* (2001) parameterization in Equation 4.4. Similarly, we denote non-nitrate-forming RO<sub>2</sub> + NO reactions with "k\_alkoxy[X,Y,Z,n]", where the same parameters are used with only a minor adjustment:

$$k_{alkoxy} = \left( X \times e^{-Y/T} \right) \times \left( \frac{Z}{Z + A(T, [M], n)} \right) \quad (4.12)$$

While this parameterization is significantly more complex than other rate coefficients in the model, the yield dependence on temperature and pressure is necessary to accurately describe radical cycling through organic nitrates in the atmosphere. However, for some applications of the model, the full parameterization may not be necessary; in these cases, we recommend calculating branching ratios at the desired

temperature and pressure before running the simulation, and scaling the Arrhenius parameterization for the rate coefficients by the relative yields of each pathway.

### **4.8.3 Photolysis rates**

Photolysis rates coefficients for photolytic reactions included in the mechanism are the rates calculated when the sun is directly overhead. When input into a box model, this rate can then be scaled with the sunlight intensity at a particular time of day. These rates are multiplied in the mechanism by the variable "SUN" to denote this.

## 4.9 Supporting Information

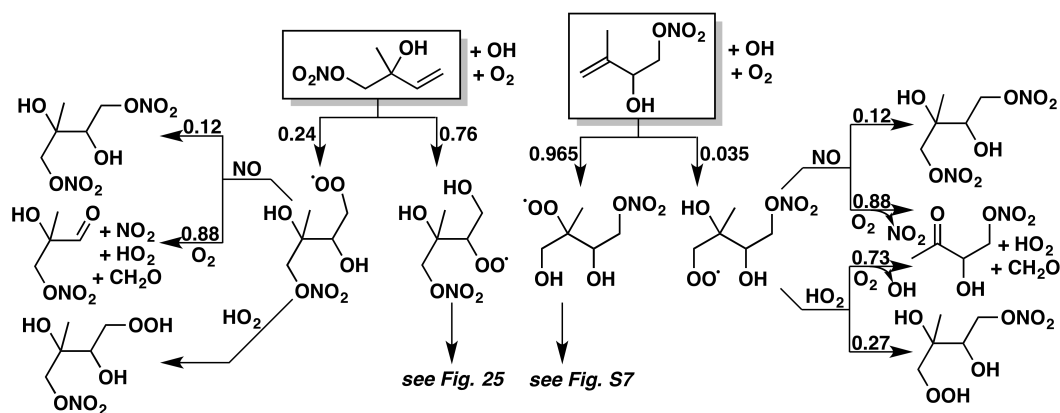


Figure 4.31: Mechanisms of the reactions of OH with (1-ONO<sub>2</sub>,2-OH)-IHN and (3-OH,4-ONO<sub>2</sub>)-IHN. Yields are for 298 K and 1 atm; in reactions of peroxy radicals with NO, the relative contributions of the nitrate and alkoxy pathways vary with both temperature and pressure. For the reduced mechanism, we combine the  $\beta$ -IHN isomers into a single species, and scale the product yields of its subsequent reactions according to the relative contributions of the isomers. We also combine the various isomers of stable C<sub>5</sub> tetrafunctionalized products.

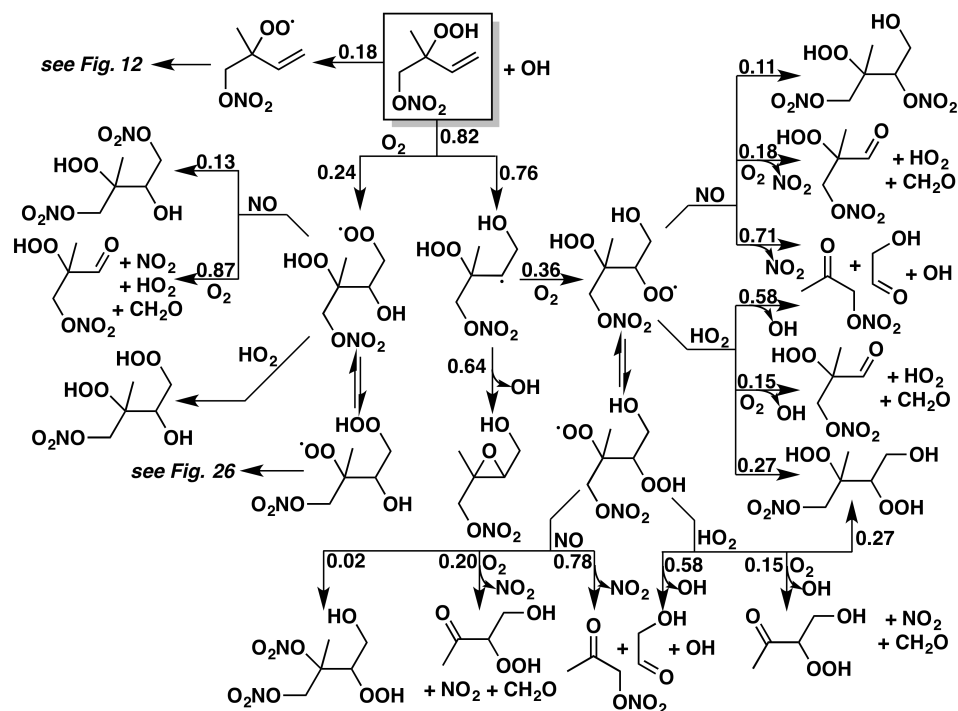


Figure 4.32: Mechanism of the reaction of OH with (1-ONO<sub>2</sub>,2-OOH)-IPN. Yields are for 298 K and 1 atm; branching ratios between OH-addition and -abstraction, epoxide formation and O<sub>2</sub> addition, and nitrate and alkoxy formation all vary with temperature and/or pressure. For the reduced mechanism, we combine the  $\beta$ -IPN isomers into a single species, and scale the product yields of its subsequent reactions according to the relative contributions of the isomers. We also combine the various isomers of stable C<sub>5</sub> tetrafunctionalized products.

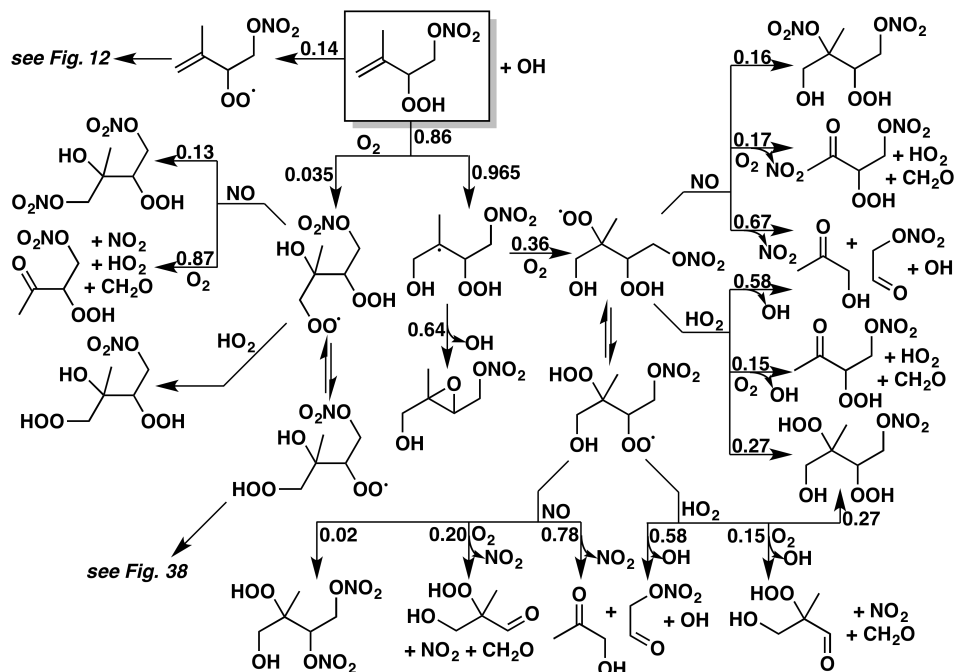


Figure 4.33: Mechanism of the reaction of OH with (3-OOH,4-ONO<sub>2</sub>)-IPN. Yields are for 298 K and 1 atm; branching ratios between OH-addition and -abstraction, epoxide formation and O<sub>2</sub> addition, and nitrate and alkoxy formation all vary with temperature and/or pressure. For the reduced mechanism, we combine the  $\beta$ -IPN isomers into a single species, and scale the product yields of its subsequent reactions according to the relative contributions of the isomers. We also combine the various isomers of stable C<sub>5</sub> tetrafunctionalized products.

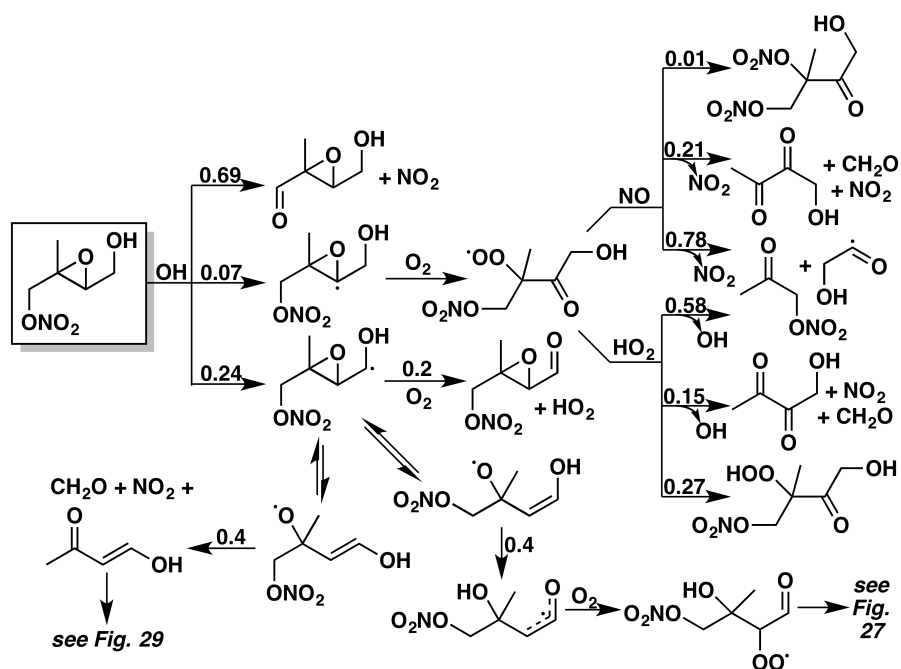


Figure 4.34: Mechanism of the reaction of OH with (1-ONO<sub>2</sub>,2,3-O,4-OH)-INHE. The *cis* and *trans* isomers are not treated separately, as they are expected to react identically. Yields are for 298 K and 1 atm; branching ratios between nitrate and alkoxy formation in reactions with NO vary with both temperature and pressure. For both the full and reduced mechanisms, we simplify the INHE and ICN systems by combining some intermediate peroxy radicals and distributing their products according to the relative contributions of the isomers. For the reduced mechanism, we also combine the  $\beta$ -INHE isomers into a single species, and scale their product yields similarly. We further combine the various isomers of stable C<sub>5</sub> tetrafunctionalized products.

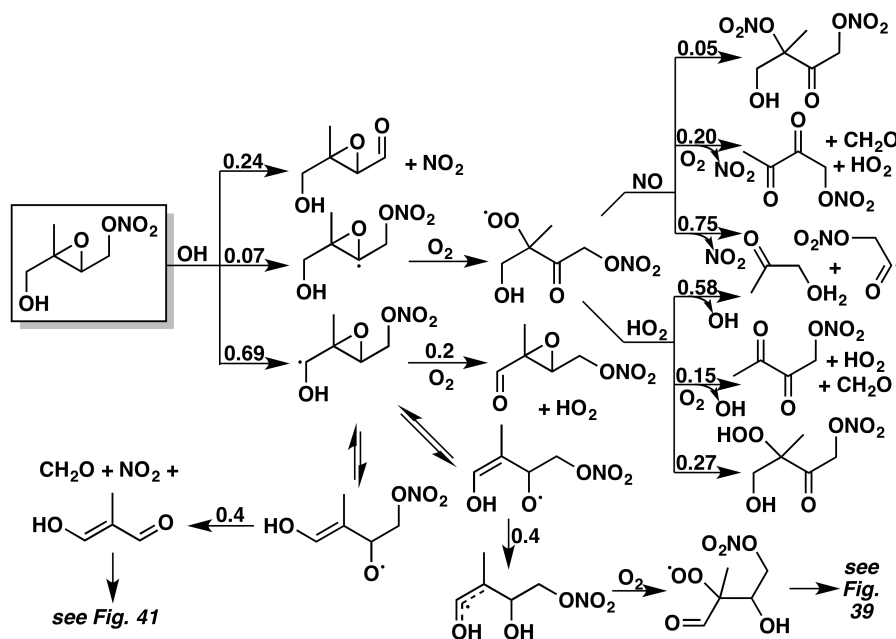


Figure 4.35: Mechanism of the reaction of OH with (1-OH,2,3-O,4-ONO<sub>2</sub>)-INHE. The *cis* and *trans* isomers are not treated separately, as they are expected to react identically. Yields are for 298 K and 1 atm; branching ratios between nitrate and alkoxy formation in reactions with NO vary with both temperature and pressure. For both the full and reduced mechanisms, we simplify the INHE and ICN systems by combining some intermediate peroxy radicals and distributing their products according to the relative contributions of the isomers. For the reduced mechanism, we also combine the  $\beta$ -INHE isomers into a single species, and scale their product yields similarly. We further combine the various isomers of stable C<sub>5</sub> tetrafunctionalized products.

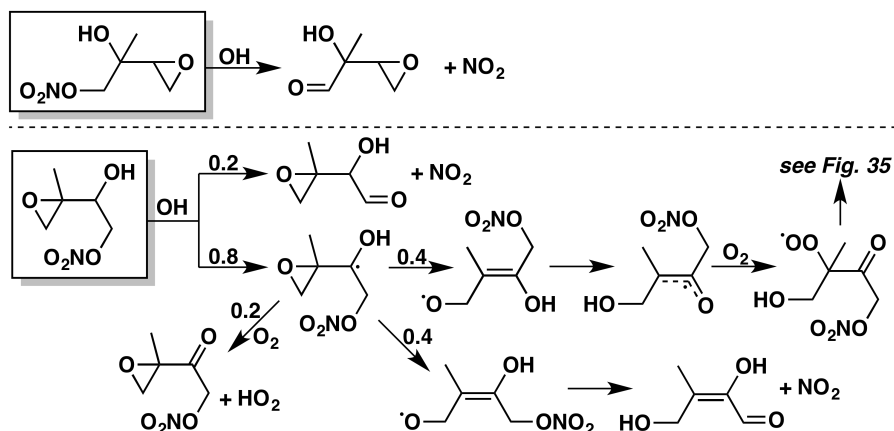


Figure 4.36: Mechanisms of the reactions of OH with (1,2-O,3-OH,4-ONO<sub>2</sub>)- and (1-ONO<sub>2</sub>,2-OH,3,4-O)-INHE. For both the full and reduced mechanisms, we simplify the INHE and ICN systems by combining some intermediate peroxy radicals and distributing their products according to the relative contributions of the isomers. For the reduced mechanism, we also combine the  $\delta$ -INHE isomers into a single species, and scale their product yields similarly. We further combine the various isomers of stable C<sub>5</sub> tetrafunctionalized products.

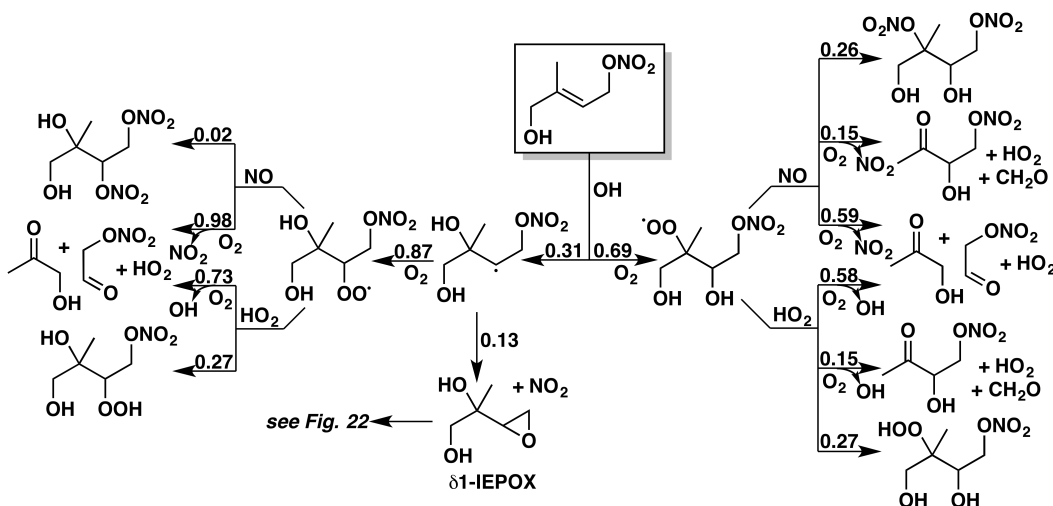


Figure 4.37: Mechanism of the reaction of OH with *E*-(1-OH,4-ONO<sub>2</sub>)-IHN. *Z*-(1-OH,4-ONO<sub>2</sub>)-IHN is expected to react identically. Yields are for 298 K and 1 atm; in reactions of peroxy radicals with NO, the relative contributions of the nitrate and alkoxy pathways vary with both temperature and pressure, and the branching ratio between IEPOX formation and O<sub>2</sub> addition also varies with pressure. For the reduced mechanism, we combine the  $\delta$ -IHN isomers into a single species, and scale the product yields of its subsequent reactions according to the relative contributions of the isomers. We also combine the various isomers of stable C<sub>5</sub> tetrafunctionalized products.

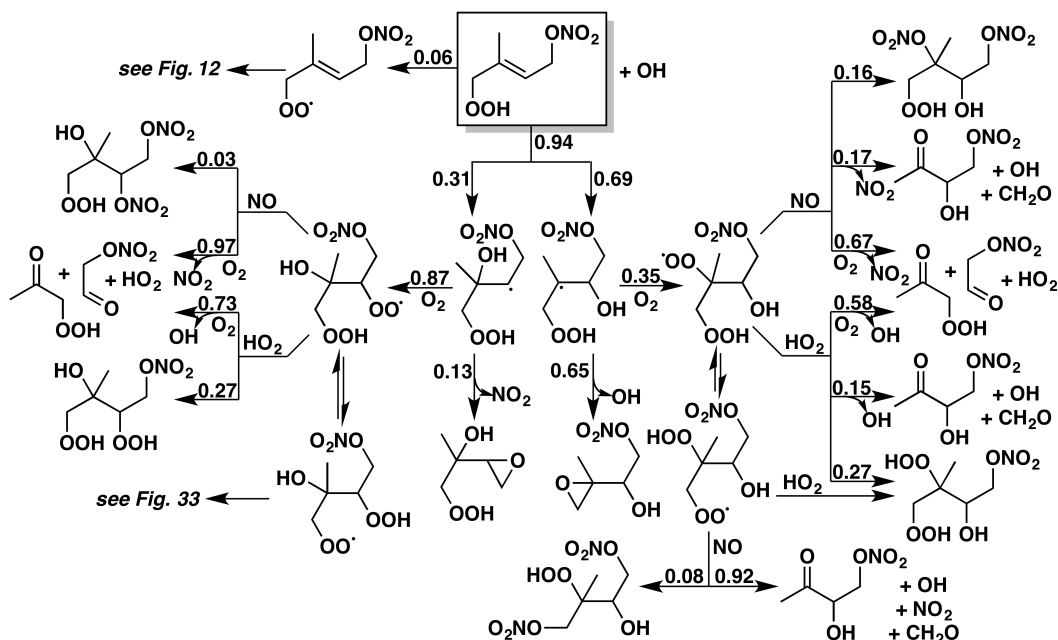


Figure 4.38: Mechanism of the reaction of OH with *E*-(1-OOH,4-ONO<sub>2</sub>)-IPN. *Z*-(1-OOH, 4-ONO<sub>2</sub>)-IPN is expected to react identically. Yields are for 298 K and 1 atm; branching ratios between OH-addition and -abstraction, epoxide formation and O<sub>2</sub> addition, and nitrate and alkoxy formation all vary with temperature and/or pressure. For the reduced mechanism, we combine the  $\delta$ -IPN isomers into a single species, and scale the product yields of its subsequent reactions according to the relative contributions of the isomers. We also combine the various isomers of stable C<sub>5</sub> tetrafunctionalized products.

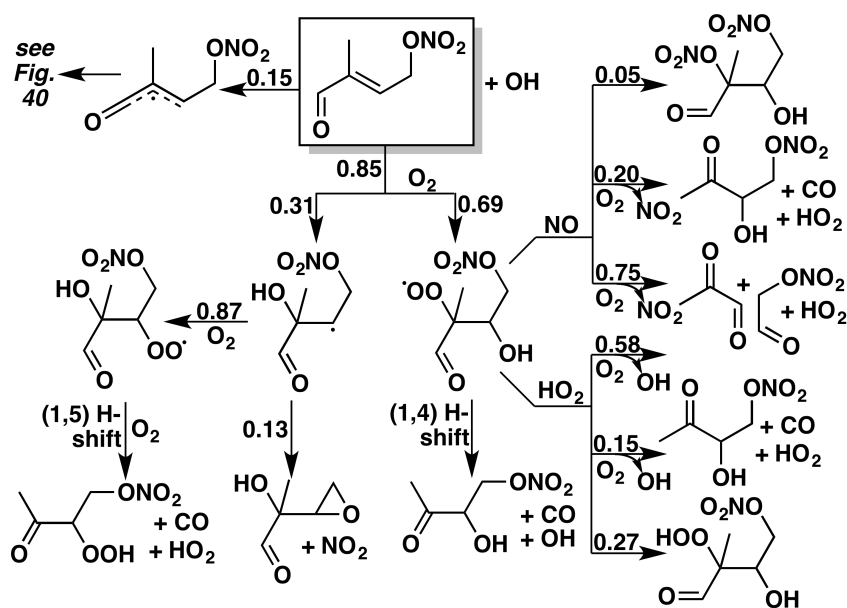


Figure 4.39: Mechanism of the reaction of OH with *E*-(1-CO,4-ONO<sub>2</sub>)-ICN. *Z*-(1-CO,4-ONO<sub>2</sub>)-ICN is expected to react identically. The terminal radical formed by H-abstraction (upper left) is presumed to add oxygen and react further like the analogous (though not identical) acyl peroxy radical in Figure 13. Yields are for 298 K and 1 atm; branching ratios between OH-addition and -abstraction, epoxide formation and O<sub>2</sub> addition, and nitrate and alkoxy formation all vary with temperature and/or pressure. For the reduced mechanism, we combine the four isomers of peroxy radicals derived from the addition of OH and O<sub>2</sub> to the  $\delta$ -ICN isomers, and scale the product yields of its subsequent reactions with NO and HO<sub>2</sub> according to the relative contributions of the isomers. We also combine the various isomers of stable C<sub>5</sub> tetrafunctionalized products.

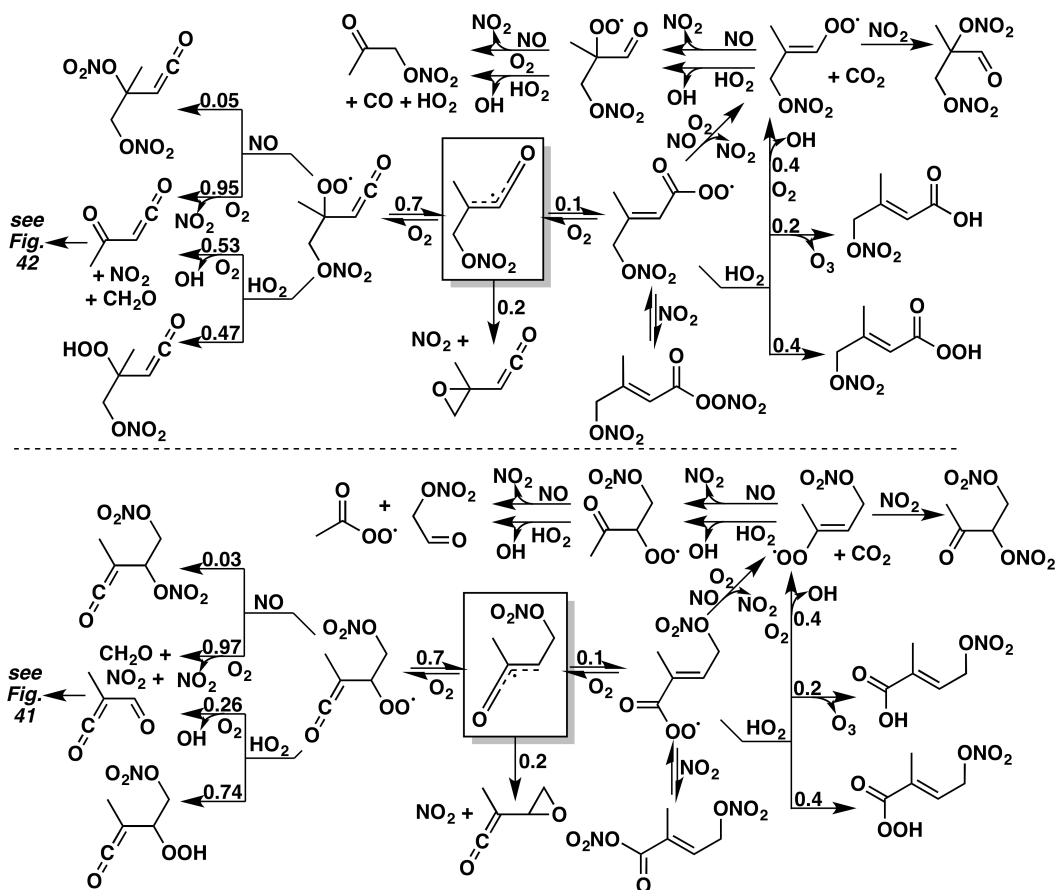


Figure 4.40: Mechanisms following the abstraction of an aldehydic hydrogen from the  $\delta$ -ICNs that form from the reaction of isoprene with  $\text{NO}_3$ . Yields are for 298 K and 1 atm; branching ratios between epoxide formation and  $\text{O}_2$  addition, as well as nitrate and alkoxy formation, vary with temperature and/or pressure. For the reduced mechanism, we group the ICN isomers together, and simplify the H-abstraction scheme to represent its effects on  $\text{HO}_x$  and  $\text{NO}_x$  budgets.



